DESIGN AND DEVELOPMENT OF REAL-TIME SINGLE AND DUAL-WAVELENGTH DCS SYSTEMS TO STUDY SKELETAL MUSCLE BLOOD PERFUSION AND OXYGEN METABOLISM

by

CHANDAN GANESH BANGALORE YOGANANDA

Presented to the Faculty of the Graduate School of

The University of Texas at Arlington in Partial Fulfillment

of the Requirements

for the Degree of

MASTER OF SCIENCE IN BIOMEDICAL ENGINEERING

THE UNIVERSITY OF TEXAS AT ARLINGTON

MAY 2017

Acknowledgement

I would like to take this opportunity to express my sincere indebtedness to Dr. Hanli Liu for offering me this chance of working on her vision and having complete confidence and faith in me and my work throughout. She has been to a great degree steady, understanding and has urged me to wind up distinctly a free learner. I am exceptionally appreciative for every one of the assets and information that I picked up over the span of my lords from Dr. Liu. I am amazingly roused by her and her work.

I would want to sincerely thank Dr. Hanli Liu, Dr. Michael Nelson and Dr. George Alexandrakis for being on my thesis defense committee notwithstanding their busy schedule and offering me their significant and invaluable counsel.

I might likewise want to express my gratitude to Dr. Fenghua Tian for mentoring me and being to a great degree understanding with my pace of learning over the span of this project. I value every one of his commitments of time, thoughts and advices amid the whole course of the project. I would want to thank my senior and lab-mate Mr. Xinlong Wang for his suggestions, advices, for tolerating all my questions and answering it to the best of his knowledge. I also want to express my appreciation to all my lab-mates who have helped me at different phases of this project.

I need to thank every one of my companions who have supported, prompted and perked me up completely through. At long last, I might want to thank my parents Mr. Yogananda B, Mrs. Sujatha V, my sibling Mr. Bharath Ganesh B Y and my sister Miss. Sandhya Manjunath for their approval, empowering blessings and for having faith in me for the duration of my life.

May 05, 2017

Abstract

DESIGN AND DEVELOPMENT OF REAL-TIME SINGLE AND DUAL-WAVELENGTH DCS SYSTEMS TO STUDY SKELETAL MUSCLE BLOOD PERUFSION AND OXYGEN METABOLISM

Chandan Ganesh Bangalore Yogananda

The University of Texas at Arlington, 2017

The aim of this study was to utilize Diffused Correlation Spectroscopy (DCS) to design and develop real-time single and dual wavelength systems and assess the physiological impacts of exercises on blood perfusion. The study consisted of 4 parts. Part 1 was to Re-design and develop a real-time single wavelength DCS system, part 2 was to validate this system by a cross validation method with the help of a concurrent study alongside Doppler ultrasound. Part 3 was to design & develop a real-time dual wavelength DCS system and part 4 was to validate the dual wavelength DCS system.

DCS is a developing non-obtrusive procedure to test profound tissue hemodynamics. DCS utilizes time-averaged intensity autocorrelation function for the fluctuations caused by moving scatterers (RBCs) in natural tissue. I introduced a software based autocorrelator framework to finish the securing and handling parts. I led approval considers on an intralipid phantom and human forearm. Both the studies demonstrated smooth decays which aid in showing signs of an improved fitting and subsequently more exact blood flow index (BFI). I

appear that the software based autocorrelation framework can be a contrasting option to the traditional equipment based correlators in DCS frameworks with advantages, for example, adaptability in raw photon count information handling, data processing, minimal effort and low cost.

Coordinate nonstop noninvasive estimation of neighborhood muscle blood stream in people stays constrained. Routine estimations of appendage blood stream, for example, Doppler ultrasound or venous impediment plethysmography, measure changes in mass channel stream and don't give provincial data. Near infrared diffused correlation spectroscopy (DCS) is a rising system for non-intrusive estimation of neighborhood muscle blood stream at the microvascular level. To better comprehend the qualities and restrictions of this novel approach, I played out an approval think about by looking at muscle blood stream changes measured by DCS and Doppler ultrasound during a small exercise.

The design and development of a real-time dual Wavelength DCS system consisted of 2 laser sources. An optical switch was used to toggle the light between laser 1 and laser 2. With this dual wavelength system conc. of HbO (Oxy hemoglobin) & conc. of Hb (de-Oxy hemoglobin) can be calculated along with the other parameters like rBFI (relative blood flow index), dOD (delta Optical density) and total intensity of the detected photons. I led validation studies on intralipid phantom and human forearm (arm cuff measurement). Both the studies demonstrated smooth decays which aid in showing signs of an improved fitting for rBFI and conc. of HbO (Oxy hemoglobin) & conc. of Hb (de-Oxy hemoglobin) was also obtained in real-time.

Table of Contents

Acknowledgements.....ii

Abstract.....iii

List of Figures & Illustrations.....viii

List of Tables.....xii

Outline of this Thesis.....xiii

Chapter 1 Introduction.....01

1.1 Diffused Correlation Spectroscopy.....01

1.1.1 Optical Window.....01

1.1.2 Diffusion of light in tissue.....03

1.2 Fundamentals of Diffused Correlation Spectroscopy.....06

1.3 DCS instrumentation & Fiber-Optic Probe.....07

Chapter 2 Re-Design & Development of a real-time, Single-Wavelength DCS System.....11

2.1 Design of the User Interface.....12

2.1.1 To embed Matlab inside LabVIEW.....12

2.1.2 Data management 14

2.1.3 User friendly input options.....15

2.2 Design of data acquisition module.....18

2.2.1 Principle of Data Acquisition.....18

2.2.2 Re-designed GATE Signal VI.....20

2.2.3 Re-designed Photon counting VI.....20

2.2.4 Advances from the previous VI.....22

2.2.5 Real time data display.....32

Chapter 3 System validation and Experiment on real-time, Single-Wavelength DCS System 35

3.1 Basic science study on hand Grip exercise…….....35

3.1.1 Ethical approval and subjects.....36

3.1.2 Experimental Protocol & Instrumentation.....36

3.1.3 Data processing.....40

3.1.4 Statistical analysis.....47

3.1.4.1 Correlation.....47

3.1.4.2 Regression analysis.....50

3.1.5 Results & Conclusions.....57

Chapter 4 Design & Development of a real-time, Dual-Wavelength DCS System.....60

4.1 Programming the optical switch.....62

4.2 Design of the User Interface.....68

4.3 Design for the data acquisition.....69

4.4 Real time data display.....70

Chapter 5 System validation on real-time, Dual -Wavelength DCS System.....71

5.1 Intralipid Phantom Test…….....71

5.2 Human Cuff Test…….....74

Chapter 6 Discussion and future work.....76

6.1 Discussions……..…….....77

6.2 Limitations…….....78

References.....79

Biographical information.....82

List of Figures and Illustration

Figure 1: Absorption Spectrum of Hb, HbO_2 and water invisible and near-infrared range.....02

Figure 2: Diffusion of light in biological tissue.....03

Figure 3: Block diagram of single wavelength DCS system.....08

Figure 4: Flow Cart for functioning of DCS system.....08

Figure 5: DCS fiber optics probes used for the experiment 10

Figure 6: Flow chart of Steps to reach MATLAB script in LABVIEW.....12

Figure 7: Block diagram Steps to reach MATLAB script in LABVIEW.....13

Figure 8(a): Screenshot of the user prompt to create a new folder in the name of the subject.....14

Figure 8(b): Screenshot of LABVIEW block diagram window to program a user option to create a new folder.....14

Figure 9(a): Screenshot of the user option to input the μ_a and μ_s values.....15

Figure 9(b): screen shot of LABVIEW block diagram window to program a user option to input the μ_a and μ_s values.....16

Figure 10(a): Screenshot of the prompt for user option to input the experimental time.....17

Figure 10(b): screenshot of LABVIEW block diagram window to program a user option to input the experimental time.....17

Figure 10(c): LABVIEW front panel window that shows experimental clock.....17

Figure 11: Buffered Period Measurement.....19

Figure 12(a): screenshot of LABVIEW block diagram for the generation of a gate signal.....20

Figure 12(b): screenshot of first half of the LABVIEW block diagram for the data acquisition.....21

Figure 12(c): screenshot of second half of the LABVIEW block diagram for the data acquisition.....21

Figure 13(a): Drawbacks of the previous system.....23

Figure 13(b): Front panel to control GATE Signal.....24

Figure: 13(c): Front panel to for data acquisition.....25

Figure 14(a): Block diagram of previous version with errors encircled with red.....26

Figure 14(b): Block diagram of new version with fixed errors encircled with green.....27

Figure 14(c): Front panel of previous version for gate generation with errors encircled in red.....27

Figure 14(d): Block diagram of new version for gate generation with fixed errors encircled in green.....28

Figure 15(a): Block diagram of part 1 new version for putting everything into one program.....29

Figure 15(b): Block diagram of new version part 2 for putting everything into one program.....29

Figure 15(c): Block diagram of new version part 3 for putting everything into one program.....30

Figure 15(d): Final front panel of new version for putting everything into one program.....30

Figure 15(e): Screenshot of CRO representing the data acquisition when GATE is on for 2 seconds with 99.9% Duty cycle.....31

Figure 15(f): Screenshot of CRO representing the data acquisition when GATE is on for 2 seconds with 99.9% Duty cycle.....32

Figure 16: a screen shot of the real-time data display.....34

Figure 17: Diagrammatic explanation of the Experimental Protocol.....37

Figure 18(a): DCS Probe affixed over the belly of the flexor digitorum profundus.....38

Figure 18(b): Pictorial representation of DCS Probe affixed over the belly of the flexor digitorum profundus.....38

Figure 19(a): DCS Probe covered with a black cloth and Doppler ultrasound on the brachial artery together.....38

Figure 19(b): LABVIEW Block diagram to design an audio feedback “GRIP”.....39

Figure 19(c): LABVIEW Block diagram to design an audio feedback “RELAX”.....39

Figure 20(a): plot of rBFI of all 14 subjects before and after normalization.....40

Figure 20(b): plot of rBFI of 1 subject after normalization.....41

Figure 20(c): plot of mean rBFI of all subjects after normalization.....41

Figure 21(a): plot of dOD of all 14 subjects before and after normalization.....42

Figure 21(b): plot of dOD of 1 subject after normalization.....42

Figure 21(c): plot of mean dOD of all subjects after normalization.....43

Figure 22(a): plot of Brachial Artery Flow of all 14 subjects before and after normalization.....44

Figure 22(b): plot of Brachial Artery Flow of 1 subject after normalization.....44

Figure 22(c): plot of mean Brachial Artery Flow of all subjects after normalization.....45

Figure 23: plot of normalized mean values of all the 3 interested parameters.....46

Figure 24(a): correlation plots.....48

Figure 24(b): correlation plot.....49

Figure 25(a): Linear data fitting for rBFI (relative blood flow index) vs Brachial artery flow (Doppler data).....51

Figure 25(b): Linear data fitting for dOD (delta optical density) vs Brachial artery flow (Doppler data) 53

Figure 25(c): Linear data fitting for dOD (delta optical density) vs rBFI (relative blood flow index) 55

Figure 26: Block diagram of Dual wavelength DCS system.....61

Figure 27: Flow Cart for functioning of dual wavelength DCS system.....61

Figure 28: MEMS MxN Blocking Switch electrical connections.....62

Figure 29(a): MEMS MxN Blocking Switch Module Pin Assignment Table for TTL.....63

Figure 29(b): MEMS MxN Blocking Switch Module Electrical specifications.....63

Figure 30(a): Timing Diagram for MEMS MxN Blocking Switch Module using TTL interface.....64

Figure 30(b): Timing parameters for MEMS MxN Blocking Switch Module using TTL interface.....65

Figure 30(c): Pin diagram connections from NI USB 6501 to Optical Switch.....65

Figure 31(a): Labview Block diagram to program the optical switch for parking position using NI USB 6501.....66

Figure 31(b): Labview Block diagram to program the optical switch for IN1 – OUT1 using NI USB 6501.....67

Figure 31(c): Labview Block diagram to program the optical switch for IN2 – OUT1 using NI USB 6501.....67

Figure 31(d): Photograph of the hardware enclosure for dual wavelength DCS system.....68

Figure 32: Photograph of the real-time data display of dual wavelength DCS system.....70

Figure 33(a) & 33(b): Photograph of probe placement during intralipid phantom test.....71, 72

Figure 34(a) & 34(b): Auto correlation functions of inralipd phantom test.....72

Figure 34(c): Intensity plot.....73

Figure 35: Schematic representation for cuff test protocol.....74

Figure 36(a): Plots for rBFI of cuff test.....75

Figure 36(b): Plot for change in conc. of Hb and HbO during cuff test.....76

List of Tables

TABLE 1: Slope and intercept table for rBFI vs Brachial artery flow.....52

TABLE 2: Slope and intercept table for dOD vs Brachial artery flow.....54

TABLE 3: Slope and intercept table for dOD vs Brachial artery flow.....56

TABLE 4: Logic table to control the MEMS based optical switch.....66

Outline of this Thesis

Chapter 1 gives a concise introduction about the basic principle of DCS system, fiber optic probe and about the instrumentation of Diffused Correlation Spectroscopy (DCS) system. It also contains a few concepts of the theoretical background of DCS. Chapter 2 will discuss about Re-Design & Develop of a real-time, Single-Wavelength DCS System, design of the user interfaces and the data acquisition principle. Chapter 3 deals with the verification, validation and cross validation of the system with an experiment where a concurrent measurement with Doppler Ultrasound is performed and about Data analysis, methodology, results and conclusions. Chapter 4 will discuss about Design & Development of a real-time, Dual-Wavelength DCS System, programming the optical switch, design of the user interfaces and the data acquisition principle and real time output display. Chapter 5 discusses about the verification and validation of the system with an experiment on liquid phantoms and human cuff occlusion. Chapter 6 deals with discussion, future work and limitations of the systems.

Chapter 1

Introduction

1.1 Diffused Correlation Spectroscopy

Diffused Correlation Spectroscopy is a rapidly emerging optical modality/technology that uses light to measure/monitor blood flow across various tissues. Several models for light propagation have made ready for extensive assortment of uses. Diffused Correlation Spectroscopy (DCS) utilizes time averaged autocorrelation function of the fluctuating diffuse reflectance Signal. DCS has the potential to non-invasively acquire data about a tissue for its optical and dynamic properties, subsequently advertising the energizing and conceivable outcomes in the field of medical imaging [1]. Diffuse optics has opened new conceivable outcomes for non-invasive medical devices to find for injuries in profound tissue. Diffuse optics-based devices are likewise generally financially savvy and convenient. These benefits develop the uses of such restorative devices to essential care unit, bedside observing, and operation theater as an optical methodology for examining hemodynamic properties in the microvasculature of profound tissue [2]. DCS innovation has been broadly created, approved and utilized in the most recent decade to test the blood perfusion data in the deep tissue vasculature, for example, brain, muscle and breast [3].

1.1.1 Optical Window

The **near-infrared (NIR) optical window** (also known as optical window or therapeutic window) defines the range of wavelengths from 650 to 1350 nm where light has its maximum depth of penetration in tissue [4]. Since scattering builds the separation went by photons inside tissue, the likelihood of photon absorption likewise increments. Since scattering has weak

reliance on wavelength, the NIR window is fundamentally restricted by the light absorption of blood at short wavelengths and water at long wavelengths.

DCS operates in this window where there is very low absorption of light by the biological tissue which enables deep penetration of light [3].

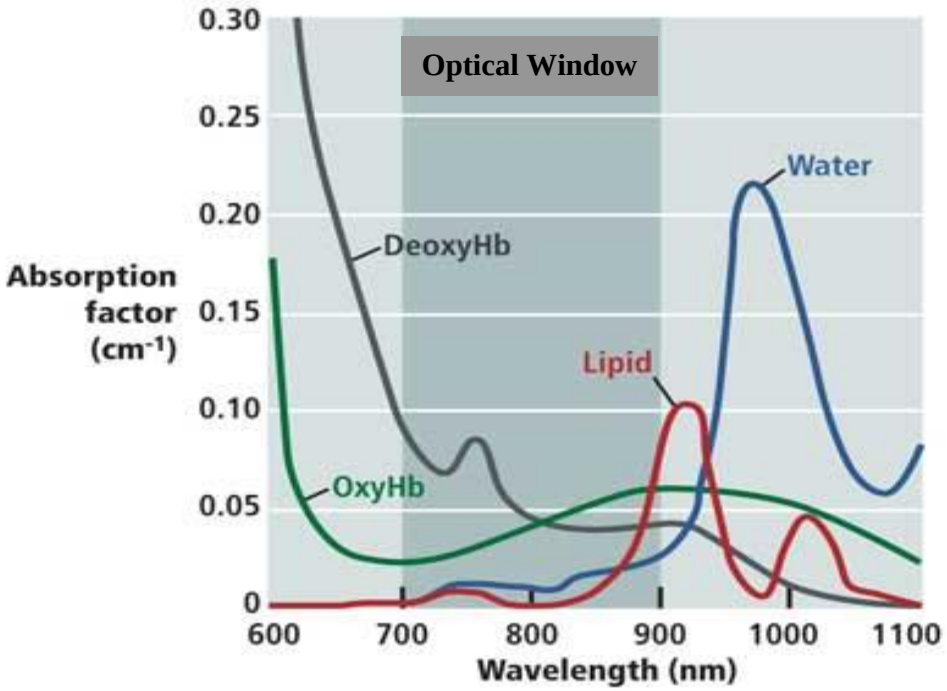

Figure 1: Absorption Spectrum of Hb, HbO_2 and water invisible and near-infrared range [5]

The lower wavelengths such as violet and ultraviolet have poor tissue penetration due to the increased absorption of light by the blood and tissue components [6]. Correspondingly, water altogether retains the light higher than 1000nm. In the middle of these wavelengths the entrance of light is higher because of low absorption. This locale (~650nm - 1100nm) is named as optical window for non-invasive optical imaging (allude figure 1). In this window, scattering is the overwhelming cooperation which happens in the tissue. The light diffuses into the tissue due to this scattering and light is able to propagate through the tissue thickness of ~15 cm for limbs,

brain and breast [7]. Hence, NIR optical window is the perfect range for non-invasive investigation of microvascular blood perfusion in a tissue.

1.1.2 Diffusion of light in tissue

Photon propagation in natural tissue is portrayed by the essential optical properties of absorption and scattering. These properties represent the quantities of photons that are transmitted between focuses on the surface of tissue. Out of these two interactions scattering is more dominant and as a result a tissue is considered a scattering or turbid media [8,9] as a result the diffused light trajectory will also change.

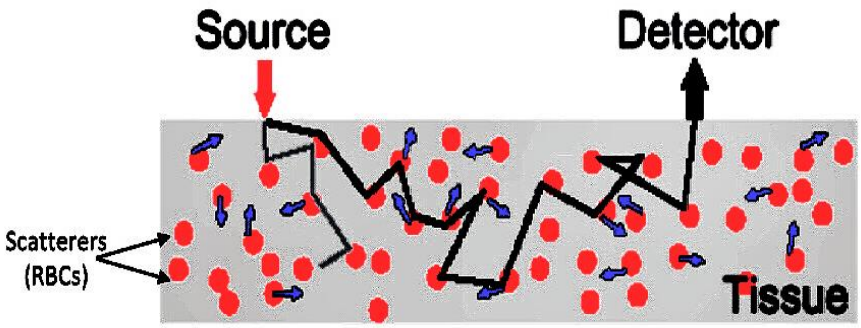

Figure 2: Diffusion of light in biological tissue [10]

DCS is an expansion of single-scattering dynamic light scattering (DLS) [11-13] to multiple scattering limit. At the point when light photons are diffused in the tissue, they may encounter stage shifts furthermore, at the detector side, speckle fluctuations are observed. The movement information of the scatter is conveyed by the electric field of the attenuated light and can be gotten from the electric field autocorrelation function [3].

The Function is defined as:

$$G(\vec{r}, \tau) = \langle E(\vec{r},t)\, E^*(\vec{r},t+\tau) \rangle$$

Also, WKT ,

$$G_1(\mathbf{r},\tau) = \frac{vSe^{-K(\tau)r_1}}{4\pi D r_1} - \frac{vSe^{-K(\tau)r_2}}{4\pi D r_2}, \quad \text{..... 1.1}$$

where $K^2(\tau) = 3\mu_a\mu_s' + \mu_s'^2 k_0^2 \alpha \langle \Delta r^2(\tau) \rangle.$

and $\langle \Delta r^2(\tau) \rangle = 6D_b\tau.$

Experimentally, the autocorrelation for diffusion is calculated as:

$$g(\vec{r},\tau) = \frac{\langle E(\vec{r},\tau)E*(\vec{r},t+\tau)\rangle}{\langle I\rangle^2}$$

OR

$$g_2(\mathbf{r},\tau) = \langle I(\mathbf{r},0)I(\mathbf{r},\tau)\rangle / \langle I(\mathbf{r},0)\rangle^2 \quad \text{..... 1.2}$$

Also, according to Siegert, the phase information will be conserved.

$$g(\vec{r},\tau) = 1 + \beta \frac{|G(\vec{r},\tau)|}{\langle I(\vec{r},t)\rangle^2} \quad \text{..... 1.3}$$

Equation 1.3 is derived from using Siegert Relation [3,14]. Where,

$I(\vec{r},t)$ ⟶ Will be the intensity of the detected diffused light at time t and position r

$\langle \ldots \rangle$ ⟶ Is the angle bracket which denotes and ensemble average

β ⟶ Factor related to geometry, number of speckles detected and certain other experimental factors [3].

And, To associate equation 1.2 to a theoretical equation, we need to get g_1 (Calibrated theoretical value).

$$g_2(\mathbf{r},\tau) = 1 + \beta\,|g_1(\mathbf{r},\tau)|^2. \quad \text{..... 1.4}$$

g_1 is directly equal to the normalized photon density of the scattered light due to both static and dynamic scatterers.

$$g_1(\mathbf{r},\tau) = G_1(\mathbf{r},\tau)/G_1(\mathbf{r},0) \quad \text{..... 1.5}$$

If $\tau = 0$, we have

$$G_1(r,\ 0) = \frac{vse^{-K(0)r_1}}{4\pi D r_1} - \frac{vse^{-K(0)r_2}}{4\pi D r_2}$$

where $K(0) = \sqrt{3\mu_a\mu_s'}$.

It is the solution for diffusion equation in steady state.

If $\tau \neq 0$, we have the original expression,

$$G_1(r,\tau) = \frac{vse^{-K(\tau)r_1}}{4\pi D r_1} - \frac{vse^{-K(\tau)r_2}}{4\pi D r_2}$$

where $K(\tau) = K(0) + 6m_s'^2 k_0'^2 (\alpha D_b)\ \tau$

The grouped parameter, , αD_b, reflects the flow of scatterers.

The term $G_1(r,\ 0)$ will remain constant in equation 1.5.

The Siegert relation is used to obtain the electric field autocorrelation function with the assumption that the systems' time average is equal to ensemble average [3]. Examines have demonstrated that, in spite of the fact that the motion of RBCs is considered as an irregular movement, The Brownian movement indicated better fitting in the larger part of the cases going from muscle to brain and furthermore tumor models. Thus, $G_1(r,\tau)$ Can be fitted to obtain αD_b and further Relative Blood Flow (rBF).

1.2 Fundamentals of Diffused Correlation Spectroscopy

Microvascular Blood Perfusion (MBP) and oxygen metabolism are the important features for determination of abnormal tissue and for treating the same. Microvascular MBP conveys supplements, for example, oxygen to tissue and expels metabolic waste items from tissue. Inconsistent MBP is identified with cardiovascular sickness stroke, head injury, peripheral vascular infection (PVD), malignancy. The perfect skill for estimation of MBP and oxygen metabolism gives quantitative data about small scale what's more, large scale vasculature with capacity to probe deep tissues. [15]. The perfect BF estimation ought to give quantitative data about full scale and microvasculature with millisecond temporal resolution. The estimations ought to be carried out persistently, noninvasively, and without hazard to subjects. Moreover, perfect estimations would not be restricted to the tissue surface, i.e., it is alluring to probe BF in profound tissues. A variety of noninvasive methods are employed for the measurement of BF and blood cell velocity (Wintermark et al. 2005) but Diffused Correlation Spectroscopy (DCS) otherwise called diffusing-wave spectroscopy (DWS) is built up as a rising method for consistent non-invasive estimation of blood perfusion and oxygen metabolism in tissues.

NIR DCS is a "static" technique since it gauges the generally moderate varieties in tissue absorption and scattering. "Dynamic" techniques specifically measure the movements of the scatterers. As far as biological tissue is considered, the RBCs are the essential moving scatterers. The recognized flag from biological tissue is identified with the movement of the RBCs, BF can be determined utilizing a numerical model of the propagation of light photon through tissue [15].

1.3 DCS instrumentation & Fiber-Optic Probe

The previous DCS system was designed similar to Dong et al 2012 paper [3]. The new system is re-designed based on the concepts obtained from the same paper but with different specifications and a lot of advancements.

Both the old and the new system consists of

- A long coherence length (>10m) CW laser at 785nm (DL785- 100-S, ~100 mW, CrystaLaser, Reno, Nevada, USA) is used as the source.
- A photon counting avalanche photo diode (APD) (SPCM AQRH-14-FC, Excelitas Technologies, Vaudreuil (Quebec), Canada) is used as the detector.
- The output of the APD is transistor-transistor logic (TTL) pulses.
- The output of the APD is connected to a computer (CPU: Intel Core 2 Duo, RAM: 4 GB) with a 32-bit, 8 channel data acquisition card (PCI-6602, National Instruments) through a shielded BNC connector block (BNC-2121, National Instruments).
- The optical probe used to obtain light from the CW laser source is a multi-mode optical fiber of 125 μm diameter (M31L02, THORLABS).
- The detector fiber use to collect light photons is a single-mode optical fiber operating in few-mode configuration (P1-980AR-2, THORLABS).
- A single mode fiber (P1-780AR-2, THORLABS) was also used in early development of the system. Another end of the detector fiber is connected to the APD.
- LabView software was used to communicate with the hardware components for acquiring data and to control the data acquisition using the gate signal from PCI-6602.
- Matlab software was used for inbuilt data processing and real time output display.

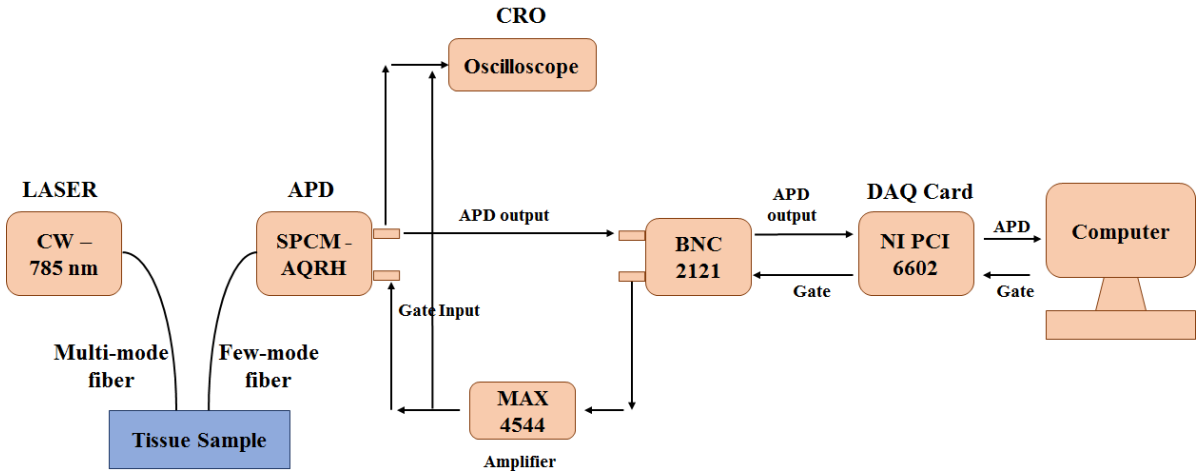

Figure 3: Block diagram of single wavelength DCS system.

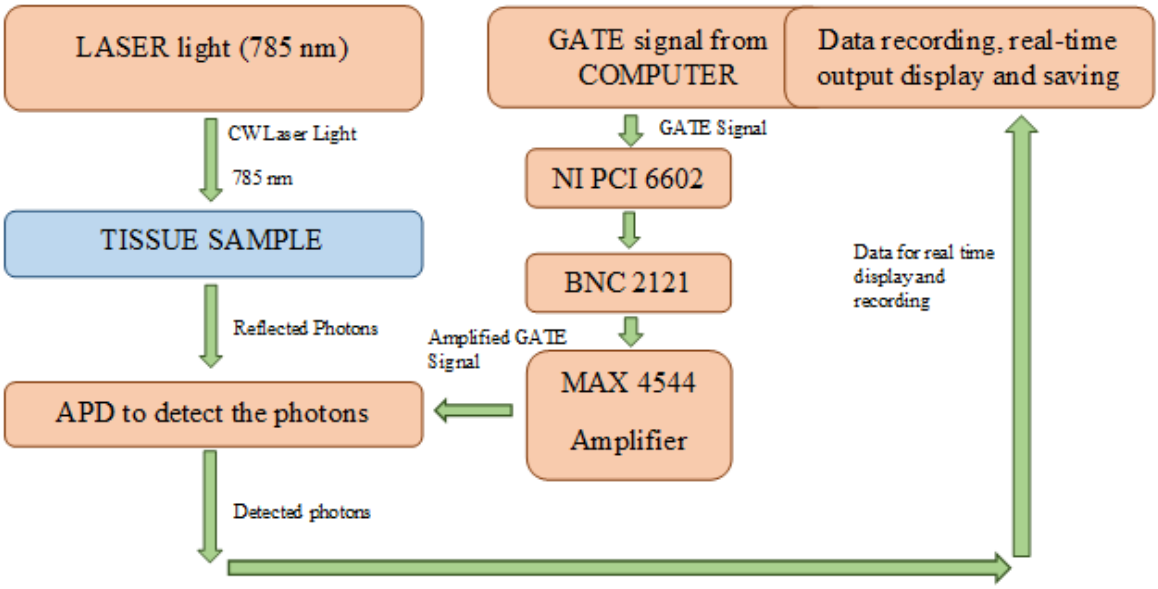

Figure 4: Flow Cart for functioning of DCS system.

As discussed earlier about the components used for building the real-time DCS system with single wavelength, Figure 3 represents the block diagram of the entire DCS system with all the discussed and required components. Figure 4 represents the flow chart for functioning of the DCS system. The DCS system consists of a 785nm laser which acts the source of light that is shined on the tissue sample and Avalanche photodiode detector (APD) is used for detecting the reflected photons. A software gate signal is produced using LABVIEW software and amplified using MAX 4544 amplifier. Then an amplified gate signal is obtained which controls the data acquisition from the APD. Simple understanding is that, when the gate is open or high, data will be acquired and if the gate is closed i.e. low then there will not be any data acquired. The acquired data is then recorded, processed, saved and the output is displayed in real-time using MATLAB script inside of LABVIEW.

Fiber-Optic Probe

DCS empowers utilization of huge assortment of tests. The most fundamental test comprises of source fibers (multimode) and at least one detector fiber (single or few-mode). For an optical fiber, the number of guided modes is dependent on the core radius (a), the operating wavelength (λ) and relative-refractive index (NA), otherwise called numerical aperture. The number of modes and the properties of a dielectric optical waveguide is related which can be best described by introducing a normalized frequency V [16].

$$V = \frac{2\pi a}{\lambda} N_A \qquad \text{..... 1.12}$$

At the point when V is lesser than the basic cutoff recurrence V_c, only the basic mode of LP01 can be guided through the fiber. At the point when V is higher than V_c the fiber can guide more

than one mode and turns into a few-mode fiber [16]. $V^2/2$ gives us the total number of optically guided modes permitted by a single mode fiber. For the detector, a few-mode fiber (P1980AR-2, THORLABS) which can pass 5 guided modes is used. Source and detector is separated by 1.5cm. Enhancing the SNR is significant when the detected signal is to a great degree low, which is not unordinary for DCS frameworks, particularly with bigger source detector separations. On utilizing, a few-mode fiber the light intensity at the detector is altogether increased, in this way enhancing the SNR of the DCS system [16].

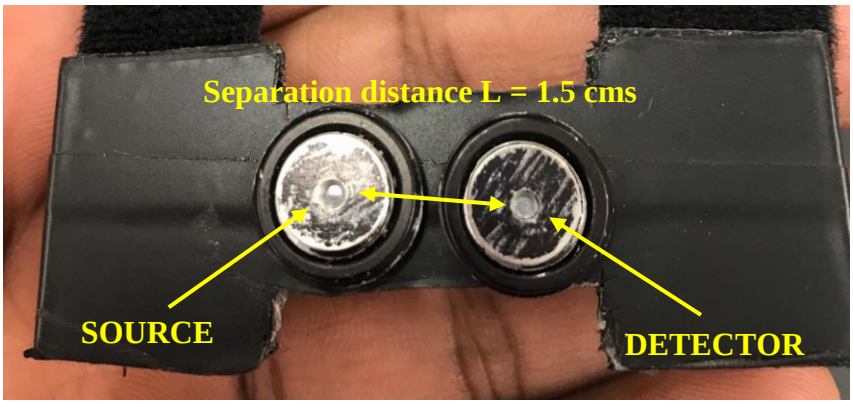

Figure 5: DCS fiber optics probes used for the experiment

Figure 5 represents the DCS fiber optics probe used in this particular system with the source fiber being a multimode fiber and the detector being a few mode fiber. The separation distance between the source and the detector was kept constant throughout as L=1.5 cms. A small probe holder was used to affix the source and detector at a constant separation distance of L=1.5 cms and also which would help us strap it up on the skeletal muscle during any experiment.

Chapter 2

Re-Design & Development of a real-time, Single-Wavelength DCS System

Re-Design & Development was done using National Instruments' LabVIEW 2013 software.

The previous DCS system was designed similar to Dong et al 2012 paper [3].

The new system is re-designed based on the concepts obtained from the same paper but with different specifications and a lot of advancements.

The goals of this re-design were:

- To fix all the errors in the data acquisition program from the previous version.
- To have all the programs running under one code and a single user interface unlike the previous one which had 3 separate parts. Separate VIs for Gate signal and data acquisition and another separate MATLAB code for data processing.
- To assure that there is no data loss during data acquisition.
- Completely time synchronized.
- Ensure proper functioning of the algorithm and to keep it user friendly.
- Proper data management.
- To give some open options for user inputs.
- To embed MATLAB in LabView which will:
    - Reduce time and man power for data processing post data acquisition.
    - Cut off the use of MATLAB separately for data processing.
    - Help in output data display.

- To have a user-friendly interface that would be capable of controlling the algorithm based on the experimental time without disturbing the data acquisition and functioning of the algorithm.
- To have a real-time output data display which will help the physician/clinician and the engineer monitor the output directly.

2.1 Design of the User Interface

A user-friendly interface was designed/programed which would help any person even without the knowledge of DCS to use the system very easily.

2.1.1 To embed MATLAB inside LabVIEW

The main reason of using MATLAB script inside of LABVIEW was to reduce time and man power for data processing post data acquisition, cut off the use of MATLAB separately for data processing, help in output data display.

Steps to reach MATLAB script in LABVIEW

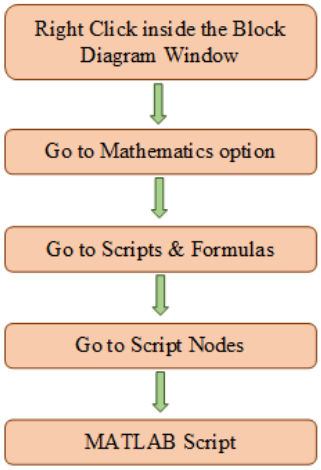

Figure 6: Flow chart of Steps to reach MATLAB script in LABVIEW

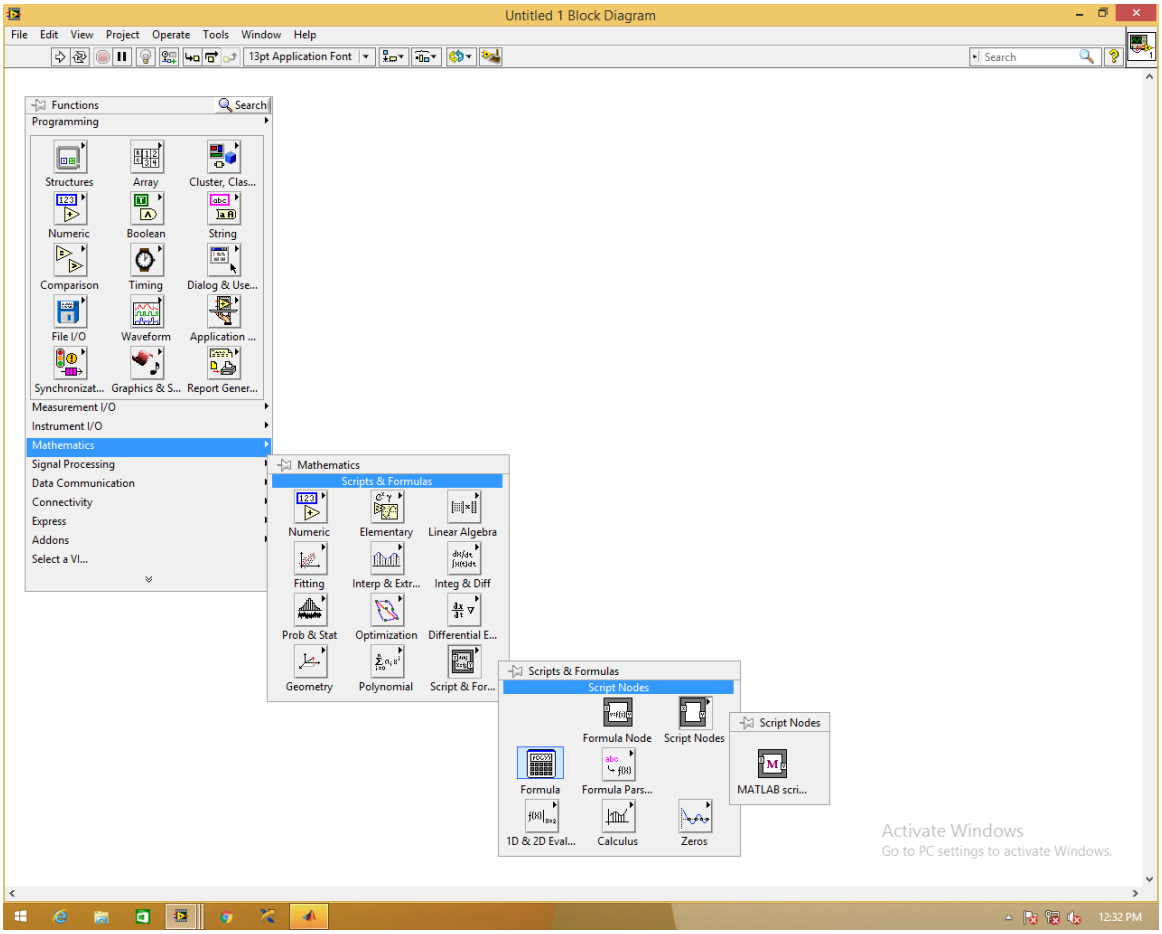

Figure 7: Block diagram Steps to reach MATLAB script in LABVIEW

Figure 6 represents a flow chart of Steps to reach MATLAB script in LABVIEW and Figure 7 represents the block diagram Steps to reach MATLAB script in LABVIEW where

- Step 1 - Right click on any open space on the block diagram to get a pop up window showing all the functions.
- Step 2 - Select the Mathematics option from the list of functions.
- Step 3 - Select the Scripts & Formulas options from the mathematics pop up window.
- Step 4 - Select the Script Nodes option from the Scripts & Formulas pop up window.
- Step 5 - Find the MATLAB script option in the Script Nodes pop up window.

2.1.2 Data management

This section will discuss about managing data obtained from a subject. A user-friendly option was designed/programmed where the user had an option to enter the name of the subject for that experiment. A New folder in the name of the subject would be created and all the related data files, figures and plots would be saved in that particular folder. This will avoid any sort of confusions related in matching a subject's data with its figures and plots. Also, it will be very well organized.

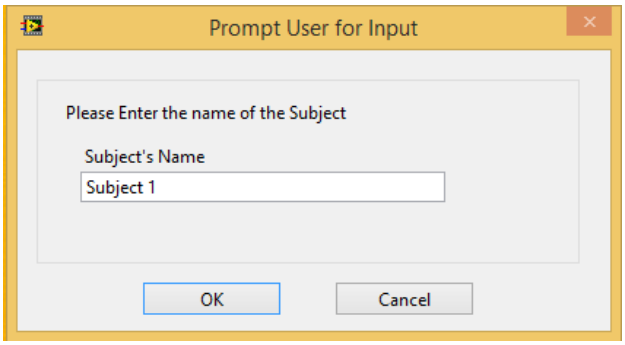

Figure 8(a): Screenshot of the user prompt to create a new folder in the name of the subject.

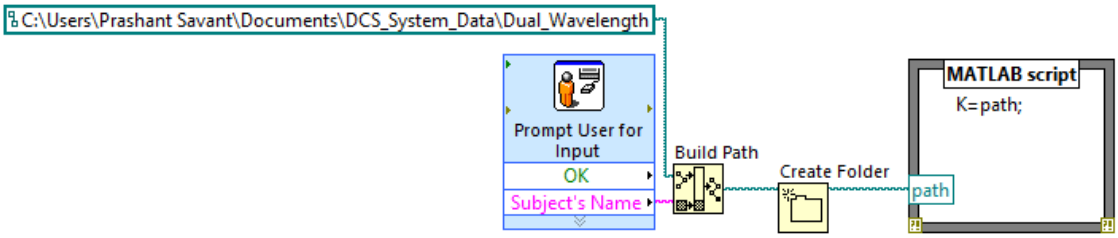

Figure 8(b): Screenshot of LABVIEW block diagram window to program a user option to create a new folder.

Figure 8(a) represent the prompt generated to enter the name of the subject for the experiment with which a folder is created in that particular name and Figure 8(b) gives us the idea about how the prompt is designed in LABVIEW for a user option to create a new folder.

2.1.3 User friendly input options

A user interface with an option to input the absorption coefficient (μ_a), scattering co-efficient(μ_s) and experimental time was designed/programmed. The input of μ_a and μ_s values will help in fitting the for data in real time also reducing the time, effort and man power to process the data post data acquisition. The option to input the experimental time will help in controlling the system based on the given time. Once the time limit has been reached, the system will close automatically without any required supervision. Also, this will in no way affect the system's performance, data acquisition or data processing inside the algorithm.

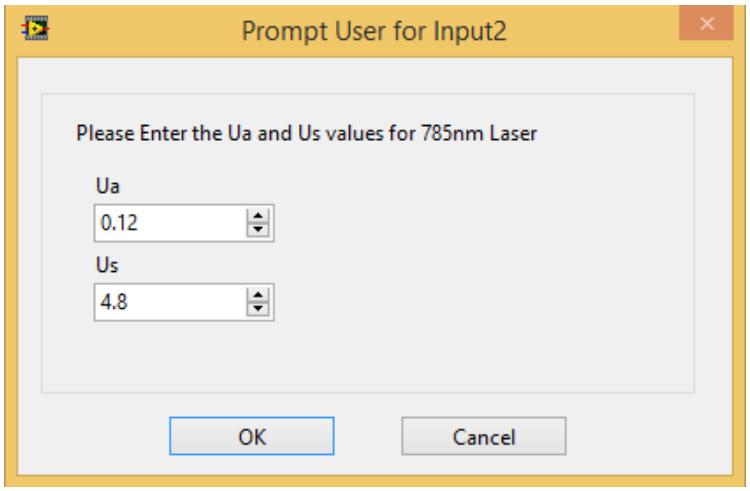

Figure 9(a): Screenshot of the user option to input the μ_a and μ_s values.

Figure 9(a) represent the prompt generated to enter the μ_a and μ_s values of the subject for the experiment with which the initial fitting model is created. This will also help in real time data display because the model that is used for fitting the data is created once even before the start of the experiment which will remain constant for a particular subject throughout the experiment and it need not be remodeled again and again for every data set we acquire during the experiment.

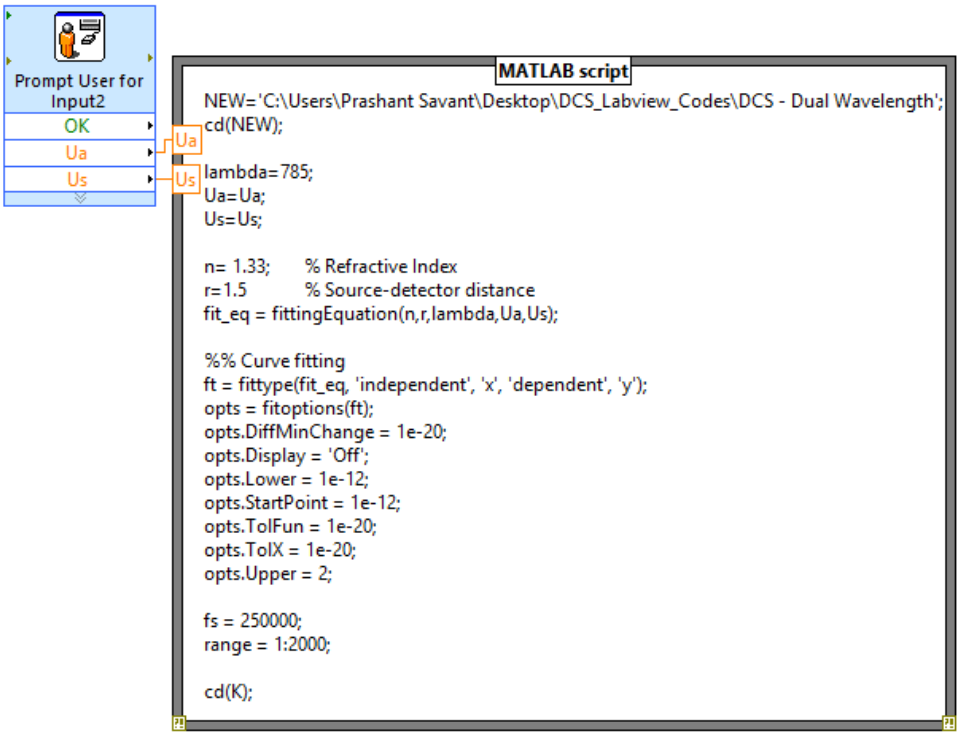

Figure 9(b): screen shot of LABVIEW block diagram window to program a user option to input the μ_a and μ_s values

Figure 9(b) gives us the idea about how the prompt is designed in LABVIEW using a prompt option for the for a user to input the μ_a and μ_s values of that particular subject and also use MATLAB script for generating a model once which will be used again and again over the course of the experiment to fit for the data .

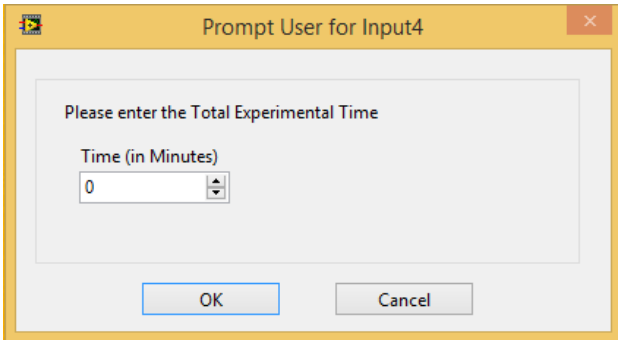

Figure 10(a): Screenshot of the prompt for user option to input the experimental time.

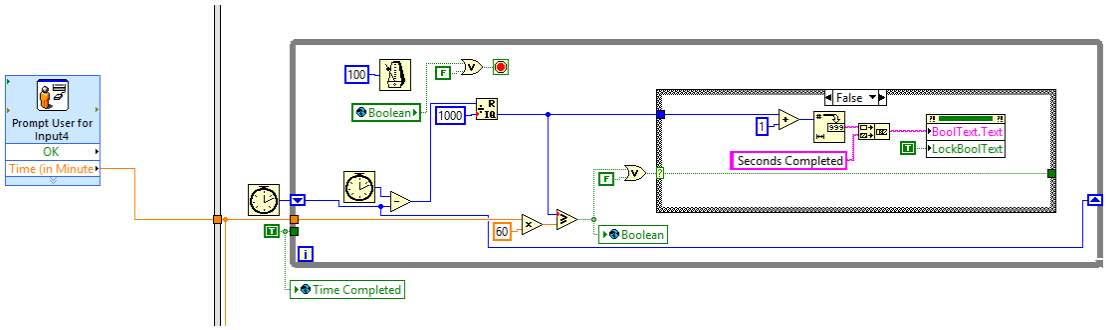

Figure 10(b): screenshot of LABVIEW block diagram window to program a user option to input the experimental time.

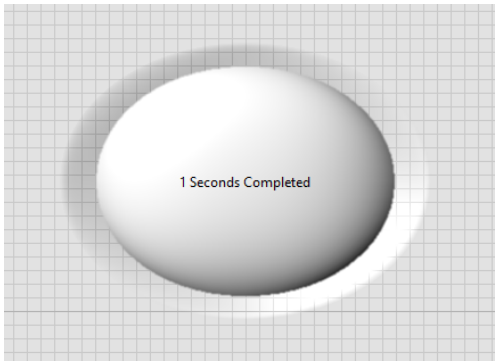

Figure 10(c): LABVIEW front panel window that shows experimental clock.

Figure 10(a), (b) and (c) are related to the experimental time that a user can input. The system will function only for this particular length of time without affecting the data acquisition or algorithm flow after which it will stop automatically.

2.2 Design of data acquisition module

A virtual instrument (VI) was designed for a real-time single wavelength DCS system in LabVIEW. This VI generated a gate signal to drive the APD and at the same time was responsible for data acquisition and recording. The APD's output is a TTL signal which was counted over the sampling time τ. The maximum frequency of the DAQ card i.e.., PCI-6602 is 80MHz which means that the fastest counting between 2 consecutive pulses would be (1/8MHz) 12.5ns [3]. Also, because the DAQ card i.e.., PCI-6602 is a 32-bit counter it can count up to 4,294,967,295 ($2^{32} - 1$) after which it moves over. For any time resolution, less than 2μs the buffer size would be limited and would overflow in less than 1 second [3]. The maximum sampling rate that the system can have is ~400kHz which intern enables a lag time of minimum ~2.5 μs. This lag time is very much shorter than the decay constant in DCS applications [36].

2.2.1 Principle of Data Acquisition

A Gate signal was utilized to drive the APD and to count the TTL output pulses from the APD. The gate signal has a time resolution of 2 seconds with 99.9% duty cycle. For counting these photon pulses a technique called buffer period measurement was used [36]. In this technique, the source edges account for an increment while the gate edges will buffer the immediate count and furthermore reset the count register back to 0 for the following interval. Along these lines, for our application each APD pulse would increment the internal count register and each active gate edge would store the immediate next count value in the buffer task and will reset the count register to 0. The total number of pulses that occur per interval will characterize the period of the gate signal and hence we use an implicit timing when we generate the gate signal [36]. This implies that the period measure of a signal would set the timing of

sampling which stands on when its' edges arrive [34] (refer Figure 11). Subsequently the net impact is to perform "binning" measurement where the "periods" are used and read to discover the number of APD pulses recorded inside each interim of the gate signal. When we use such a technique, the initially acquired points would represent awful information in period measurements and subsequently were overlooked. The initial data point is the measured interval between the point when the counter is started and the initial edge transition which actually takes place on the counter gate [35]. Since there is no particular method or any technique to indicate as to when the counter is really armed, the initial value might be mistaken and any acquired data point after this will not have such a problem. Therefore, the first reading is neglected [35].

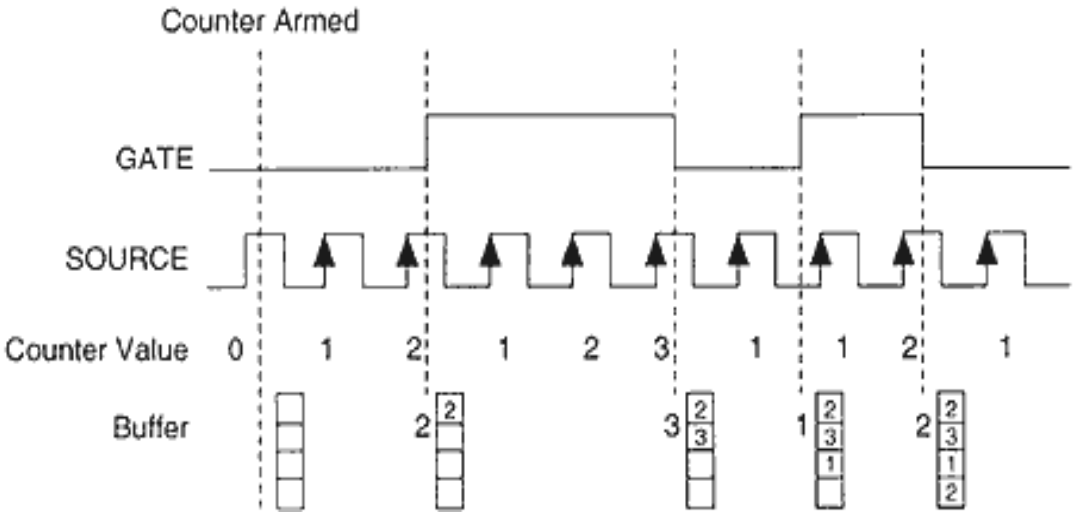

Figure 11: Buffered Period Measurement [20]

2.2.2 Re-designed GATE Signal VI

The Gate signal we utilized to drive the APD and to count the TTL output pulses from the APD has a time resolution of 2 seconds or frequency of 0.5 with 99.9% duty cycle.

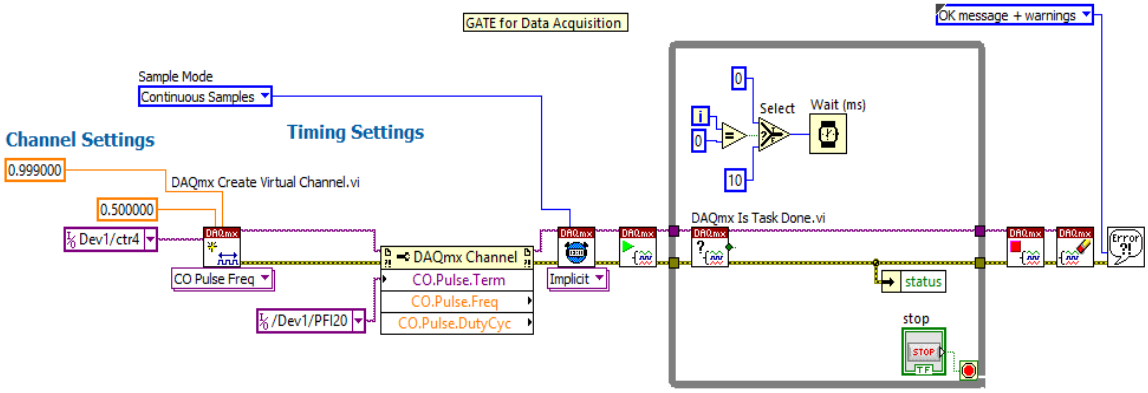

Figure 12(a): screenshot of LABVIEW block diagram for the generation of a gate signal.

Figure 12(a) represents the programming technique used in LABVIEW to generate a gate signal with a time resolution of 2 seconds or frequency of 0.5 with 99.9% duty cycle to drive the APD. It also means that the APD will acquire data only for the 2 seconds resolution time after which it will stop or a delay of desired time is given even before the data gate drives the APD to acquire data again.

2.2.3 Re-designed Photon counting VI

For counting the photon pulses, we used a technique called buffer period measurement in which the source edges account for an increment while the gate edges will buffer the immediate count and furthermore reset the count register back to 0 for the following interval. The total number of pulses that occur per interval will characterize the period of the gate

signal and hence we use an implicit timing when we generate the gate signal [36]. This implies that the period measure of a signal would set the timing of sampling which stands on when its' edges arrive [34]. Subsequently the net impact is to perform "binning" measurement where the "periods" are used and read to discover the number of APD pulses recorded inside each interval of the gate signal. When we use such a technique, the initially acquired points would represent awful information in period measurements and subsequently were overlooked.

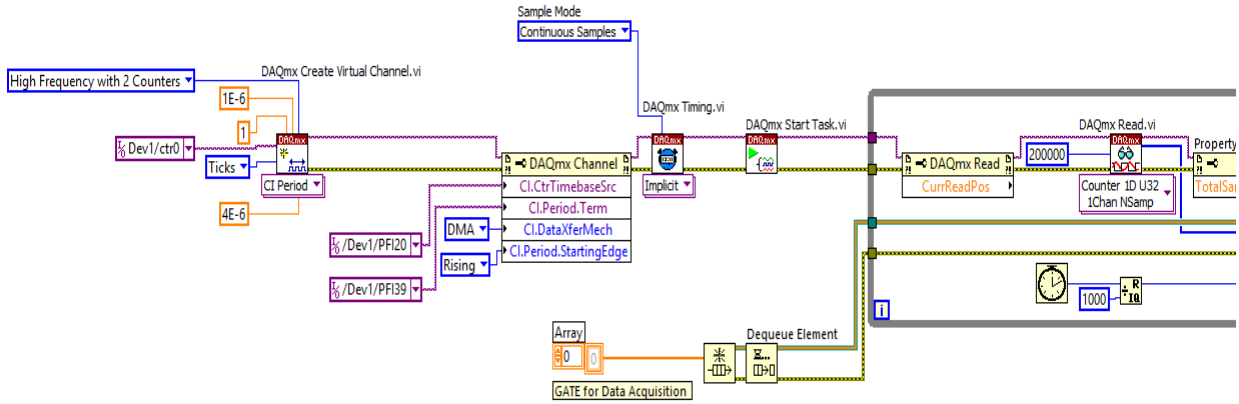

Figure 12(b): screenshot of first half of the LABVIEW block diagram for the data acquisition

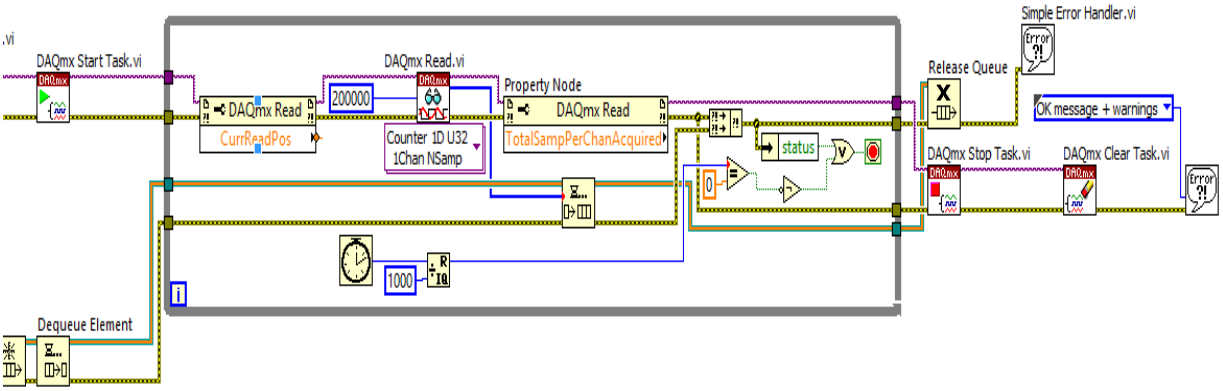

Figure 12(c): screenshot of second half of the LABVIEW block diagram for the data acquisition.

Figure 12(b) and Figure 12(c) represents the programming technique used in LABVIEW block diagram to program for data acquisition using the APD. The APD was instructed to count a photon for every 4μs which would give 500k photon counts in 2 seconds. Also, the data acquisition was designed in such a way that the data acquisition would happen only if the gate drove the APD and when the gate was open.

2.2.4 Advances from the previous VI

Drawbacks of the previous system.

- The previous system had a gate frequency of 250k which implies that the time period of the gate was 4μs with 80% duty cycle meaning that the gate would be on for a time period of 3.2μs (80% of 4μs) and off for 0.8μs (20% of 4μs).
- Also, from the data acquisition VI it was found that the time interval for counting between 2 consecutive counts was 3.4μs.
- The actual meaning of using a gate signal is, when the gate is high or open data is acquired and when the gate is closed or low data is not acquired. From the previous design, it was understood that, though the resolution time of the gate was 4μs it would be on only for 3.2μs and at the same time the data acquisition system was instructed to acquire data or count photons for every 3.4μs.
- In which case, we lose out on a lot of data even before acquisition because the gate would close 0.2μs earlier than the next count and also a lot of data overlapping.

- From the data acquisition VI it was found that the system is being instructed to acquire not more than or not less than 250k photons in one second.
- If we acquired data for every 3.4µs we will not be able to acquire 250k photons.
- Instead, we will be acquiring more than 250k photons in one second because 3.4µs x 250k will not give us back 1 sec and 3.4µs windows for 1 second > 250k.
- Moreover, in a 1 second window the gate would not only be on only for 0.8 seconds but will also miss out on recording data for 50ms (0.2µs x 250k).
- At the same time the system would record wrong data for the same 50ms.
- During the gate OFF time of 0.8 µs the photons that would be detected during that particular count will not be acquired.
- Furthermore, the preceding detected photons from the next count would be considered as those which went missing due to the OFF time of the gate.

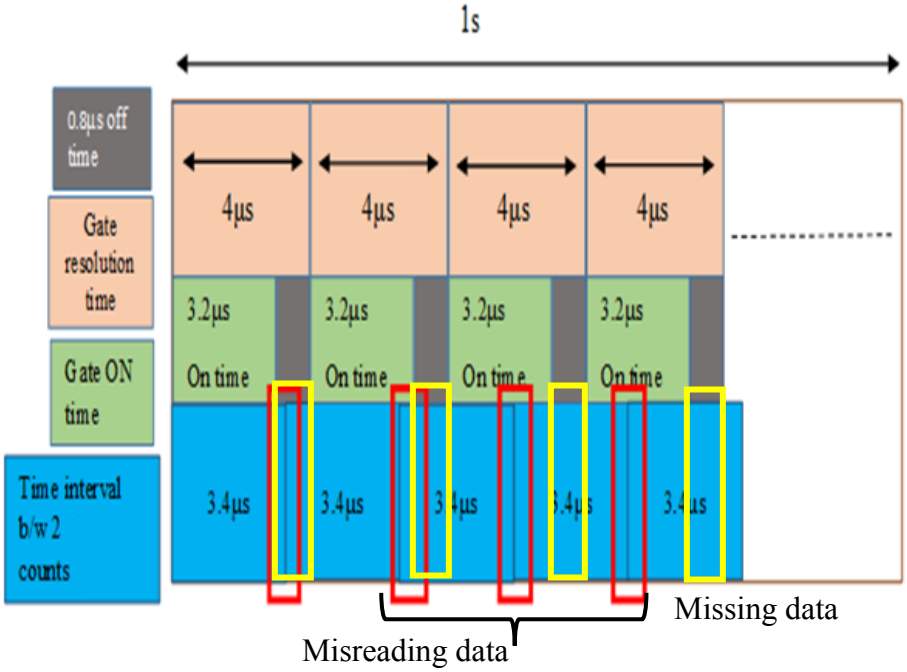

Figure 13(a): Drawbacks of the previous system.

- The data missing and the data overlapping was at random parts of the data acquisition and hence no signal processing techniques could be used to process the data.
- This 50ms is not towards any corner of the window instead is at random positions because the photons counted would be 250k+ per second and hence no data processing could be done to remove them.

Figure 13(a) represents one of the major drawbacks from the previous system in which it clearly depicts as to how the data was overlapping or had a left shift during acquisition and the missing data while the system was functioning during the experimental course of time.

This version of the system has two separate VIs

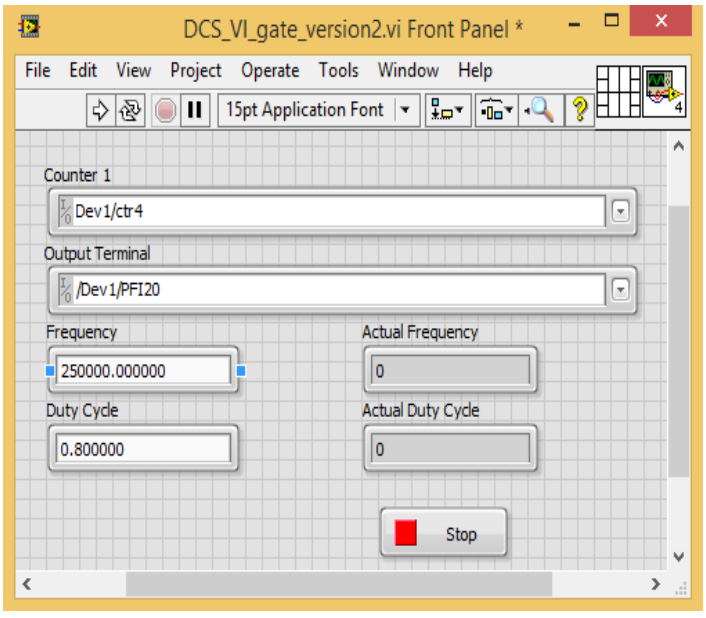

Figure 13(b): Front panel to control GATE Signal

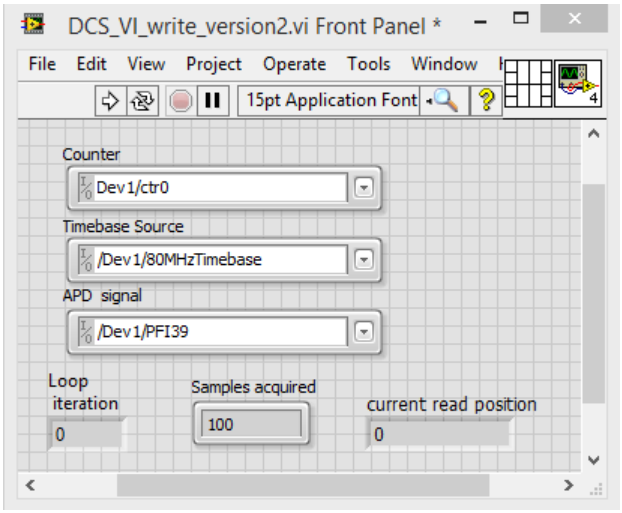

Figure: 13(c): Front panel to for data acquisition

Figure 13(b) and Figure 13(c) represents the front panel of 2 separate VIs used in the previous system. One for generating the gate signal and the other was for data acquisition respectively.

Advances in the new system

- The new system has a gate frequency of 0.5 which implies that the time period of the gate is 2 seconds with 99.9% duty cycle meaning that the gate would be on for a time period of 1.998 seconds and off for 0.002 seconds.
- Also, in the data acquisition VI the time interval for 2 consecutive counts is given as 4µs.
- The actual meaning of using a gate signal is, when the gate is high or open data is acquired and when the gate is closed or low data is not acquired. From the new design, it is clear that, the resolution time of the gate is 2 seconds in which it would be on for 1.998 seconds and at the same time the data acquisition system was instructed to acquire data for every 4µs.

- In this case, there will not be any over lapping of the data or any missing data because the gate is on for the entire ~2 seconds during which photons are counted for every 4µs.
- In the new data acquisition VI the system is instructed to count not more than or not less than 250k photons in one second.
- On cross calculation, we find that if we acquire a photon for every 4µs then we get 250k points or photons in one second.
- Also, a few of the unwanted loops and parts in the VI were removed for better functioning of the system.

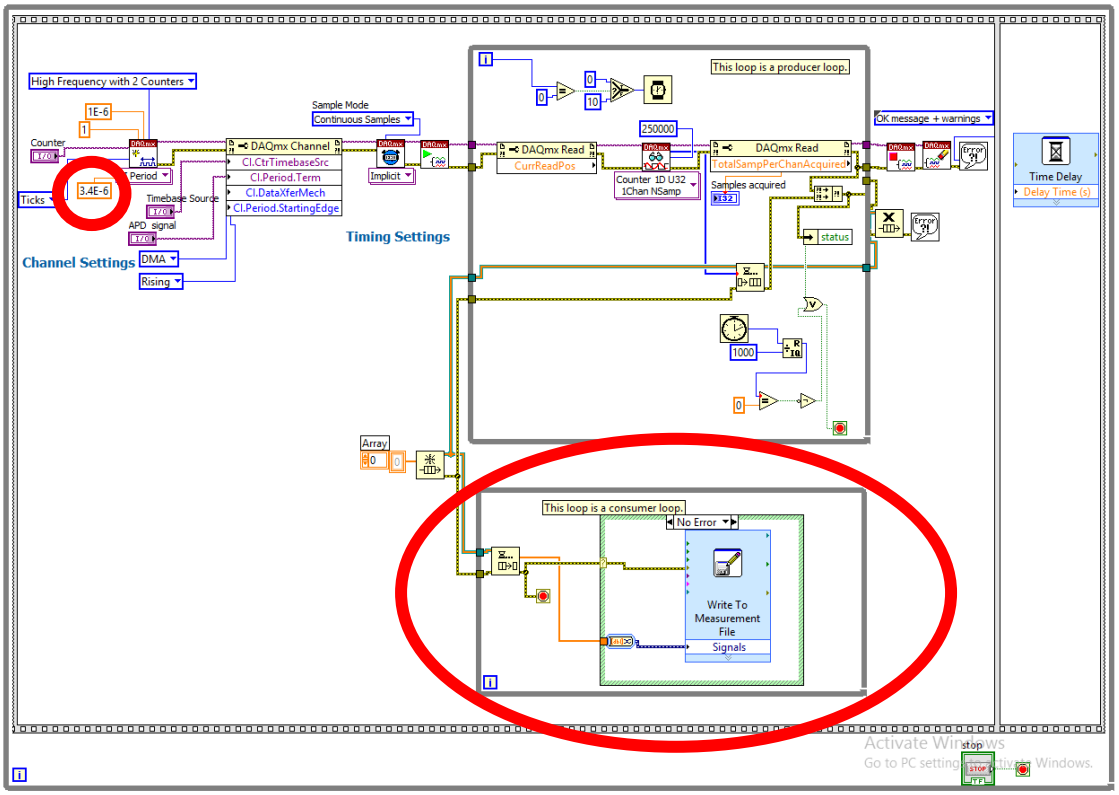

Figure 14(a): Block diagram of previous version with errors encircled with **red**

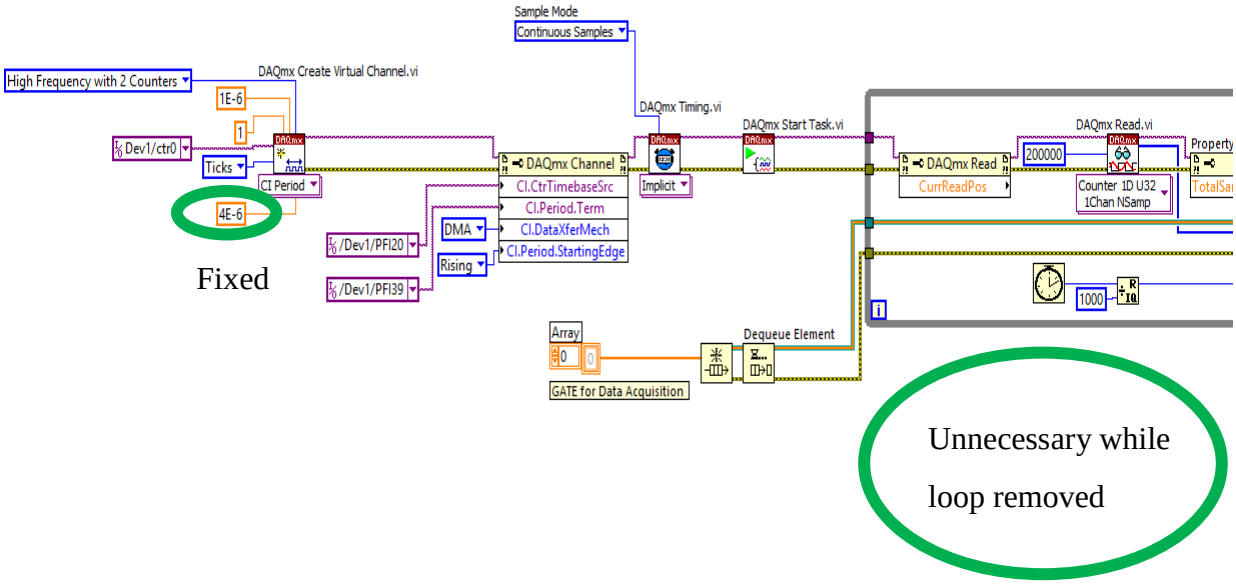

Figure 14(b): Block diagram of new version with fixed errors encircled with **green**

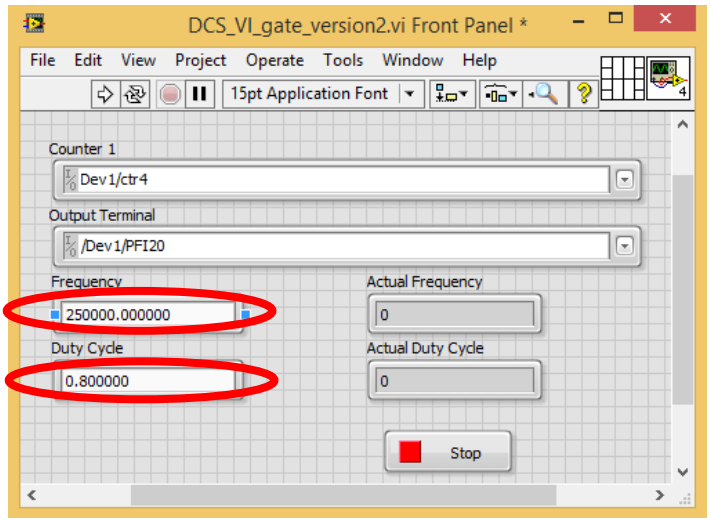

Figure 14(c): Front panel of previous version for gate generation with errors encircled in **red**

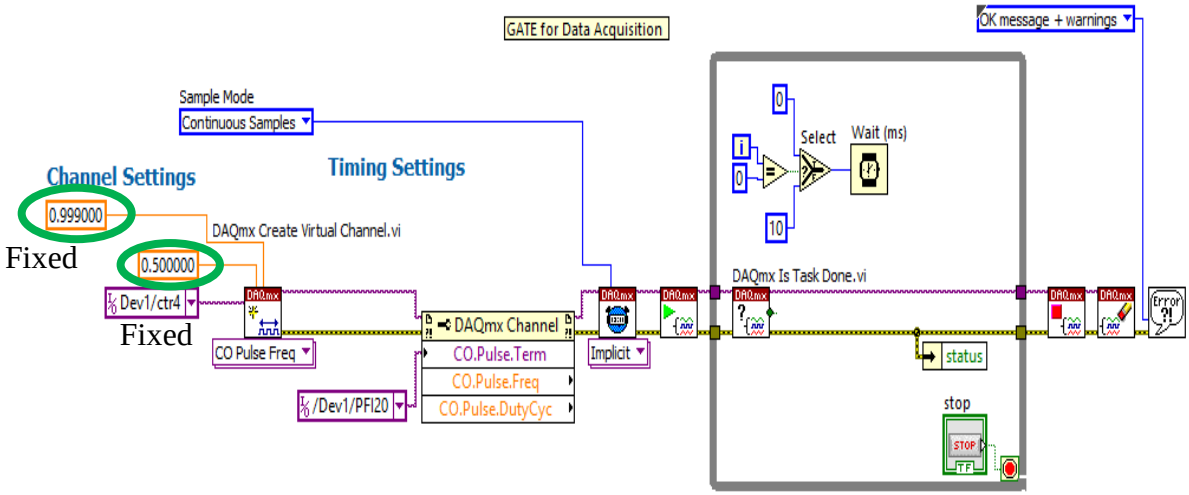

Figure 14(d): Block diagram of new version for gate generation with fixed errors encircled in **green**

Figure 14(a) and Figure 14 (c) represent the data acquisition VI and gate generation VI respectively from the previous versions with the drawbacks encircled in red. Figure 14(b) and Figure 14(d) represent the data acquisition VI and gate generation VI respectively with all the errors fixed encircled in green, where frequency was changed from 250000k to 0.5 and duty cycle from 80% (0.80) to 99.9%(0.999).

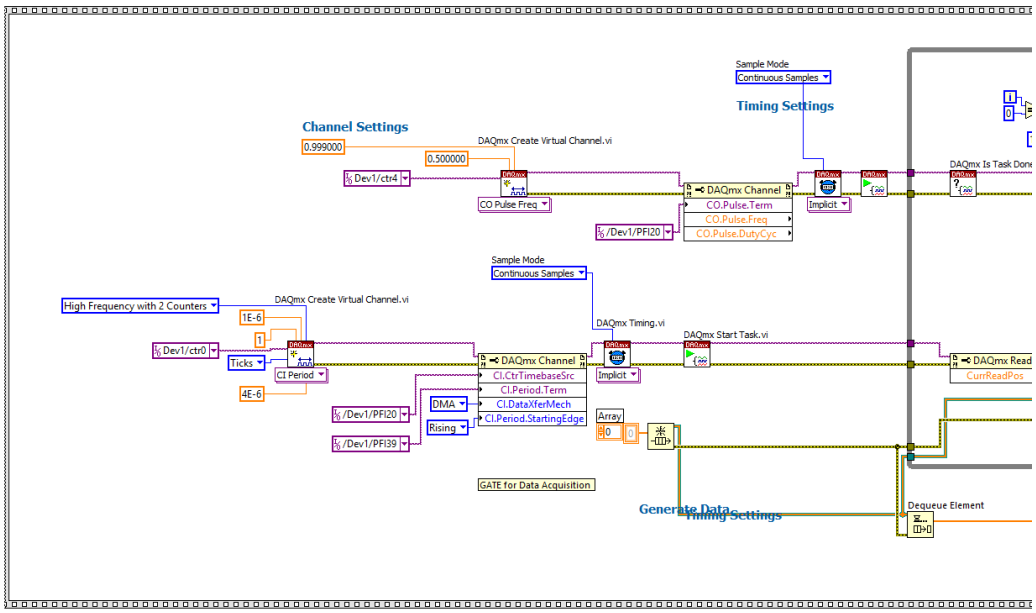

Figure 15(a): Block diagram of part 1 new version for putting everything into one program

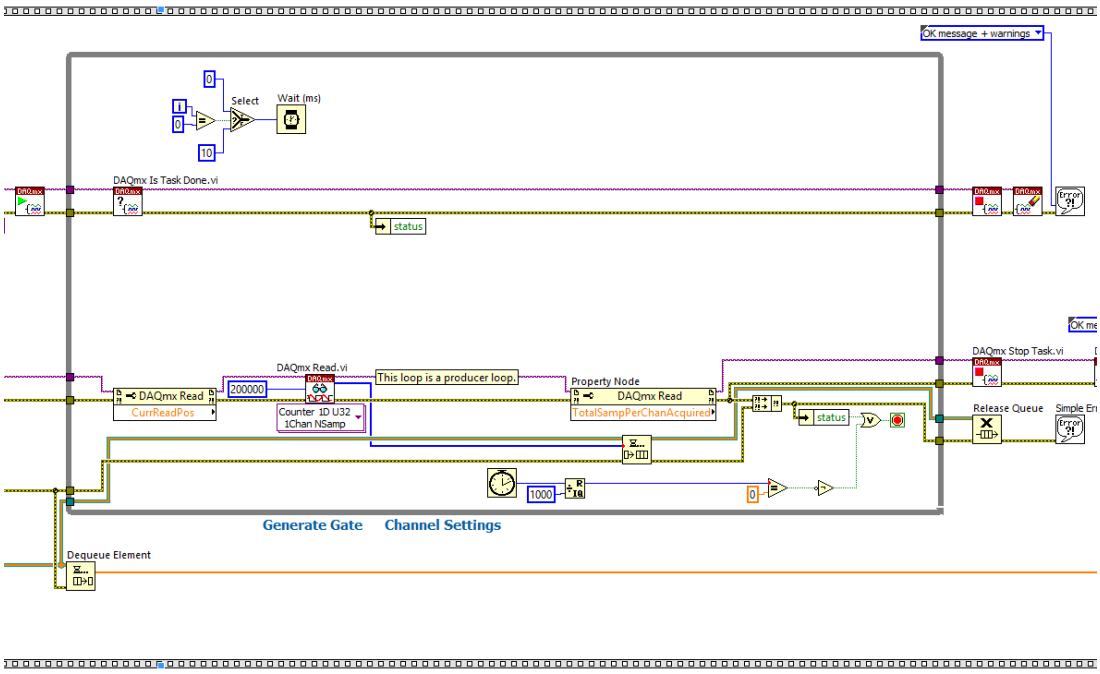

Figure 15(b): Block diagram of new version part 2 for putting everything into one program

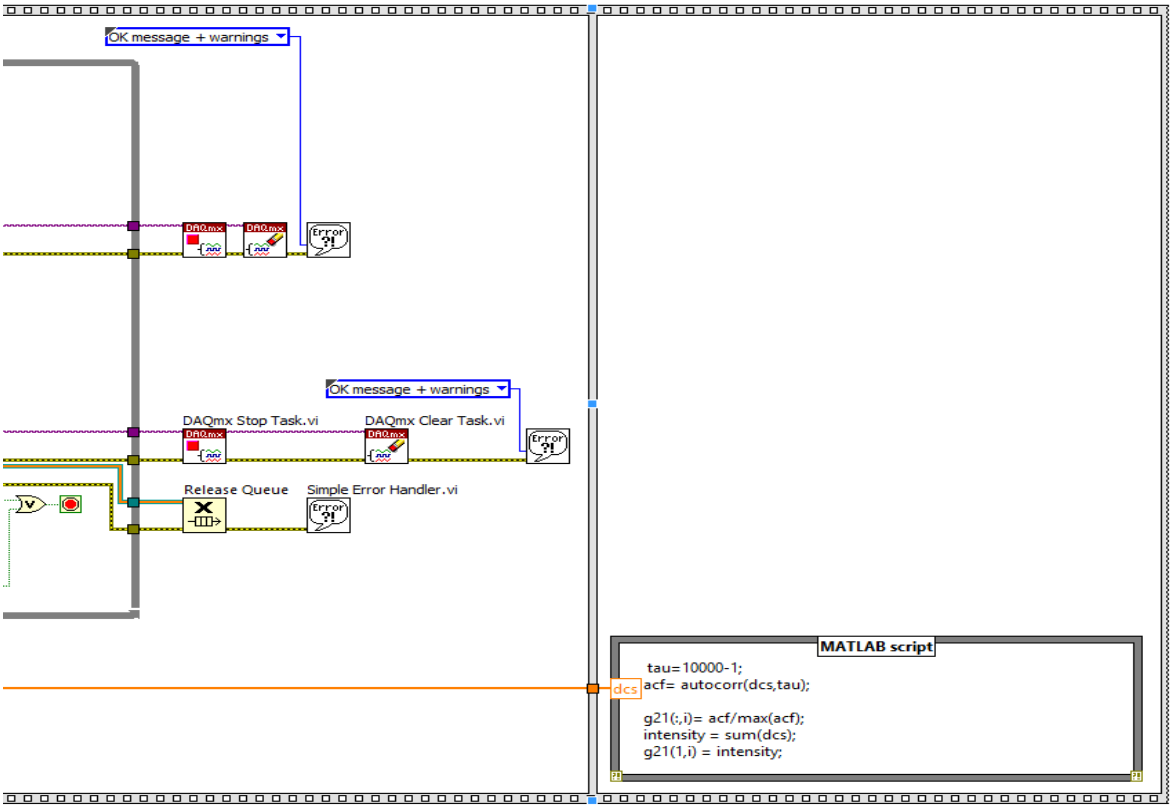

Figure 15(c): Block diagram of new version part 3 for putting everything into one program

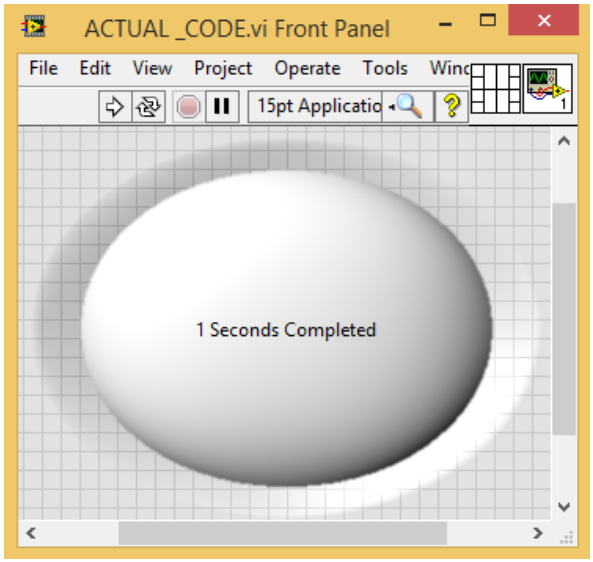

Figure 15(d): Final front panel of new version for putting everything into one program

Figure 15(a), (b) and (c) represent the technique used in LABVIEW block diagram to design and put both VIs of gate generation and data acquisition in one VI so that both the gate generation which will drive the APD for data acquisition and the actual data acquisition will start together which intern will assure that there will not be any data loss during the course of the experiment. Also, from Figure 15(c) we can see the use of MATLAB script inside LABVIEW in the first step of data processing which in the later steps will yield a real-time output display by using the processed data. Figure 15(d) represents the front panel of the entire LABVIEW VI used for single wavelength DCS system. This has only a clock display which will show us the elapsed time of the experiment. When we compare Figure 15(d) to Figure 13(b) and Figure 13(c), all the unwanted displays were removed to have the front panel look as simple as possible.

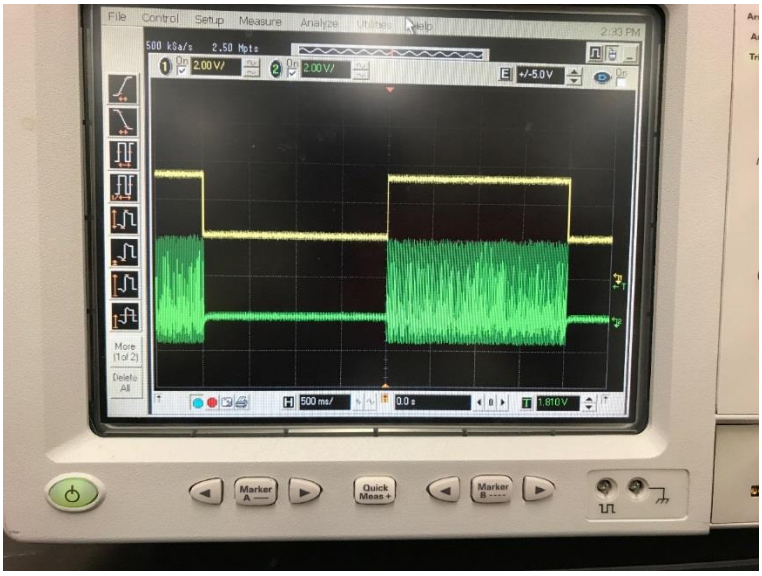

Figure 15(e): Screenshot of CRO representing the data acquisition when GATE is on for 2 seconds with 99.9% Duty cycle

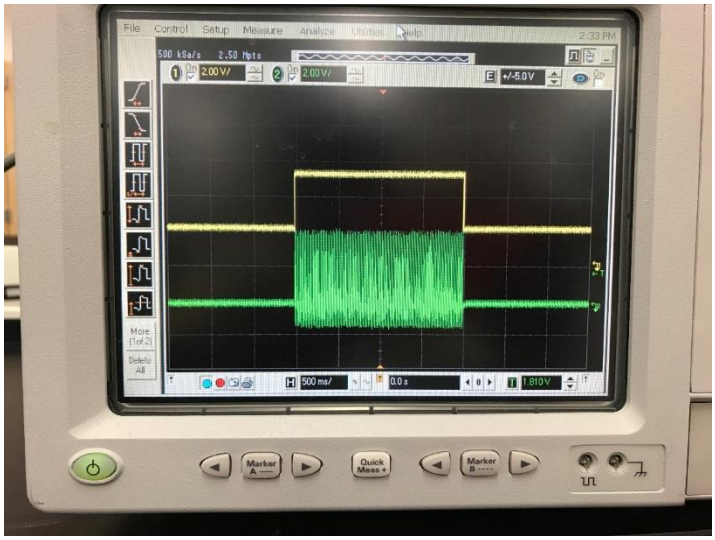

Figure 15(f): Screenshot of CRO representing the data acquisition when GATE is on for 2 seconds with 99.9% Duty cycle

Figure 15(e) and Figure 15(f) is a screenshot of the CRO representing the data acquisition when the GATE is on for the entire 2 seconds with 99.9% duty cycle. This was one of the main advancements from the previous system with which we stopped the opening and closing of the GATE for every 4μs.

2.2.5 Real time data display

One of the main goals of the re-design was to make this system a real-time bedside patient monitoring system. This would :

- Reduce time and man power for data processing post data acquisition.
- Cut off the use of MATLAB separately for data processing.
- Help in real time output data display.
- To have a real-time output data display which will help the physician/clinician and the engineer monitor the output directly.

- To have a user-friendly interface which had the capability to control the algorithm based on the experimental time without disturbing the data acquisition/recording and functioning of the algorithm at the same time giving a real-time output.

The real-time plot was achieved using the MATLAB script inside of LABVIEW. The MATLAB script inside of LABVIEW would call the MATLAB software and required functions that would perform the desired task even without opening MATLAB software separately.

The real-time plot had 4 graphs in one window.

  - Auto correlation curve.
  - Intensity of the detected light.
  - Delta OD (Optical Density) (dOD).
  - Relative Blood Flow Index (rBFI).

- Auto correlation curve is the curve of correlation between the elements of the array of the detected photons and other detected photons from the same series separated from them by some interval.
- Intensity of the detected light is the sum of all the photons detected in the given interval of time. (ex. 1 second)
- Delta OD (Optical Density) (dOD) is the measure of optical density given by the formula

  $dOD = \log(I_1) / \log(I_i)$ $i = 1,2,3,4,5\ldots\ldots\ldots n$

  I_1 is the initial total intensity of the detected photons and I_i will be the total intensity at i^{th} interval.
- Relative Blood Flow Index (rBFI) is a relative measure of the blood flow. This is calculated from αDb as $rBFI = (Db(i)./Db(1))*100$ $i = 1,2,3,4,5\ldots\ldots\ldots n$

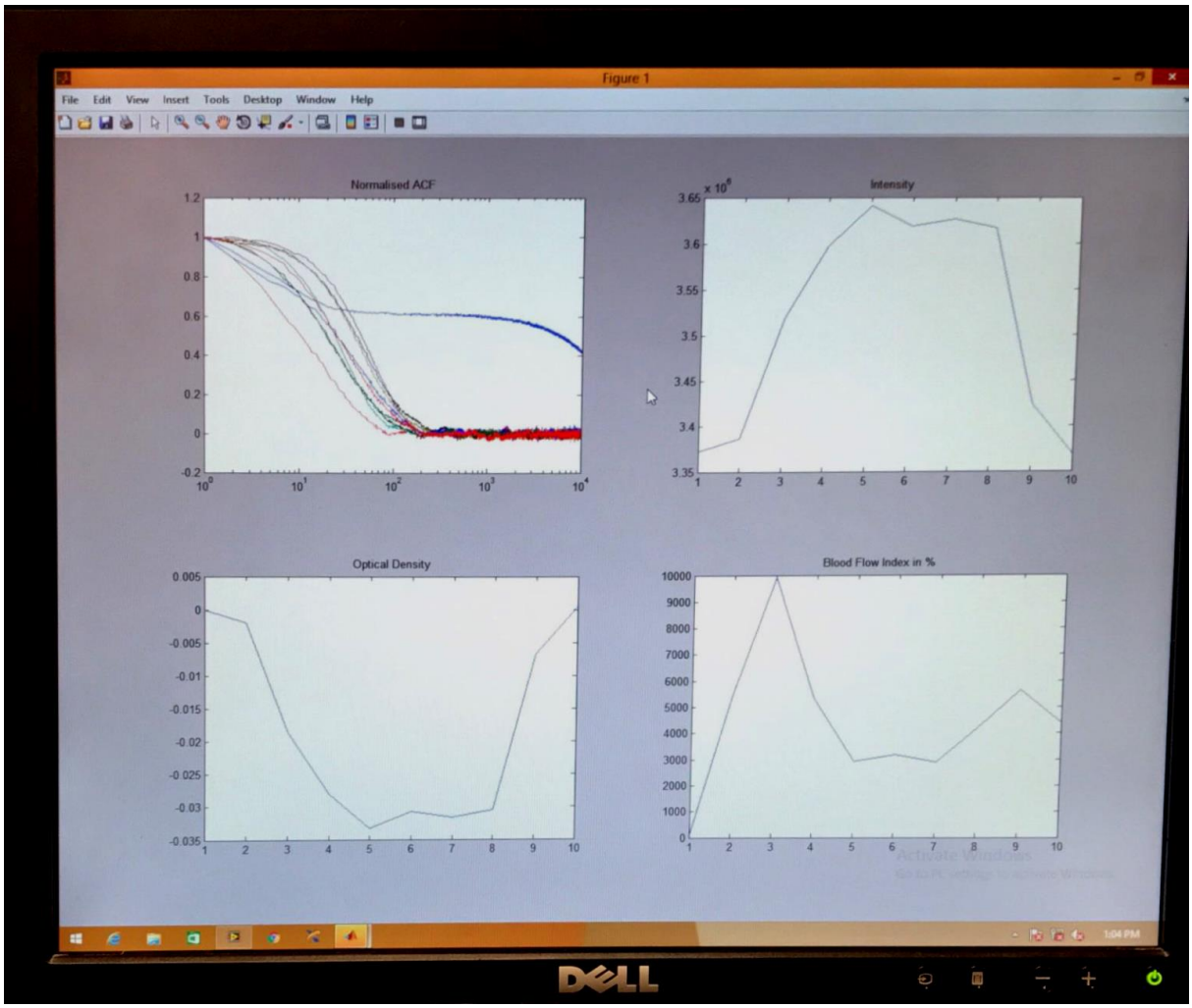

Figure 16: a screen shot of the real-time data display

Figure 16 represents a screenshot of the real-time data display during the course of the experiment. The entire plot is split into 4 subplots to show all the desired output parameters in real-time. The top left curve represents the auto correlation functions of the recorded data, while the top right curve represents the total intensity of the detected photons and the bottom left one is the curve for dOD which is calculated using the formula as discussed earlier and would follow an inverse trend of the intensity plot, while the bottom right curve is the one that represents the Relative Blood Flow Index (rBFI) which is relative measure giving information about the change in blood perfusion.

Chapter 3

System validation and Experiment on real-time, Single-Wavelength DCS System

Direct continuous noninvasive measurement of local muscle blood flow in humans remains limited. Conventional measurements of limb blood flow, such as Doppler ultrasound or venous occlusion plethysmography, do not provide regional information instead measure changes in bulk conduit flow. Near-infrared diffuse correlation spectroscopy (DCS) is an emerging technique for non-invasive measurement of blood perfusion at the microvascular level. To better comprehend the strengths and limitations of this real-time single wavelength DCS system, we performed a validation study by comparing blood perfusion (Relative Blood Flow Index) measured by DCS and brachial artery flow measured using Doppler ultrasound during a small exercise.

3.1 Basic science study on hand Grip exercise

"Mild to moderate hand grip exercise will invariably increase skeletal muscle oxygen demand. Consequently, in thermoneutral conditions, exercise-induced increases in blood flow must be directed to the muscle. Thus, we can conclude with certainty that any changes in brachial artery blood flow are due to the increase in exercise activity, and will be directed to the working muscle to accommodate the increased muscle tissue oxygen demand."

Finally, we utilized Doppler ultrasound because it a well-established, broadly used method for non-invasive measurement of brachial artery blood flow. It has been used in countless studies and is an industry standard method for measuring blood flow and imaging the artery.

3.1.1 Ethical approval and subjects

Healthy youthful people of either sex, of age ranging from 23-30 years from any ethnic foundation for around 14 subjects were considered. Volunteered participants were booked promptly for the analysis. Upon the arrival of each volunteer for the test, they were given an oral clarification and after that the volunteer was given a chance to make inquiries. Each and every volunteer had to sign a consent form and after their endorsement to begin the analysis the members' sex and age was recorded and the test was completed. The members were made a request to keep the body relaxed as the development could deliver motion artifacts. The member was given the decision to stop the investigation on the off chance that he/she felt uncomfortable.

3.1.2 Experimental Protocol & Instrumentation

Even before the start of the experiment, the μ_a and μ_s values for each subject on the belly of the flexor digitorum profundus were recorded using the ISS machine. In each experiment, the subject was made to take a supine position with the DCS Probe affixed over the belly of the flexor digitorum profundus and the Doppler ultrasound probe imaging the brachial artery and obtaining the brachial artery flow. The DCS probe consisted of 2 optical fibers out of which one with a multimode acted as the fiber to deliver light i.e., the source fiber and the other fiber with few modes acted as a detector fiber with the separation distance between the source and the detector being 1.5 cms. The subjects were made a request to keep the body relaxed as the development could deliver motion artifacts. At the start of the experiment, the maximum pressure that a subject could give at that particular supine position was recorded. The experimental protocol consisted of baseline readings for first 2 mins, 2 mins of 20% of the

subject;s maximum pressure, 2 mins of 50% of the subject;s maximum pressure and 2 mins for recovery.

Data was acquired for every 4 seconds which was split into 2 seconds for gripping and 2 seconds for relaxing out of which data were recorded for the 2 mins relaxing session. An audio feedback was designed in LABVIEW which would give an audio output saying ‘grip’ and would wait for 2 seconds and then say ‘relax’. LABVIEW software was used for the design so that the there will be proper time synchronization between the subject’s relaxing time and data acquisition. Also, a visual feedback which showed the subjects as to what percentage they should reach (either 20% or 50% of their maximum pressure) or were reaching during the experimental protocol. The aim of the study was to validate the real time single wavelength system and at the same time observe changes in rBFI, brachial artery flow and dOD in sim ilar trends.

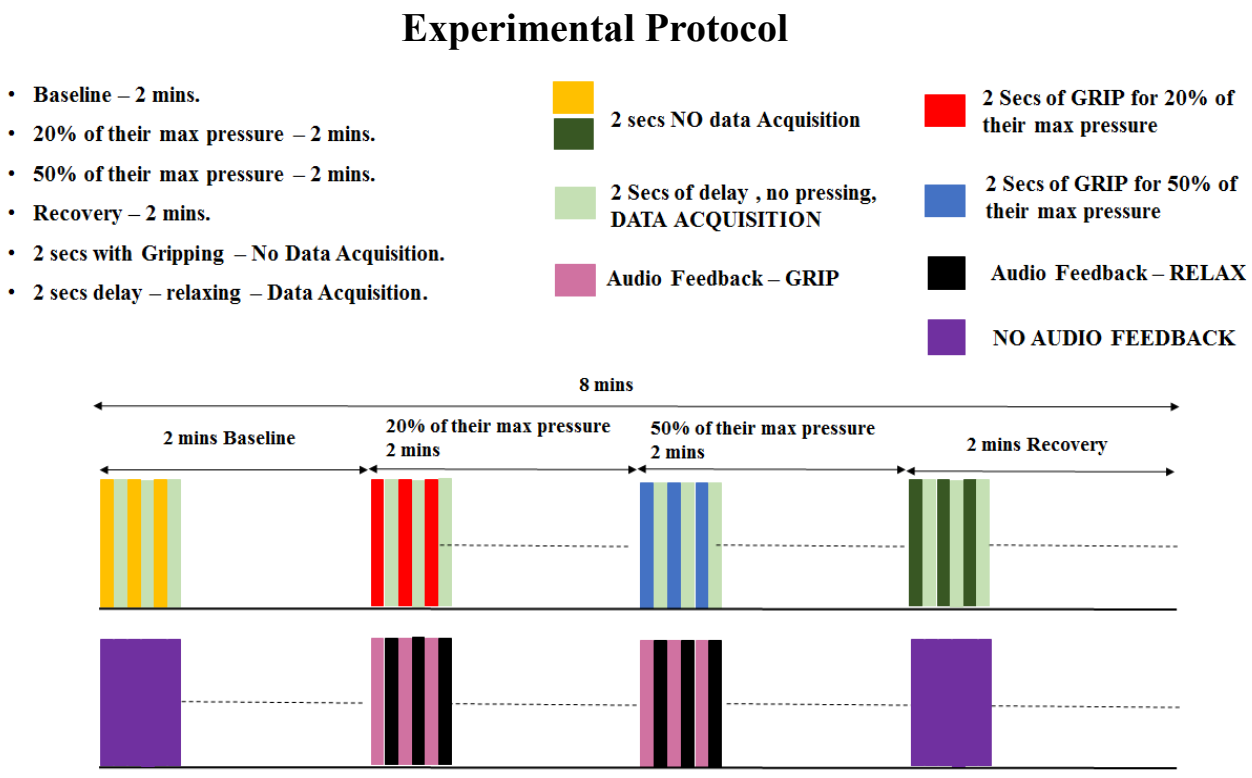

Figure 17: Diagrammatic explanation of the Experimental Protocol

The environment of the experimental room was kept as dark as possible with the DCS probe being covered with a black cloth to avoid any kind of external light detection which could affect the readings.

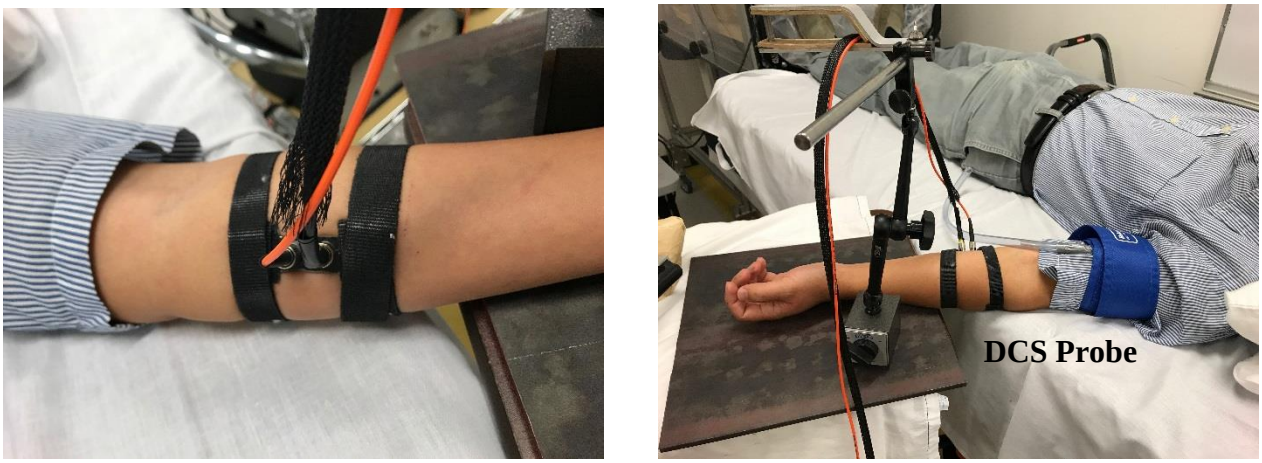

Figure 18(a): DCS Probe affixed over the belly of the flexor digitorum

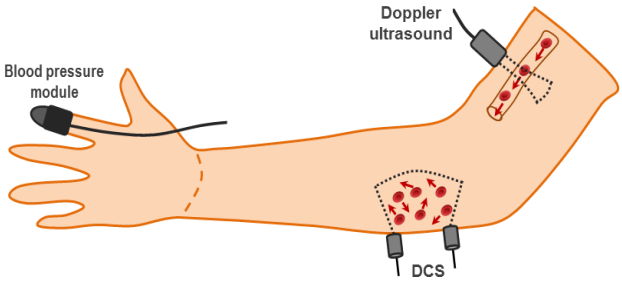

Figure 18(b): Diagramatic representation of DCS and Doppler ultrasound probe placement

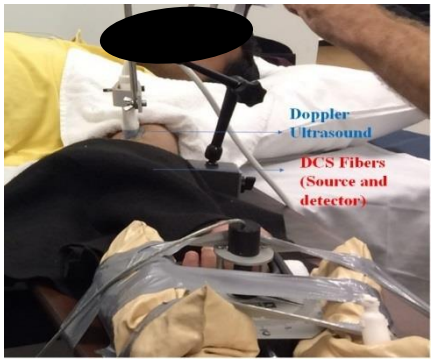

Figure 19(a): DCS Probe covered with a black cloth

and Doppler ultrasound on the brachial artery together

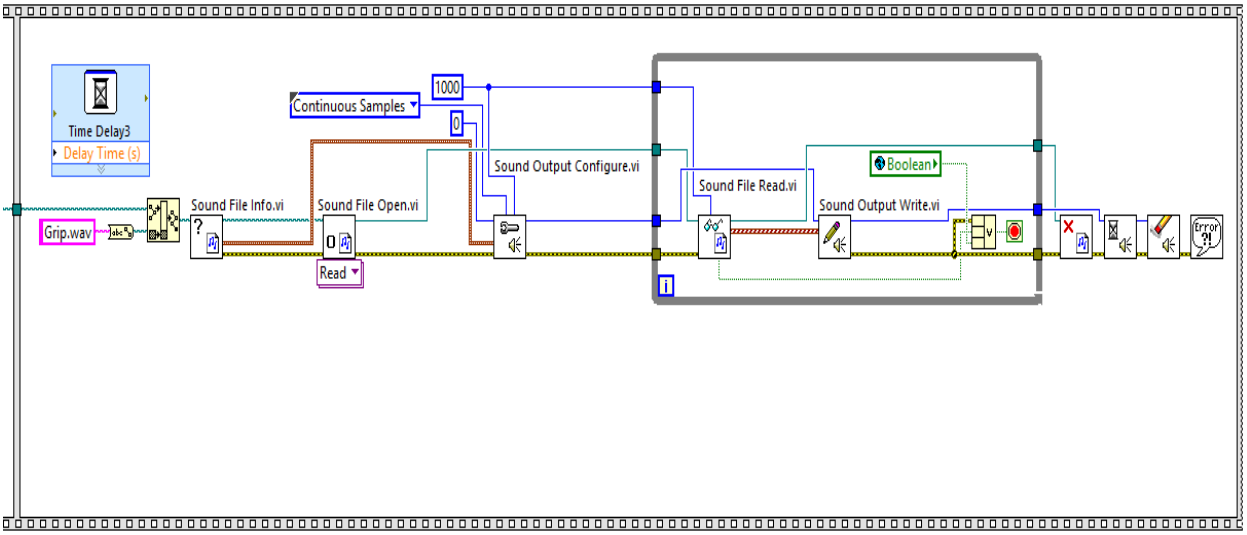

Figure 19(b): LABVIEW Block diagram to design an audio feedback "GRIP"

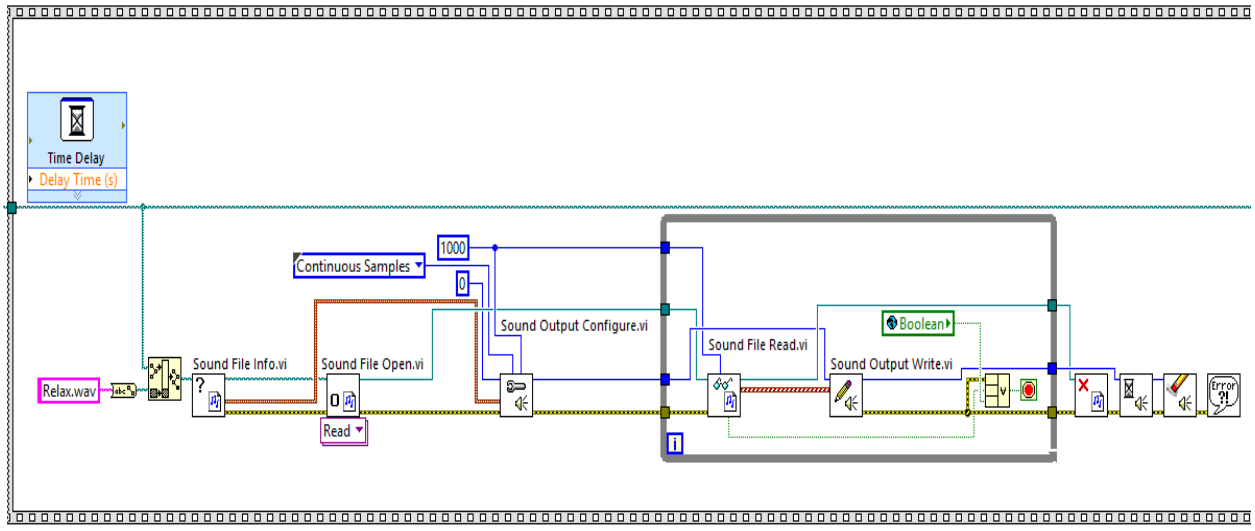

Figure 19(c): LABVIEW Block diagram to design an audio feedback "RELAX"

Figure 19(b) and Figure 19(c) represent the technique used in LABVIEW block diagram to design an audio feedback for "GRIP" and "RELAX" that was used in the experiment to alert the subject as to when he/she had to grip and relax.

3.1.3 Data processing

The data from individual subjects was acquired and no preprocessing on this data was required because the system would show a real-time output and also save all the data accordingly. To calculate the mean of all the subjects on the parameters of interest a MATLAB code was written and the data was processed. The first step was to normalize the data and an average of 14 subjects on the normalized data was performed on the interested parameters such as rBFI, brachial artery flow and dOD. Data normalization was performed for all the factors of interest to keep them on the same scale for comparison and to draw better and easy conclusions.

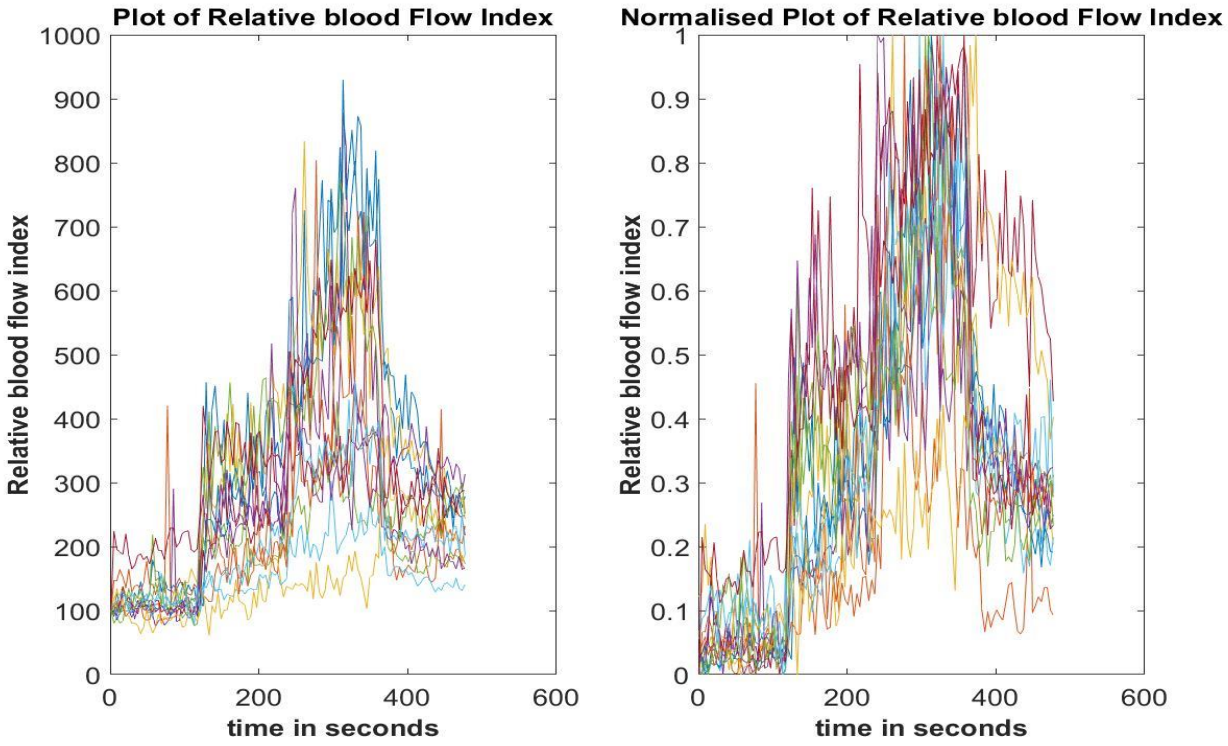

Figure 20(a): plot of rBFI of all 14 subjects before and after normalization

Figure 20(a) is the plot of rBFI over the entire course of the experiment for all the 14 subjects before and after normalization. Each curve represents the rBFI for one particular subject and both the subplots in the graph has 14 curves (14 subjects and one for each subject).

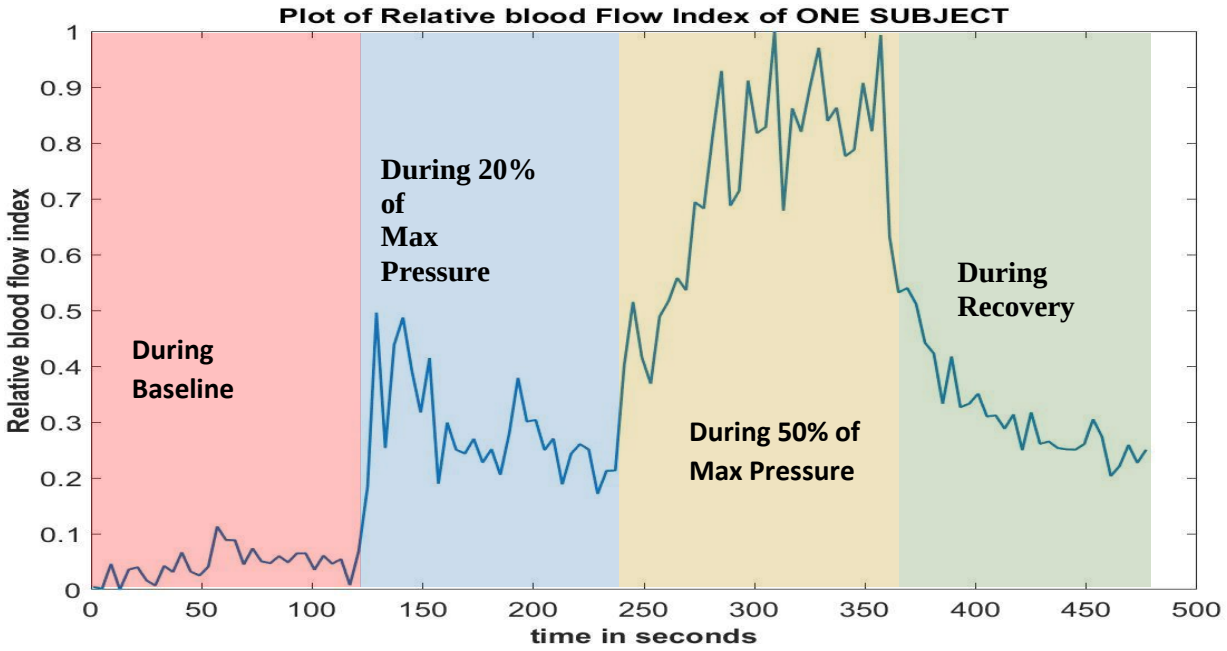

Figure 20(b): plot of rBFI of 1 subject after normalization

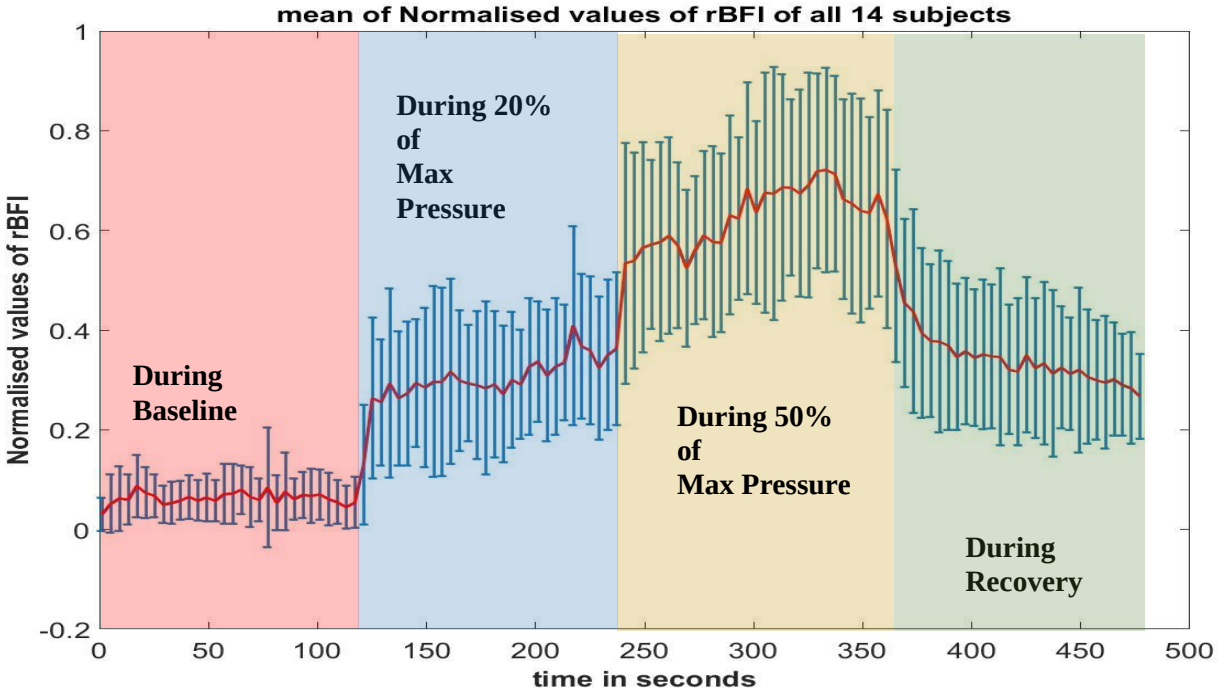

Figure 20(c): plot of mean rBFI of all subjects after normalization

Figure 20(b) represents the rBFI of one subject over the entire course of the experiment while Figure 20(c) represents the mean rBFI during the experiment of all the 14 subjects.

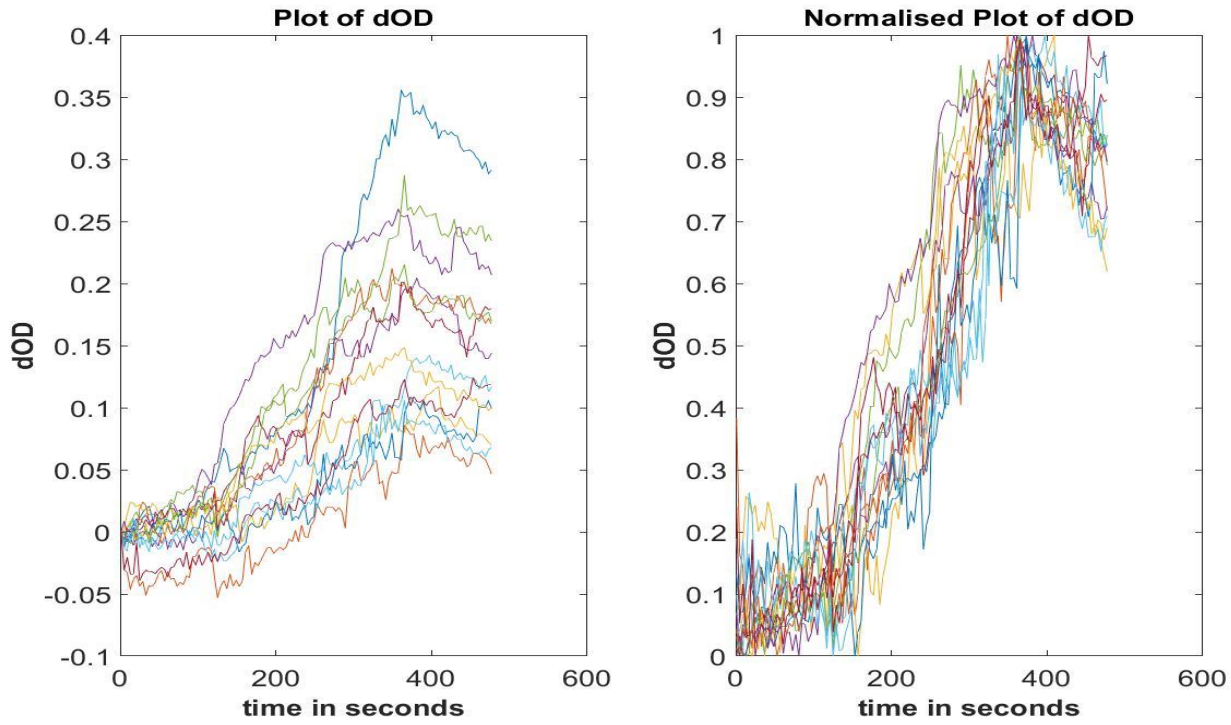

Figure 21(a): plot of mean dOD of all subjects after normalization

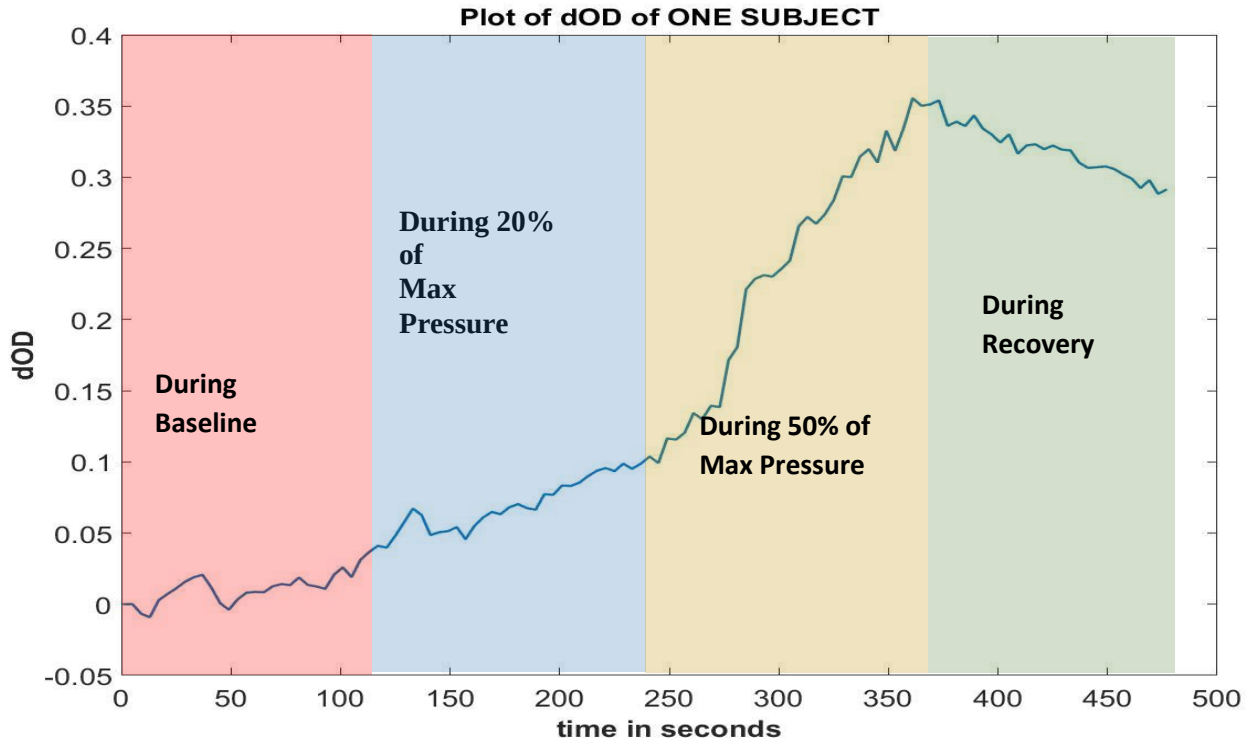

Figure 21(b): plot of dOD of 1 subject after normalization

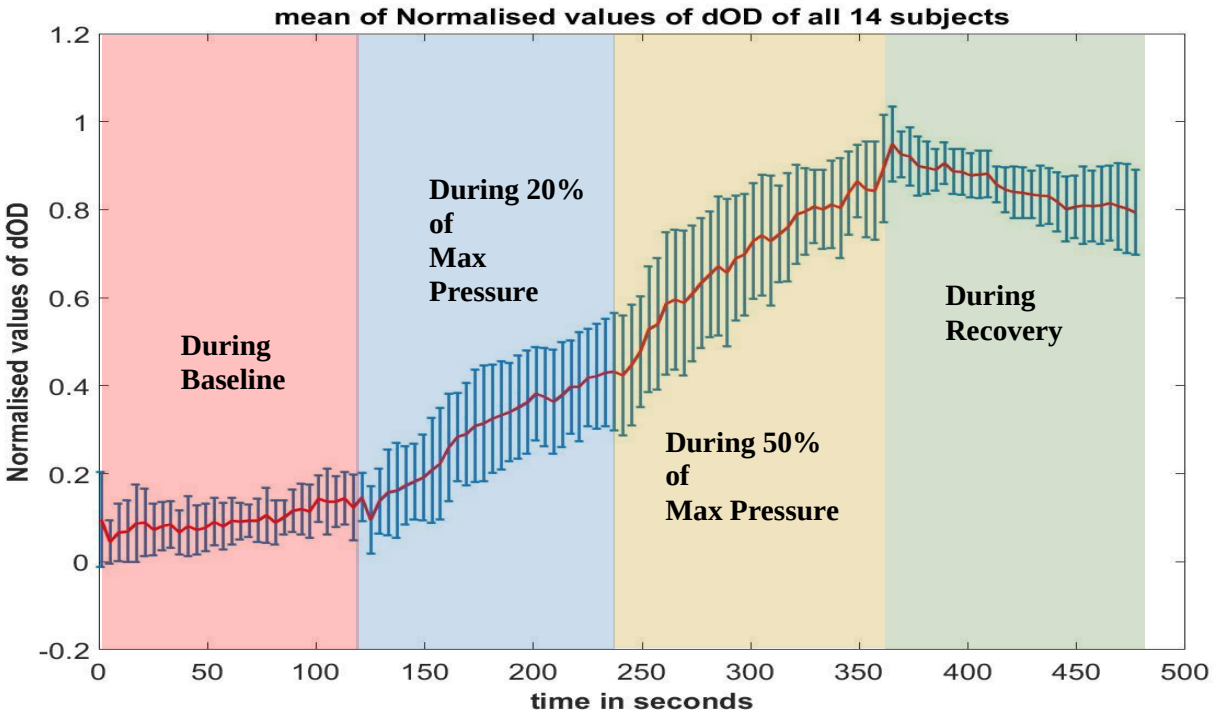

Figure 21(c): plot of dOD of all 14 subjects before and after normalization

Figure 21(a) is the plot of dOD over the entire course of the experiment for all the 14 subjects before and after normalization. Each curve represents the dOD for one particular subject and both the subplots in the graph has 14 curves (14 subjects and one for each subject).

Figure 21(b) represents the dOD of one subject over the entire course of the experiment while Figure 21(c) represents the mean dOD during the experiment of all the 14 subjects.

For a cross validation study, the brachial artery flow data that was recorded using Doppler ultrasound was also processed in the same way as rBFI and dOD.

I.e. the first step was to normalize the data and an average of 14 subjects on the normalized data was performed on the brachial artery flow data obtained from the Doppler ultrasound modality.

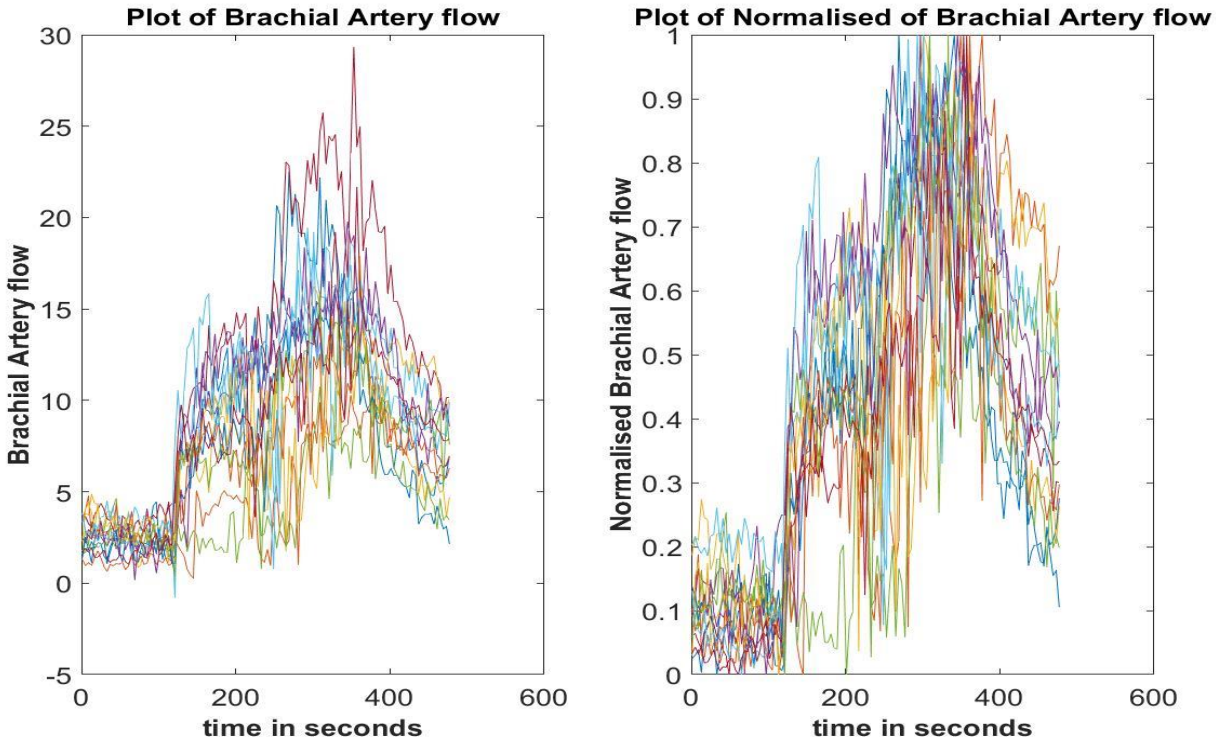

Figure 22(a): plot of Brachial Artery Flow of all 14 subjects before and after normalization

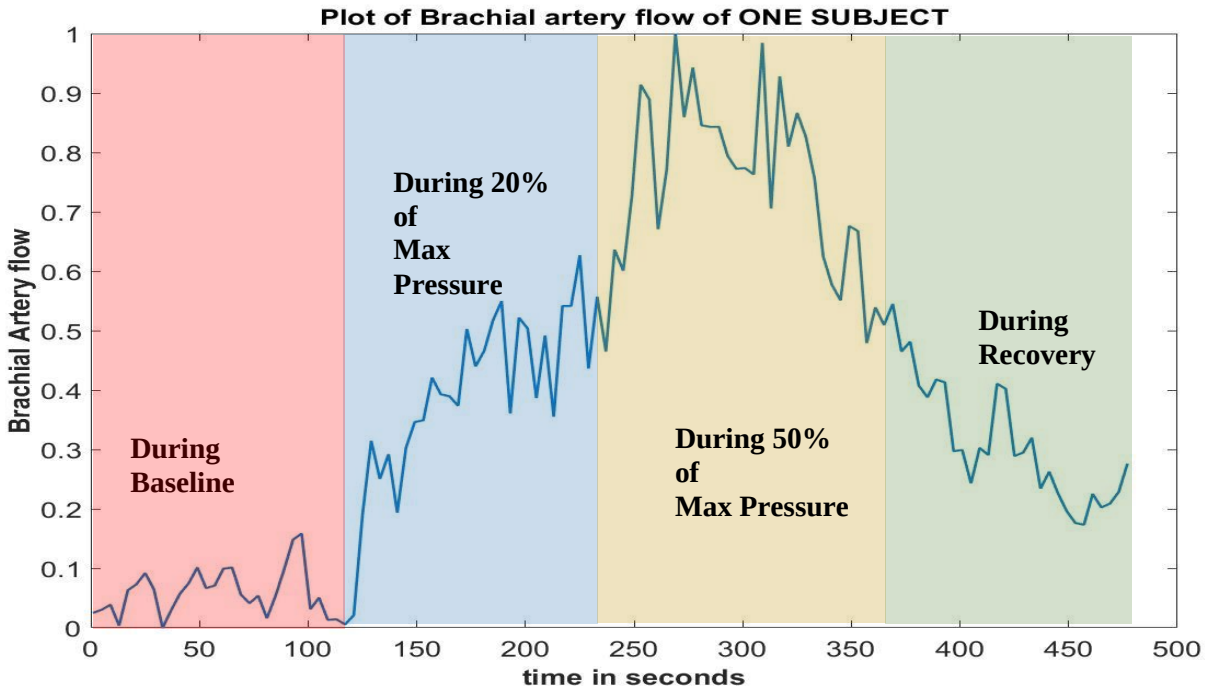

Figure 22(b): plot of Brachial Artery Flow of 1 subject after normalization

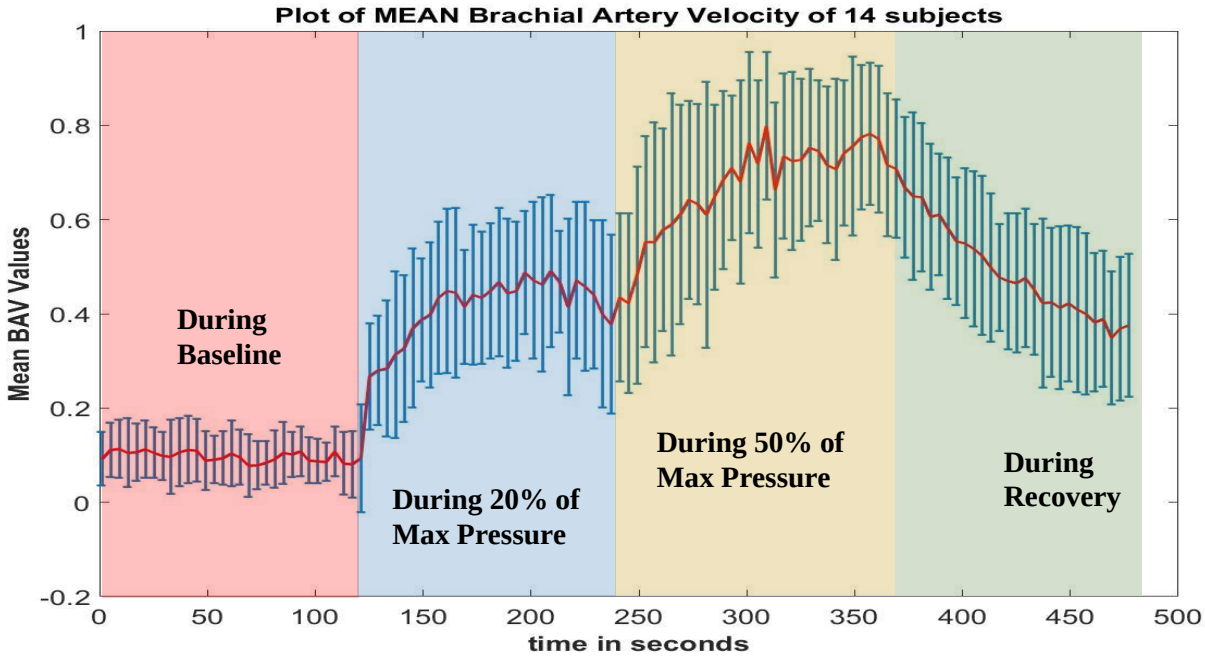

Figure 22(c): plot of mean Brachial Artery Flow of all subjects after normalization

Figure 22(a) is the plot of Brachial Artery Flow over the entire course of the experiment for all the 14 subjects before and after normalization. Each curve represents the Brachial Artery Flow for one particular subject and both the subplots in the graph has 14 curves (14 subjects and one for each subject).

Figure 22(b) represents the Brachial Artery Flow of one subject over the entire course of the experiment while Figure 22(c) represents the mean Brachial Artery Flow during the experiment of all the 14 subjects.

To better understand the changes in rBFI, dOD and Brachial Artery Flow all the three curves from Figure 20(c), Figure 21(c) and Figure 22(c) i.e. the curve which represented the normalized mean values of all the three parameters were plotted together in a single plot and the first step of conclusions were drawn.

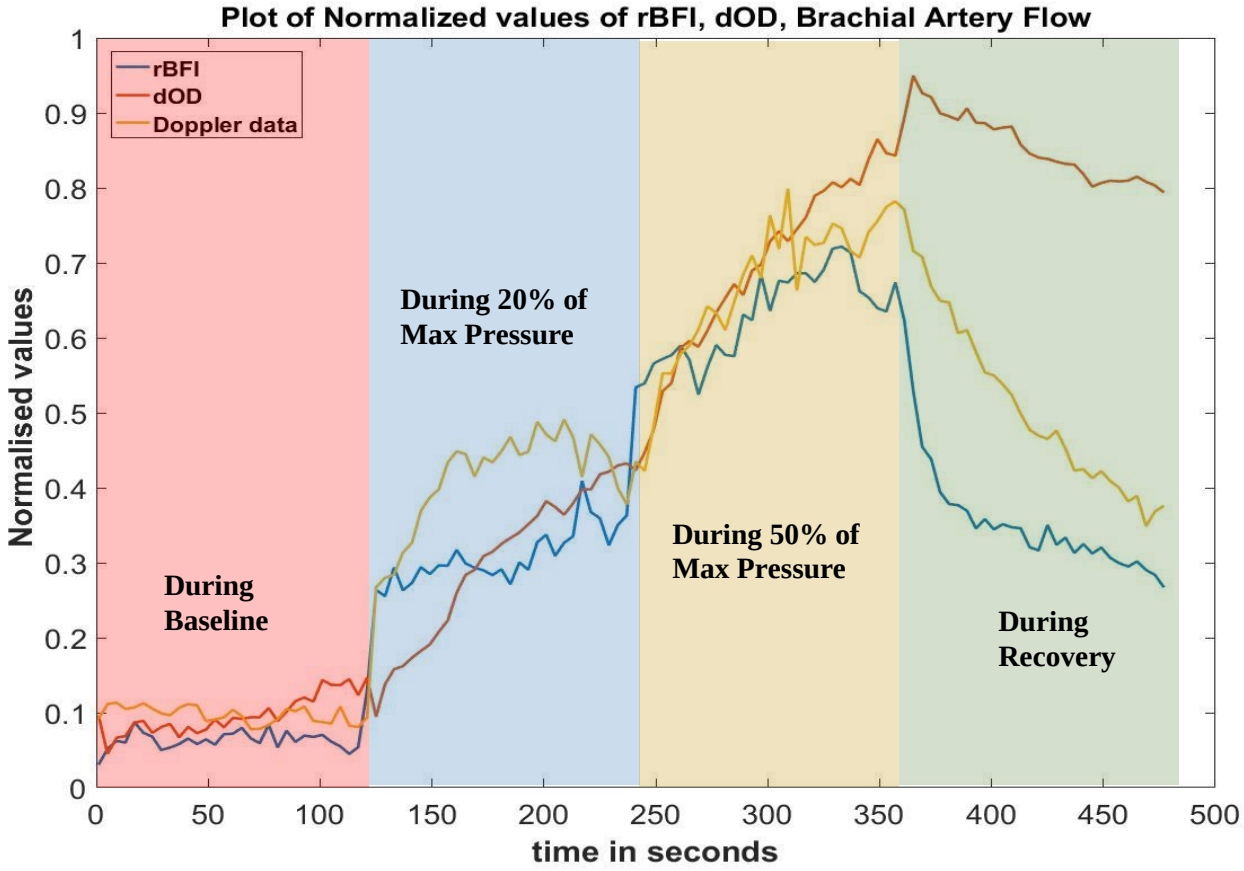

Figure 23: plot of normalized mean values of all the 3 interested parameters.

From Figure 23, we can see that all the 3 parameters (rBFI, dOD and Brachial Artery Flow) remained pretty much stable during the baseline which was for 2 mins or 120 secs, after which during the second part of the experiment which was to give 20% of the maximum pressure for 2 mins or 120 secs that was until 4th min or 240 seconds of the total experiment, there was a sudden increase in rBFI and Brachial artery flow and then they remain pretty much constant until the end of the second part of the experiment. But, we can clearly see that the dOD does not increase immediately, instead is linearly increasing until the end of the 4th minute or until 240 seconds. In the 3rd part of the experiment where the subjects gave 50% of their maximum

pressure for the next 2 mins we again see that there is a sudden increase in rBFI and Brachial artery flow and then they remain pretty much constant while the dOD does not increase immediately, instead is linearly increasing until the end of the 6th minute of the total experimental time or 360 seconds. During recovery period, the rBFI falls immediately and will remain constantly decreasing throughout. Whereas, the brachial artery flow decreases rapidly in a linear fashion while the dOD also tends to decrease but in a very small way when compared to the decrease in rBFI and brachial artery flow.

3.1.4 Statistical analysis

Keeping in mind all this, to check if the protocol worked fine to give some better results and the cross-validation study we performed statistical analysis.

3.1.4.1 Correlation

Scatter plots were used to plot the data on a vertical and horizontal axis with an attempt to show how much one parameter is correlated to the other. The initial understanding was that the relationship between two parameters is called their correlation.

Three correlation graphs were plotted as:

(a) rBFI (relative blood flow index) vs Brachial artery flow (Doppler data).

(b) dOD (delta optical density) vs Brachial artery flow (Doppler data).

(c) dOD (delta optical density) vs rBFI (relative blood flow index).

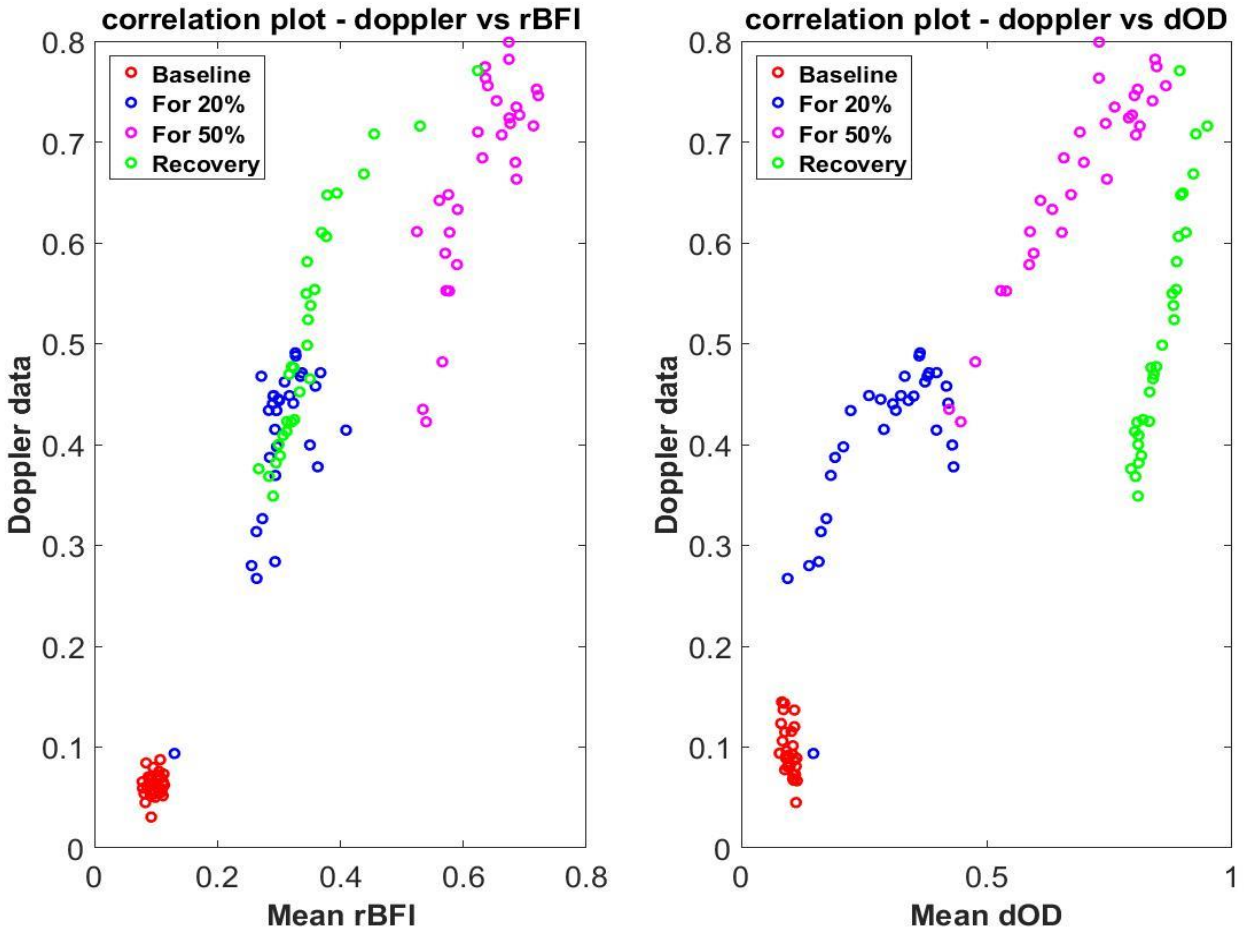

Figure 24(a): correlation plots

Figure 24(a) represents the correlation plots for rBFI vs doppler data (Brachial artery flow) and dOD vs doppler data (Brachial artery flow). From both the plots in the above figure, it is clearly evident that there are 4 separate clusters representing the 4 different sections or parts of the experiment. Also, it is pretty clear that the markers are close to making a linear increase in the plot for all the sections except baseline. This means that the 2 parameters have a good correlation. The baseline section is pretty concentrated as a cluster with no increase or decrease which means that the baseline recordings for both the parameters remained stable and were consistent throughout the baseline recording part of the experiment. Also, for the cross-validation study, this graph gives a very clear initial picture stating that the 2 different modalities measuring

similar parameters still yielded a good correlation between the parameters with which we can have the third step of conclusion as rBFI vs Brachial artery flow and dOD vs brachial artery flow have good correlation.

Figure 24(b) represents the correlation plots for rBFI vs dOD. Both rBFI and dOD were from DCS system. From the plot in the above figure, it is evident that there are 4 separate clusters representing the 4 different sections or parts of the experiment. Also, the markers are making a linear increase in the plot for all the sections except baseline which means that the 2 parameters have a good correlation. The baseline section is concentrated as a cluster with no increase or decrease telling us that the baseline recordings for both the parameters remained stable and were consistent throughout the baseline recording part of the experiment.

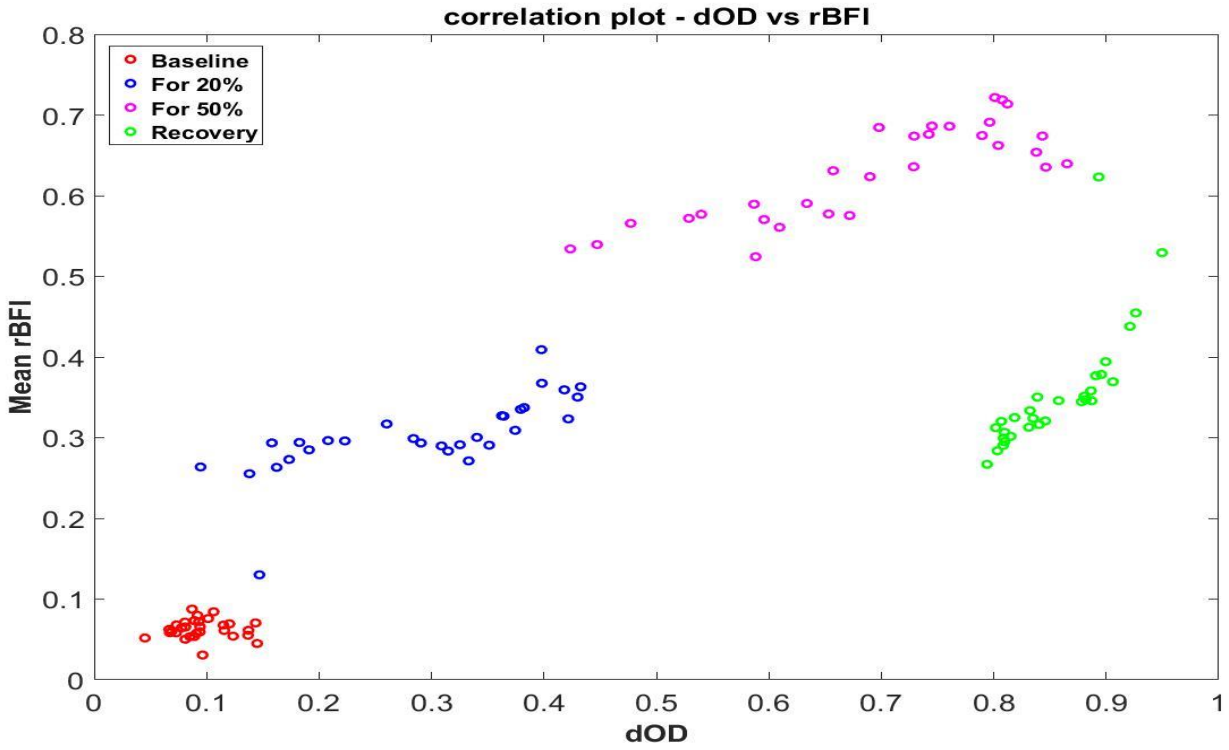

Figure 24(b): correlation plot

3.1.4.2 Regression analysis

Even though a good correlation looks to be present, this might not always be true because, both the variables could be related to another possible third variable. To confirm the correlation, we perform a Linear regression analysis that gives the percentage of linear relationship between the 2 parameters with which we can conclude if the correlation was just a variation or pure coincidence which might have caused an apparent correlation. We fit for the data while calculating the slope and intercept with which we can come up with an equation for the fitted line relating the 2 parameters that would give us information as to how one parameter is related to another or by what factor one parameter is related to another.

Three Linear regression models were fitted:

(a) rBFI (relative blood flow index) vs Brachial artery flow (Doppler data).

(b) dOD (delta optical density) vs Brachial artery flow (Doppler data).

(c) dOD (delta optical density) vs rBFI (relative blood flow index).

Each regression model was split into 3 parts based on the experimental sections to have a clear and better understanding as to how the parameters were correlated. The adjusted R^2 value obtained would tell us the percentage of linear relationship.

(a) Linear regression model for rBFI (relative blood flow index) vs Brachial artery flow (Doppler data).

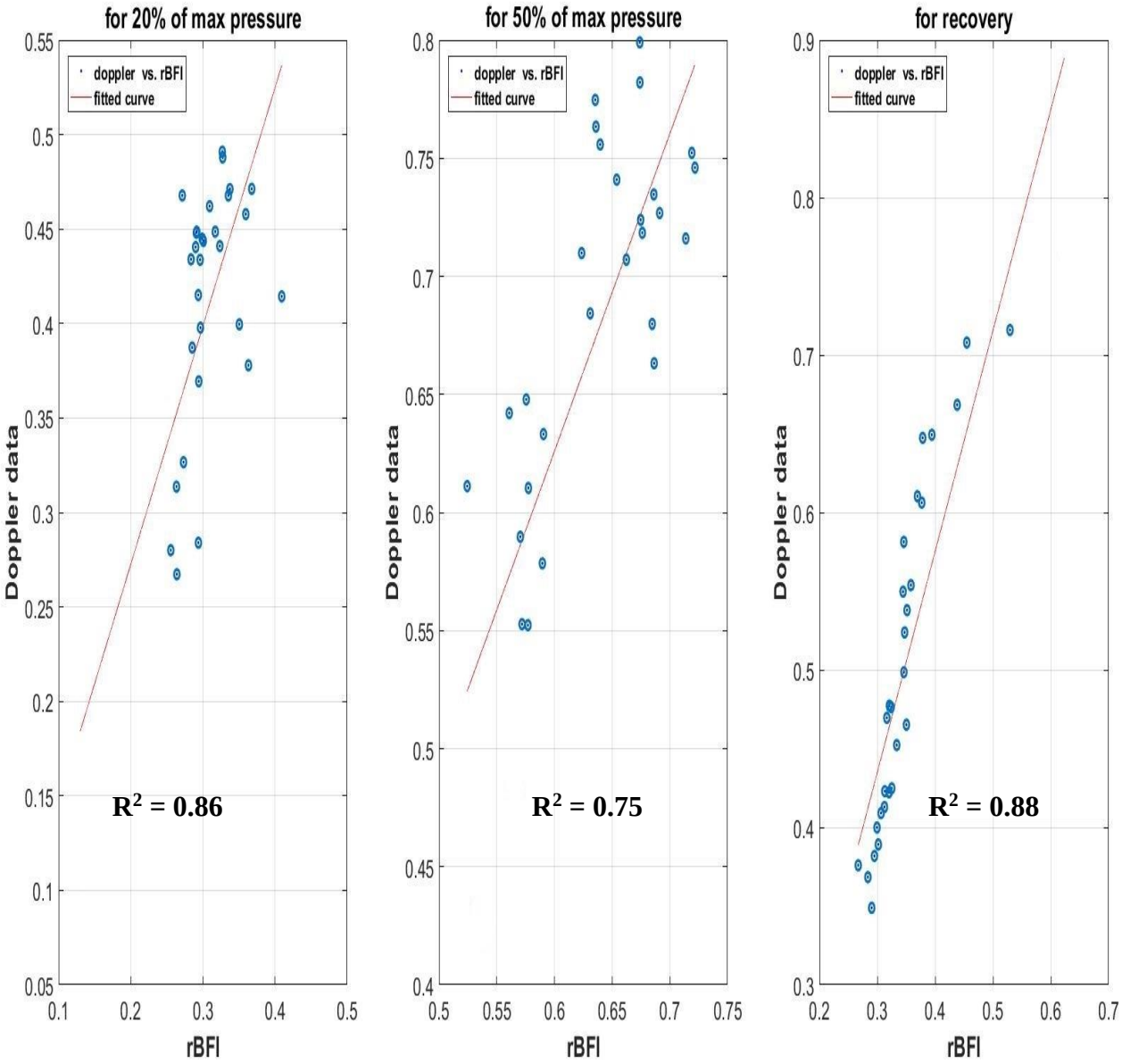

Figure 25(a): Linear data fitting for

rBFI (relative blood flow index) vs Brachial artery flow (Doppler data).

Figure 25(a) represents the Linear data fitting plots of rBFI (relative blood flow index) vs Brachial artery flow (Doppler data) for the 3 different sections in the experimental protocol. From the figure, it is clear that the fitting for the first two subplots will have a +ve slope while the last subplot which is for recovery will have a -ve slope for the fact that both rBFI (relative blood flow index) and Brachial artery flow (Doppler data) will decrease during this section of the experiment. Now, to come up with a straight-line equation for the fitted line, slope and the intercept were calculated separately for the 3 sections.

TABLE 1 : Slope and intercept table for rBFI vs Brachial artery flow

	Slope	Intercept
20% of the max pressure	**1.26**	**0.020**
50% of the max pressure	**1.344**	**-0.180**
Recovery	**1.404**	**0.0136**

TABLE 4 contains the values of slope and intercept for rBFI vs brachial artery flow.

Equations for the fitted line:

- For Model 1, i.e. during 20% of the subject's maximum pressure

  Brachial artery flow (Doppler data) = 1.26*(rBFI (relative blood flow index)) + 0.020

- For Model 2, i.e. during 50% of the subject's maximum pressure

  Brachial artery flow (Doppler data) = 1.344*(rBFI (relative blood flow index)) - 0.180

- For Model 3, i.e. during recovery

  Brachial artery flow (Doppler data) = 1.404*(rBFI (relative blood flow index)) + 0.0136

(b) Linear regression model for dOD (delta optical density) vs Brachial artery flow (Doppler data).

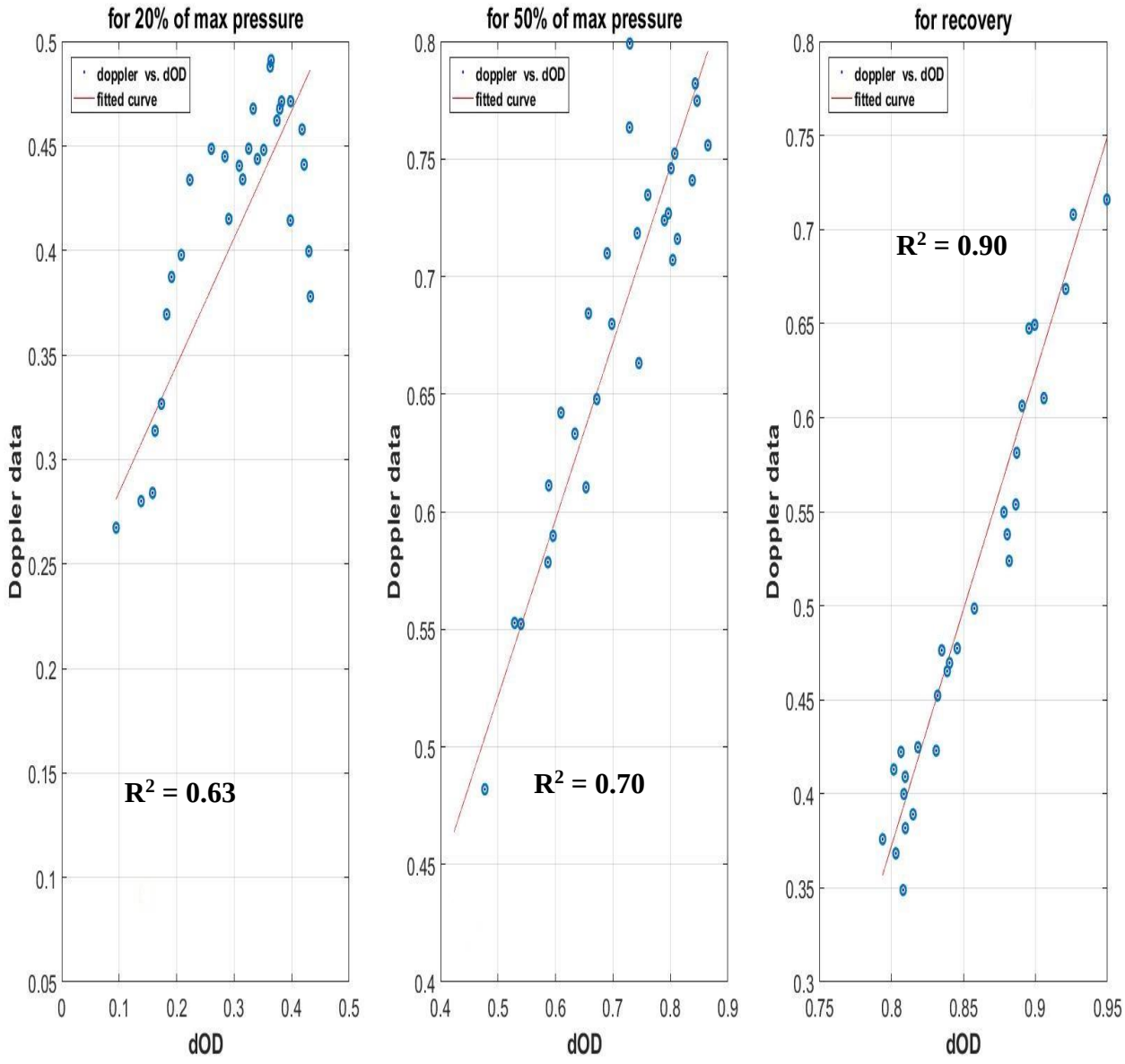

Figure 25(b): Linear data fitting for

dOD (delta optical density) vs Brachial artery flow (Doppler data).

Figure 25(b) represents the Linear data fitting plots of dOD (delta optical density) vs Brachial artery flow (Doppler data) for the 3 different sections in the experimental protocol. From the figure, it is clear that the fitting for the first two subplots will have a +ve slope while the last subplot which is for recovery will have a -ve slope for the fact that both dOD (delta optical density) and Brachial artery flow (Doppler data) will decrease during this section of the experiment. Now, to come up with a straight-line equation for the fitted line, slope and the intercept were calculated separately for the 3 sections.

TABLE 2 : Slope and intercept table for dOD vs Brachial artery flow

	Slope	**Intercept**
20% of the max pressure	**0.6077**	**0.2237**
50% of the max pressure	**0.7521**	**0.1453**
Recovery	**1.5148**	**-1.6399**

TABLE 5 contains the values of slope and intercept for dOD vs brachial artery flow.

Equations for the fitted line:

- For Model 1, i.e. during 20% of the subject's maximum pressure

  Brachial artery flow (Doppler data) = 0.6077*(dOD (delta optical density))+ 0.2237

- For Model 2, i.e. during 50% of the subject's maximum pressure

  Brachial artery flow (Doppler data) = 0.7521*(dOD (delta optical density)) + 0.1453

- For Model 3, i.e. during recovery

  Brachial artery flow (Doppler data) = 1.5148* (dOD (delta optical density)) – 1.6399

(c) Linear regression model for dOD (delta optical density) vs rBFI (relative blood flow index).

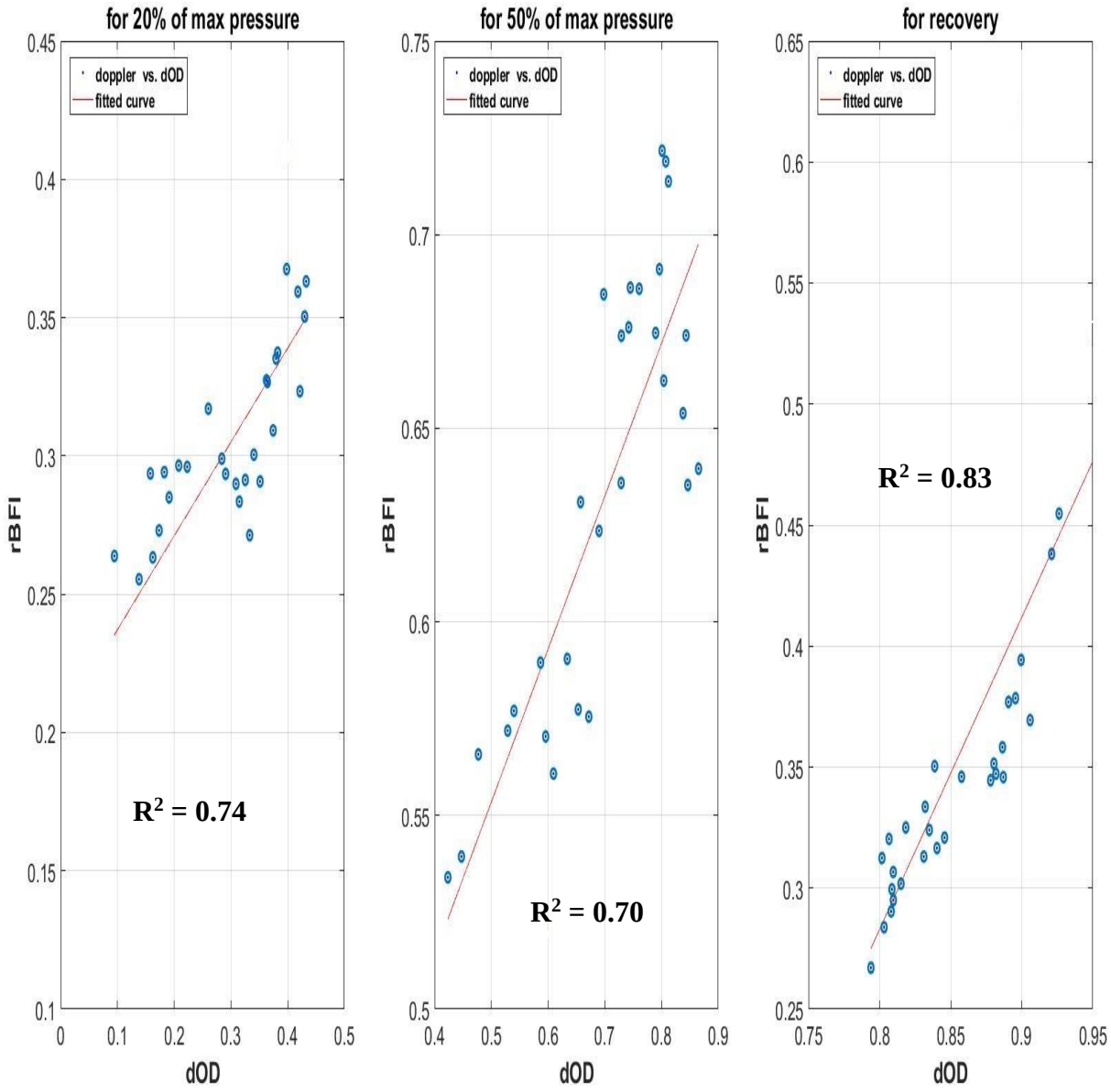

Figure 25(c): Linear data fitting for

dOD (delta optical density) vs rBFI (relative blood flow index).

Figure 25(c) represents the Linear data fitting plots of dOD (delta optical density) vs rBFI (relative blood flow index) for the 3 different sections in the experimental protocol which are measured from the same modality i.e. DCS. From the figure, the fitting for the first two subplots will have a +ve slope while the last subplot which is for recovery will have a -ve slope for the fact that both dOD (delta optical density) and rBFI (relative blood flow index) will decrease during this section of the experiment. Now, to come up with a straight-line equation for the fitted line, slope and the intercept were calculated separately for the 3 sections. Regression analysis for dOD vs rBFI was done to validate the DCS system.

TABLE 3 : Slope and intercept table for dOD vs Brachial artery flow

	Slope	**Intercept**
20% of the max pressure	**0.3391**	**0.2032**
50% of the max pressure	**0.3948**	**0.3560**
Recovery	**1.290**	**-0.7490**

TABLE 5 contains the values of slope and intercept for dOD vs brachial artery flow.

Equations for the fitted line:

- For Model 1, i.e. during 20% of the subject's maximum pressure

  rBFI (relative blood flow index) = 0.3391 *(dOD (delta optical density))+ 0.2032
- For Model 2, i.e. during 50% of the subject's maximum pressure

  rBFI (relative blood flow index) = 0.3948*(dOD (delta optical density)) + 0.3560
- For Model 3, i.e. during recovery

  rBFI (relative blood flow index) = 1.290* (dOD (delta optical density)) – 0.7490

3.1.5 Results & Conclusions

- The linear regression analysis was split into 3 parts to observe the linear relationship between the interested parameters in that physiological condition.
- The first part being the condition where the subject gave 20% of his/her max pressure, second part being the condition where the subject gave 50% of his/her max pressure and the last part being the recovery.
- The first linear regression analysis yielded an Adjusted R^2 of 0.86, 0.75 and 0.88 for the above-mentioned parts respectively for rBFI (relative blood flow index) vs Brachial artery flow (Doppler data).
- It means that the rBFI and BAF are linearly related by 86% during a physiological condition where the subject gave 20% of his/her maximum pressure, 75% during a physiological condition where the subject gave 50% of his/her maximum pressure and 88% during recovery.
- The output of the first linear regression analysis on inclusion of baseline yielded an Adjusted R^2 of 0.89 for rBFI (relative blood flow index) vs Brachial artery flow (Doppler data).
- The second linear regression analysis yielded an Adjusted R^2 of 0.63, 0.70 and 0.90 for the above-mentioned parts respectively for dOD (delta optical density) vs Brachial artery flow (Doppler data).
- It means that the dOD and BAF are linearly related by 63% during a physiological condition where the subject gave 20% of his/her maximum pressure, 70% during a physiological condition where the subject gave 50% of his/her maximum pressure and 90% during recovery.

- While the second linear regression analysis on inclusion of baseline yielded an Adjusted R^2 of 0.66 for dOD (delta optical density) vs Brachial artery flow (Doppler data).
- It means that the rBFI (relative blood flow index) measured by the DCS system and the Brachial artery flow (Doppler data) measured using Doppler ultrasound were linearly related by a proportion of 0.89 or 89% and dOD (Delta optical density) measured by the DCS system and the Brachial artery flow (Doppler data) measured using Doppler ultrasound were linearly related by a proportion of 0.66 or 66%.
- Which intern means that for every increase of 1 point in brachial artery flow, there will be an increase of 0.89 in rBFI and 0.66 in dOD.
- The third linear regression analysis yielded an Adjusted R^2 of 0.74, 0.70 and 0.83 for the above-mentioned parts respectively for dOD (delta optical density) vs rBFI (relative blood flow index).
- It means that the rBFI (relative blood flow index) measured by the DCS system and the dOD (delta Optical density) measure by DCS system were linearly related by 74% during a physiological condition where the subject gave 20% of his/her maximum pressure, 70% during a physiological condition where the subject gave 50% of his/her maximum pressure and 83% during recovery.
- In the cross-validation experiment, a 785nm laser was used as a light source which tends to correspond to the change in conc. of HbT in blood.
- For the experimental protocol that was followed, the exercise lasted for minutes or more which would increase the consumption of oxygen form the blood[17].
- For periods of exercise lasting minutes or longer, aerobic generation of ATP by the mitochondria is critical and requires oxygen and substrate [17].

- Hence, the change in conc. of HbT increases which is clearly visible from figure 21(c).
- It also means that, even after using two different modalities that use 2 different strategies for measuring similar parameters such as rBFI and brachial artery flow, similar results were obtained and it can be concluded by stating that they are linearly well related.
- With the above conclusion, it can be stated that the DCS system was validated for its working and performance and also cross validated with another modality which at the end gave us similar results.
- But, the dOD does not have a good linear relationship with brachial artery flow because, flow consists of not just Hb but also HbO and other smaller components in blood like plasma and platelets.
- Also, no assumptions or conclusions can be made for the change in conc of HbO or Hb because this is a single wavelength system with which change in conc. Of HbO or Hb cannot be calculated.
- Hence, we proceed further to build a real-time Dual wavelength DCS system to monitor skeletal muscle blood perfusion and oxygen metabolism.
- Taken together, these data show that DCS and Doppler ultrasound quantify the same temporal dynamics of skeletal muscle blood flow during exercise.
- While these results are indeed encouraging, more work is needed to fully validate this approach for measuring local microvascular blood flow in humans.

Chapter 4

Design & Development of a real-time, Dual-Wavelength DCS System

Design and development of this real-time, Dual-Wavelength DCS system was done using National Instruments' LabVIEW software (LABVIEW 2013, 64 bit).

This new system is designed based on the concepts obtained from the single wavelength system. The goals of this design were:

- To have 2 laser sources with which the change in conc. Of HbO and Hb can be calculated.
- Program a MEMS based 2x2 blocking optical switch (Dicon Fiberoptics, INC) which would toggle the source between 785nm laser and 852nm laser which intern would source laser for the dual wavelength system.
- The optical switch would also reduce the total time the laser is shining on the tissue sample.
- Completely time synchronized.
- Ensure proper functioning of the algorithm and to keep it user friendly.
- Proper data management.
- To give some open options for user inputs.
- To embed MATLAB in LabView which will:
    - Reduce time and man power for data processing post data acquisition.
    - Cut off the use of MATLAB separately for data processing.
    - Help in output data display.

- To have a user-friendly interface that would be capable of controlling the algorithm based on the experimental time without disturbing the data acquisition and functioning of the algorithm.

To have a real-time output data display which will help the physician/clinician and the engineer monitor the output directly.

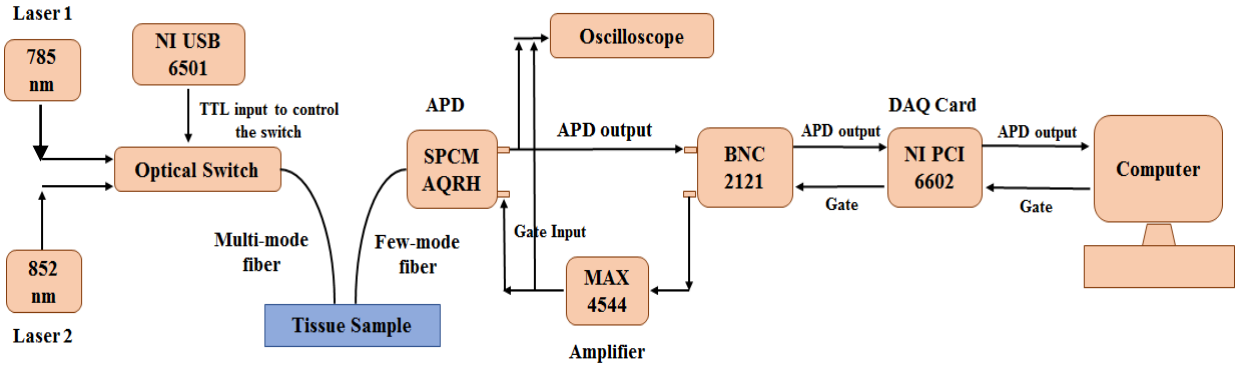

Figure 26: Block diagram of Dual wavelength DCS system.

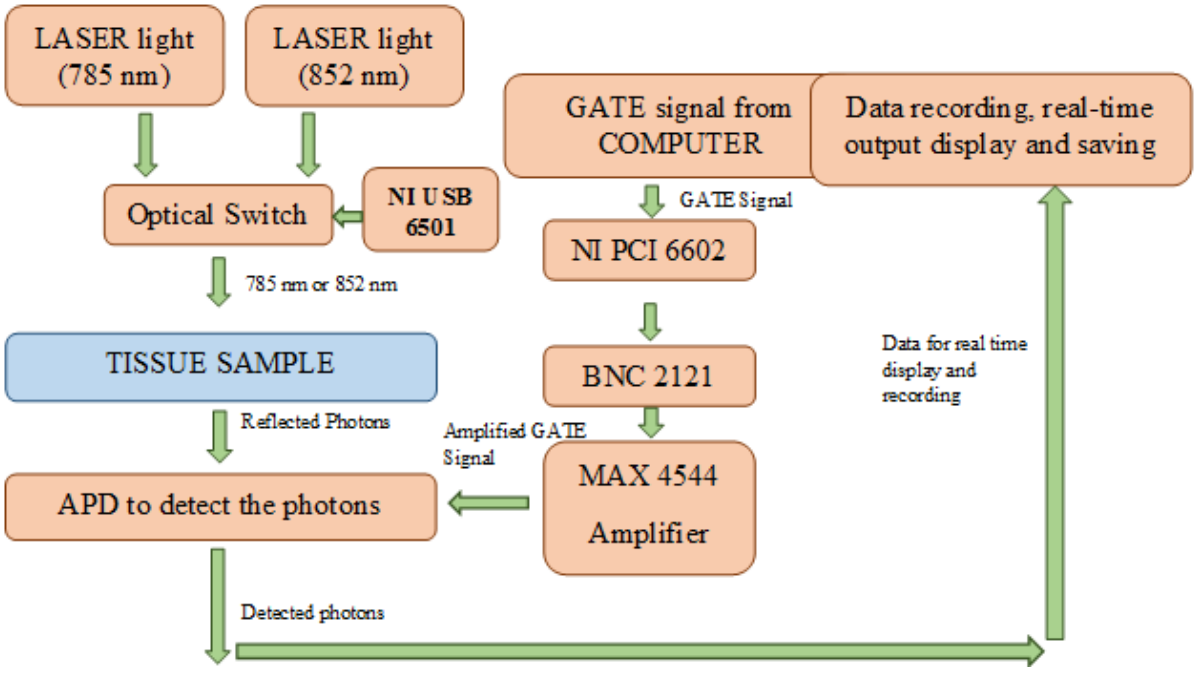

Figure 27: Flow Cart for functioning of dual wavelength DCS system.

Figure 26 represents the block diagram of the entire dual wavelength DCS system with all the components including the optical switch. Figure 27 represents the flow chart for functioning of the dual wavelength DCS system. The dual wavelength DCS system consists of a 785nm laser and an 852nm laser which goes into a MEMS based 2x2 blocking optical switch (DICON Fiberoptics, INC) which will block and allow either of the laser light which acts the source of light that is shined on the tissue sample. NI USB 6501 is used to generate a 5V TTL signal to control the switch. This software generated TTL signal is used to control the optical switch to obtain the desired laser output. An Avalanche photodiode detector (APD) is used for detecting the reflected photons. A software generated gate signal from LABVIEW software is used and amplified using MAX 4544 amplifier after which we get an amplified gate signal which controls the data acquisition from the APD.

4.1 Programming the optical switch

The dual wavelength DCS system uses a MEMS based 2x2 blocking optical switch (DICON Fiberoptics, INC). The main function of the optical switch is to block and allow either of the laser light which acts as the source of light that is shined on the tissue sample. In this system we use a TTL controllable optical switch. A TTL signal is generated using LABVIEW software which is used to control the optical switch to obtain the desired laser output. This switch operates through a 16 pin connection.

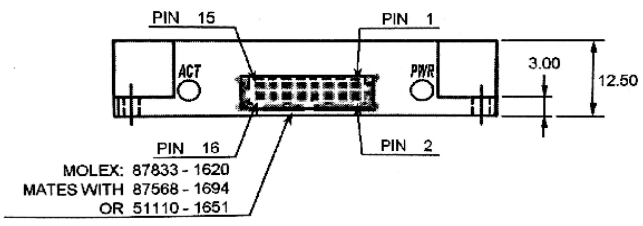

Figure 28: MEMS MxN Blocking Switch electrical connections [18]

Figure 28 represents the electrical connections of the optical switch where the electrical connector is a molex 87833-1620 male connector and mates with a female connector 87568-1694 or 51110-1651 [18]

DiCon Pin #	Name	Description	Direction	Specification	Unit
1	D0	Data 0 Input	IN	LVTTL	VDC
2	D5	Data 5 Input	IN	LVTTL	VDC
3	VIN	Power Supply	IN	+5	VDC
4	VIN	Power Supply	IN	+5	VDC
5	GND	Signal ground			
6	GND	Signal ground			
7	D4	Data 4 Input	IN	LVTTL	VDC
8	D1	Data 1 Input	IN	LVTTL	VDC
9	NC	Not connected			
10	NC	Not connected			
11	D2	Data 2 Input	IN	LVTTL	VDC
12	D3	Data 3 Input	IN	LVTTL	VDC
13	/BUSY	Normally pull low. While a module is busy, it will be pulled high.	OUT	LVTTL	VDC
14	/ALARM	Device communication error signal output, "Low" = Comm. Error	OUT	LVTTL	VDC
15	/STROBE	Falling edge active to synchronize command execution.	IN	LVTTL	VDC
16	/RESET	Low level active for hardware reset.	IN	LVTTL	VDC

Figure 29(a): MEMS MxN Blocking Switch Module Pin Assignment Table for TTL [18]

Parameter		Minimum	Typical	Maximum	Damage Threshold	Unit
Latching Type		Non-latching				
Vin voltage	For I^2C, RS232 type	10.8	12	13.2	15	VDC
	For TTL type	4.75	5	5.25	7	VDC
LVTTL		-	3.3	-	3.6	VDC
Power consumption[1]	at 12V	-	-	700	-	mW
	at 5V	-	-	1.5	-	W

Figure 29(b): MEMS MxN Blocking Switch Module Electrical specifications [18]

Figure 29(a) is a pictorial representation of a table for MEMS MxN Blocking Switch Module Pin Assignment Table for TTL [18]. Figure 29(b) is a pictorial representation of a table for MEMS MxN Blocking Switch Module Electrical specifications [18].

TTL Interface for programming the optical switch.

- V_{in} (pins 3 and 4) are the power supply pins to the optical switch. The V_{in} should be around 5V. Once the input voltage is supplied and the pins 5 and 6 are grounded, we see a yellow and green LED turning on at the back of the switch indicating that the switch is powered on.
- Data input pins from D0 to D3 are used for channel selection. No data input pins should be left floating instead, all the unused data input pins should be connected to ground.
- Pin number 13 is the busy pin which will go high during switching of channels.
- Pin number 15, the STROBE pin is the falling edge active pin that is only used for TTL interfaces [18]. This basically acts as a gate (Figure 30(a)). After giving the logical TTL input for controlling the switch, the strobe pin has to be pulled low so that this allows the logical input to reach the optical switch to obtain the desired output.

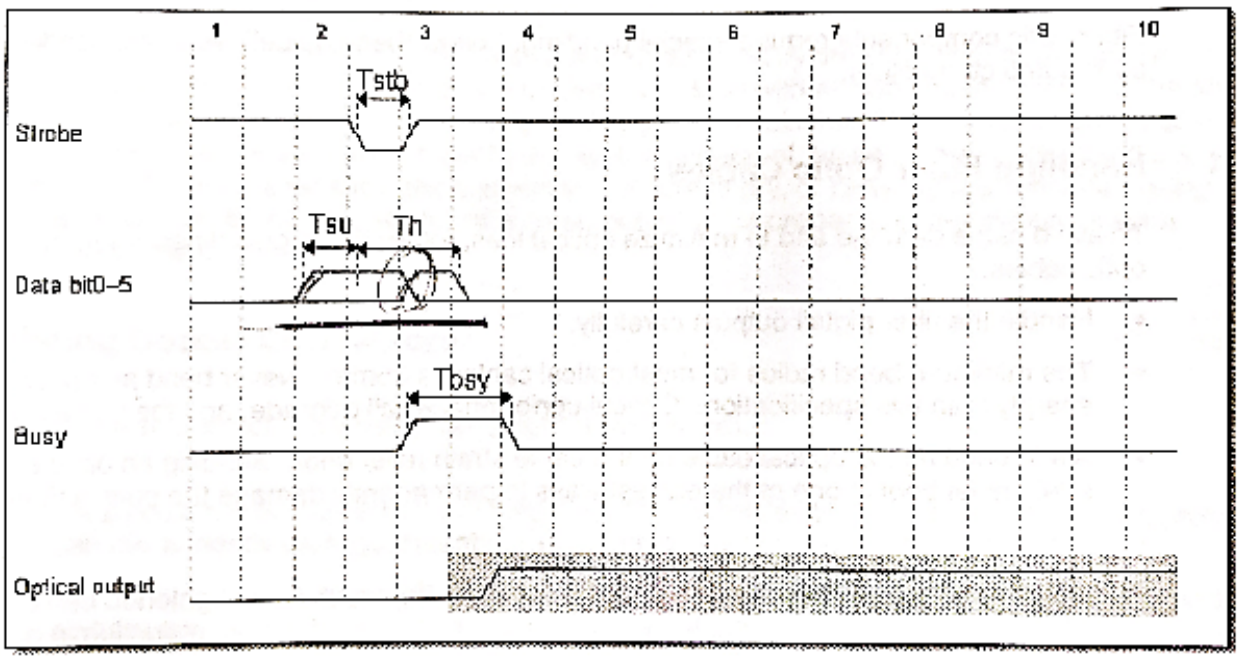

Figure 30(a): Timing Diagram for MEMS MxN

Blocking Switch Module using TTL interface [18]

Parameter	Description	Min	Max	Units
T_{su}	Setup time. The channel address (<D5:D0>) must remain stable preceding the falling edge of Strobe.	100	-	µs
T_h	Hold time. The channel address (<D5:D0>) must remain stable following the falling edge of Strobe.	100	-	µs
T_{stb}	Strobe pulse width	1	-	ms
T_{bsy}	Switching time. During this period there may be invalid optical transmission on all channel.	-	30	ms

Figure 30(b): Timing parameters for MEMS MxN
Blocking Switch Module using TTL interface [18]

- T_{su} is the minimum required data set-up time, relative to falling edge of the strobe. The channel address (D3 to D0) must remain stable preceeding the falling edge of strobe [18].
- T_h is the minimum required data hold time, relative to the falling edge of the strobe. The channel address (D3 to D0) must remain stable preceding the falling edge of strobe [18].
- T_{stb} is the minimum required pulse width of the strobe [18].

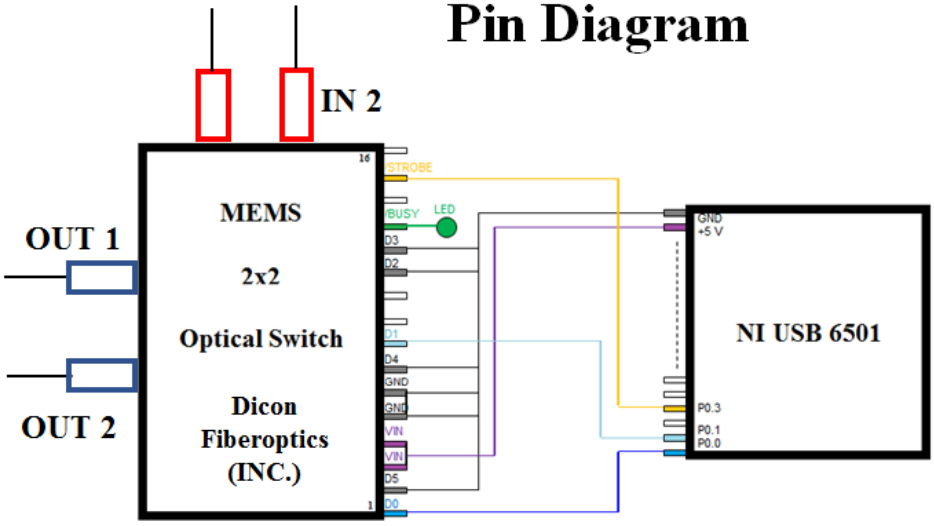

Figure 30(c): Pin diagram connections from NI USB 6501 to Optical Switch

Figure 30(b) is a pictorial representation of a table for Timing parameters for MEMS MxN Blocking Switch Module using TTL interface [18]. Figure 30(c) is a diagrammatic representation Pin diagram connections from NI USB 6501 to Optical Switch of a table for

ID	Active Channels	D3	D2	D1
1	PARKING	0	0	0
2	IN1 -OUT1	0	0	1
3	IN1 -OUT2	0	1	0
4	IN2 -OUT1	0	1	1
5	IN2 -OUT2	1	0	0

TABLE 4: Logic table to control the MEMS based optical switch [11].

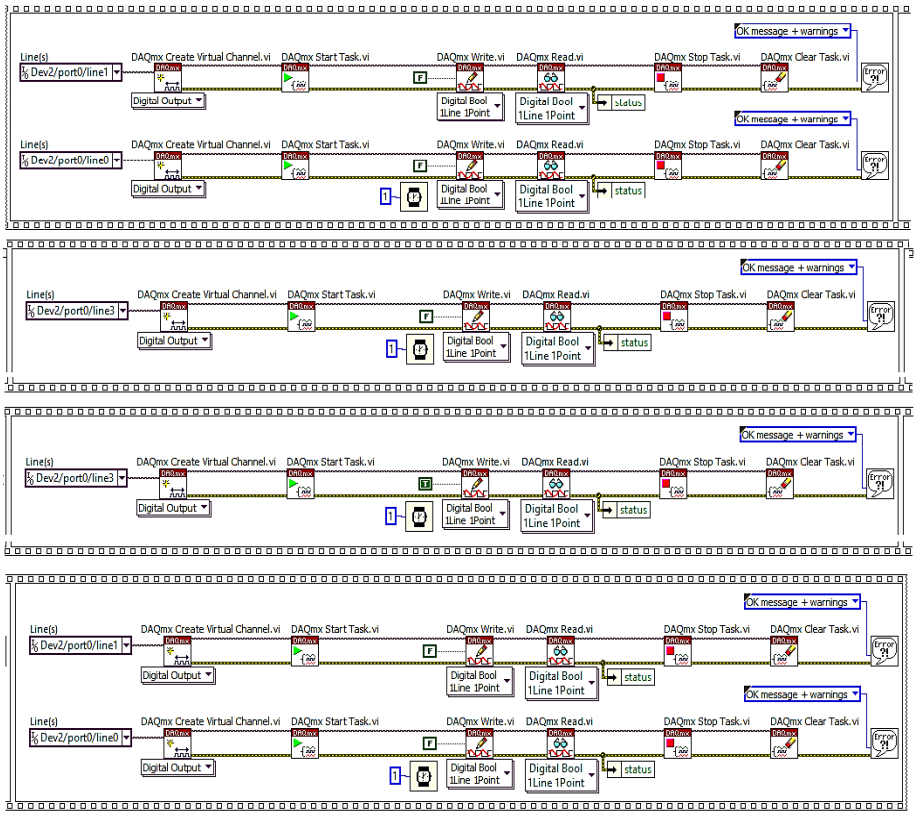

Figure 31(a): Labview Block diagram to program the optical switch for parking position using NI USB 6501

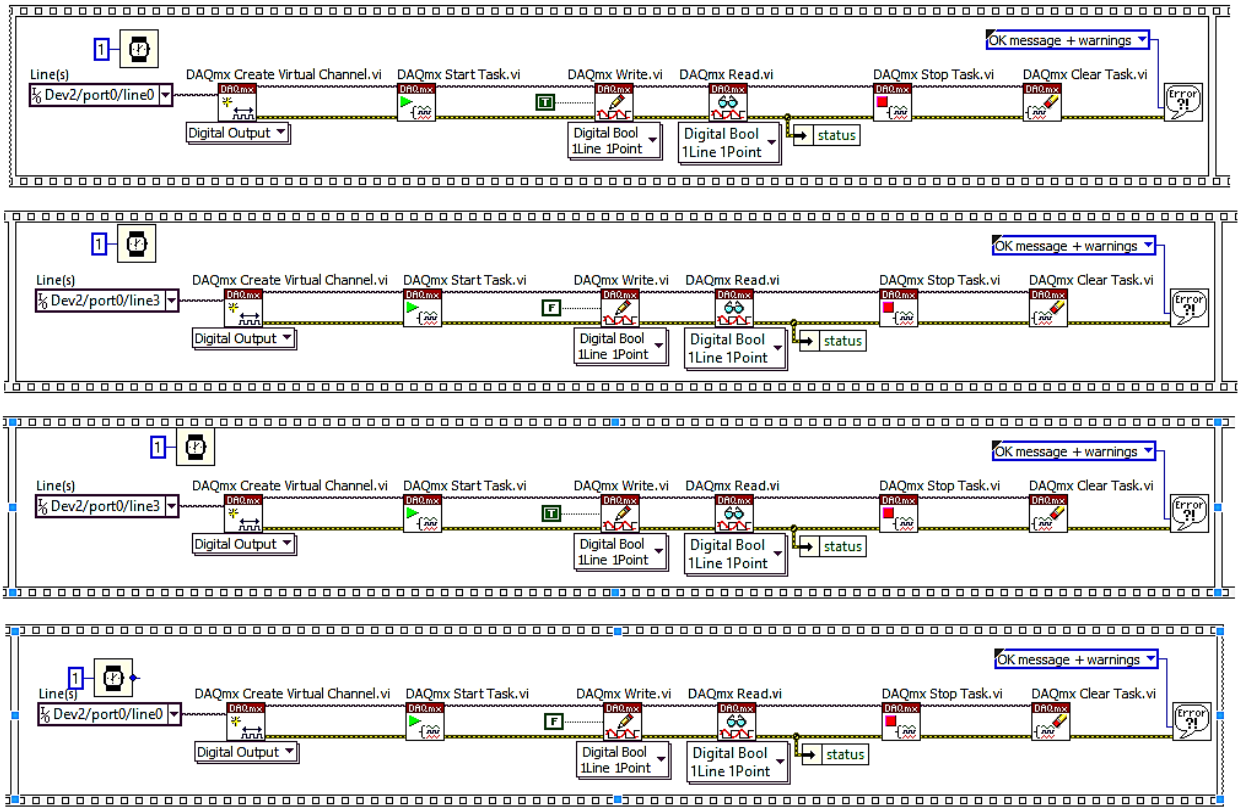

Figure 31(b): Labview Block diagram to program the optical switch for IN1 – OUT1 using NI USB 6501

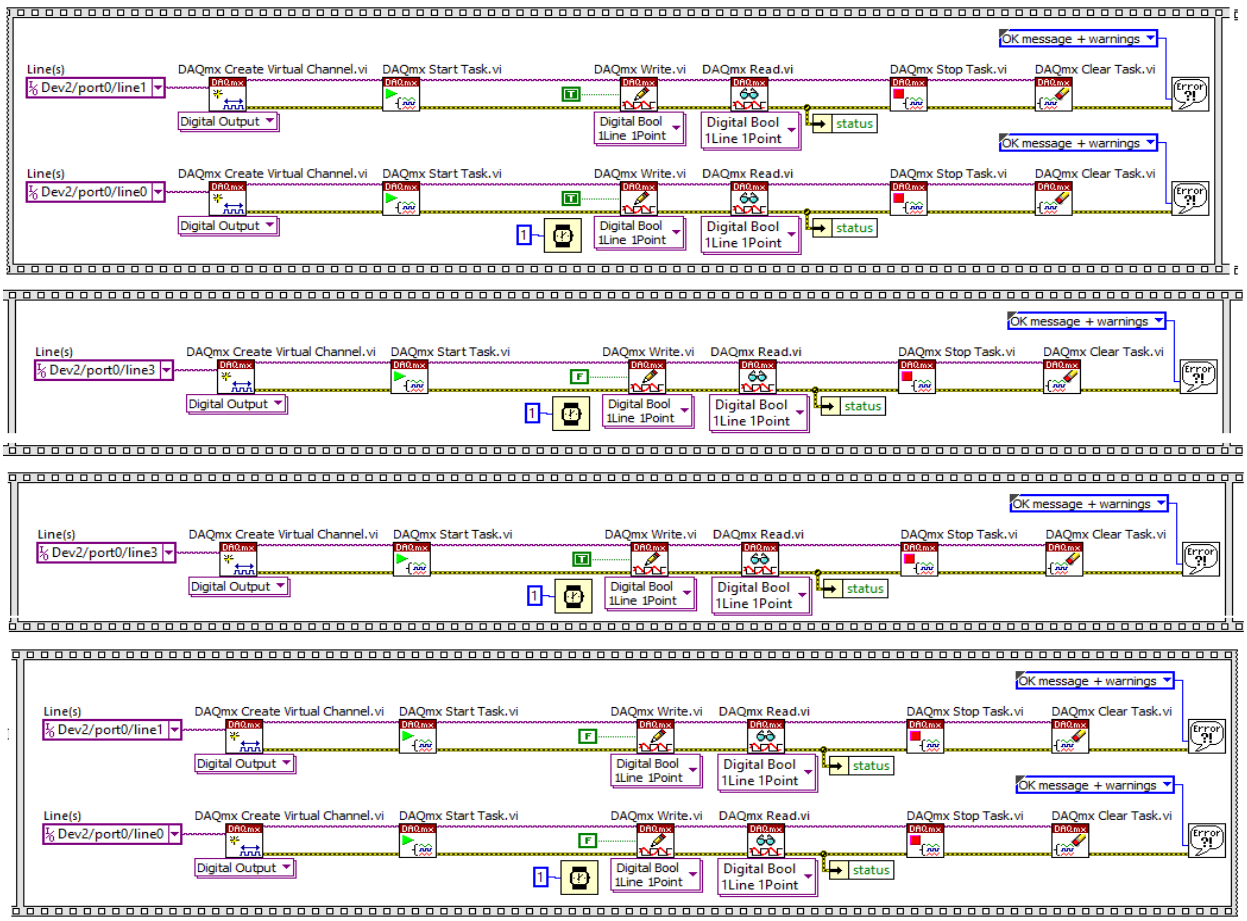

Figure 31(c): Labview Block diagram to program the optical switch for IN2 – OUT1 using NI USB 6501

Figure 31(d): Photograph of the hardware enclosure for dual wavelength DCS system.

Figure 31(d) is a pictorial representation of the hardware enclosure with all the components enclosed for dual wavelength DCS system.

4.2 Design of the User interface

As discussed in the section *2.1*, same technique was adopted in the dual wavelength DCS system as well to design user friendly input options.

- For data management, a prompt was generated for the user to input the name of the subject after which a new folder in that name would be created and all the related data would be saved in that particular folder.
- A user interface with an option to input the absorption coefficient (μ_a), scattering co-efficient(μ_s) and experimental time was designed/programmed as before.

- The input of μ_a and μ_s values will help in fitting the for data in real time also reducing the time, effort and man power to process the data post data acquisition.
- The option to input the experimental time will help in controlling the system based on the given time. Once the time limit has been reached, the system will close automatically without any required supervision.
- Also, this will in no way affect the system's performance, data acquisition or data processing inside the algorithm.

4.3 Design for the data acquisition

The Gate signal we utilized to drive the APD and to count the TTL output pulses from the APD has a time resolution of 2 seconds or frequency of 0.5 with 99.9% duty cycle as discussed in the section *2.2.3 and 2.2.4* (refer Figure 12(a)).

For counting the photon pulses, we used a technique called buffer period measurement in which the source edges account for an increment while the gate edges will buffer the immediate count and furthermore reset the count register back to 0 for the following interval. The total number of pulses that occur per interval will characterize the period of the gate signal and hence we use an implicit timing when we generate the gate signal [36]. This implies that the period measure of a signal would set the timing of sampling which stands on when its' edges arrive [34]. Subsequently the net impact is to perform "binning" measurement where the "periods" are used and read to discover the number of APD pulses recorded inside each interval of the gate signal. When we use such a technique, the initially acquired points would represent awful information in period measurements and subsequently were overlooked (refer Figure 12(a), 12(b) and Figure 15(a), (b), (c), (d)).

4.3 Real-Time data Display

The main goals for having a real-time data display is as discussed in the section *2.2.5.*

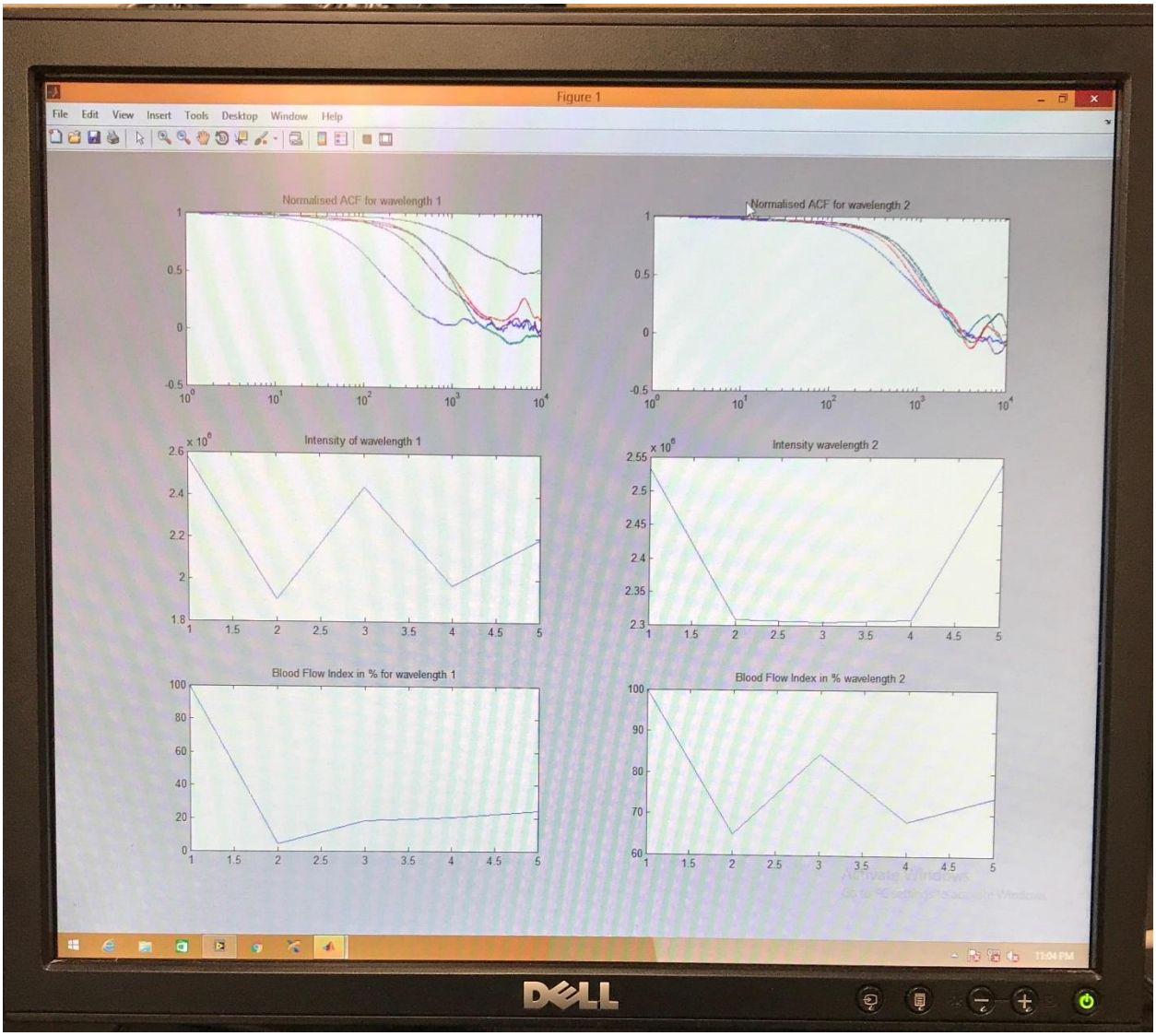

Figure 32: Photograph of the real-time data display of dual wavelength DCS system.

Figure 32 represents a photograph of the real-time data display during the course of the experiment. The entire plot is split into 6 subplots to show all the desired output parameters in real-time. The top left curve represents the auto correlation functions of the recorded data when the light source is 785nm, while the top right curve represents the auto correlation functions of

the recorded data when the light source is 852nm. The right and the left plot middle represent the total intensity of the detected photons for 785nm laser and 852nm laser respectively. and the bottom left and the right curves represent the Relative Blood Flow Index (rBFI) for 785nm and 852nm lasers respectively, which is a relative measure giving information about the change in blood perfusion.

Chapter 5

System validation on real-time, Dual -Wavelength DCS System

5.1 Intralipid Phantom test

To validate the system and its performance, an intralipid phantom was prepared and was used as a test sample to mimic the human tissue sample. Intralipid phantoms play an important role in the development of diagnostic systems [40]. These intralipid solutions can be used for initial testing of any system design, to optimize the SNR (Signal to noise ratio) of that system.

An intralipid phantom was prepared with concentration of 1% which would mimic the optical properties carried by a tissue sample.

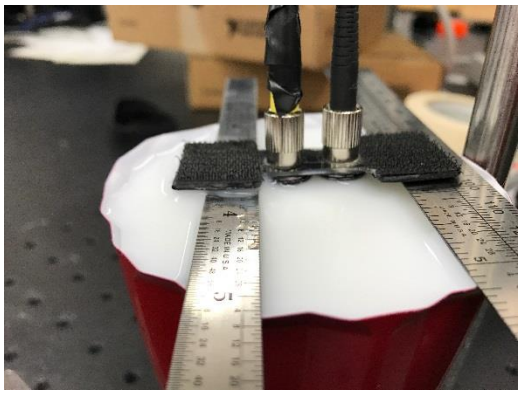

Figure 33(a): Photograph of probe placement during intralipid phantom test.

Figure 33(b): Photograph of probe placement during intralipid phantom test.

Figure 33(a) and Figure 33(b) represent the probe placement and arrangement during the intralipid phantom test. The source and the detector separation distance was kept constant with L=1.5 cms.

Figure 34(a)

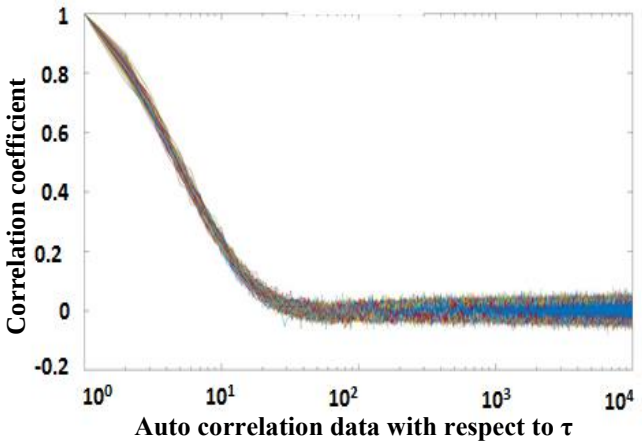

Auto correlation functions from 785 nm

Figure 34(b)

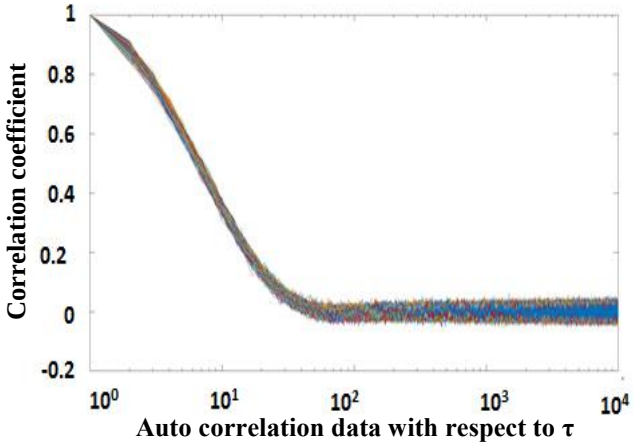

Auto correlation functions from 852 nm

Figure 34(a) and Figure 34(b) represent the auto correlation functions of the detected photons from 785nm and 852nm respectively. From both the figures it is evident that the auto correlation function has no change over the entire period of 15 mins.

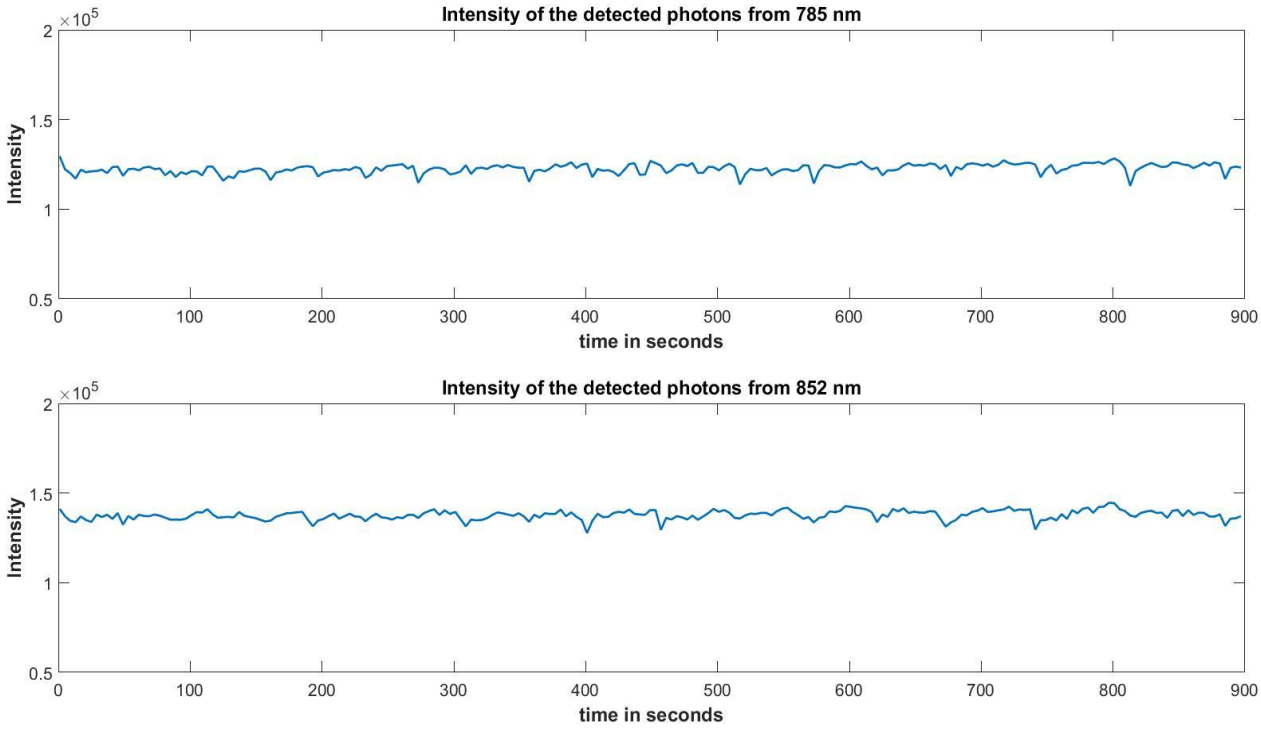

Figure 34(c)

Figure 34(c) represents the intensity plot of the detected photons. The upper curve represents the intensity when the laser source was 785nm and the lower curve represents the intensity when the laser source was 852nm. From both the curves it is clear that the there wasn't much of the change in the detected photons during the entire course of the experiment with the max change being 2%.

From the conclusions drawn from Figure 34(a), Figure 34(b) and figure 34(c) we can conclude by telling that the system was validated for its functioning and performance.

5.2 Human cuff test

The next step in system validation was to perform a cuff test on humans. An experimental protocol was separately designed for this purpose.

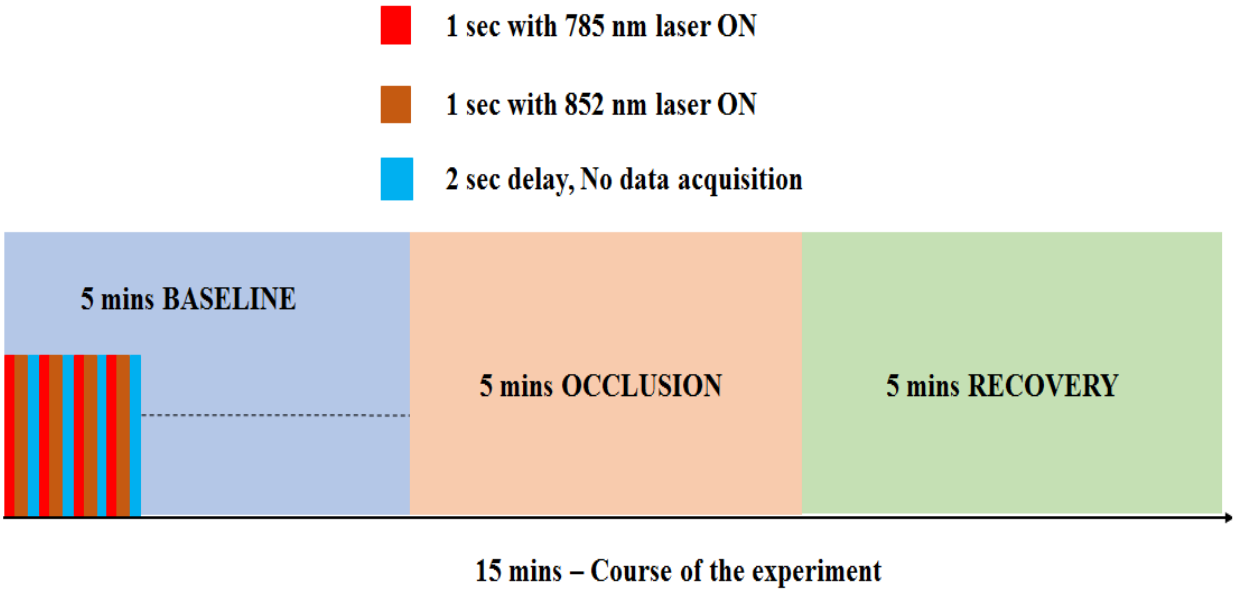

Figure 35

Figure 35 is a schematic representation of the protocol designed for the cuff occlusion test on humans. The laser light was designed to shine for 1 sec from each laser while the other was designed to go off and during 2 seconds' delay, both the lasers would go off and no data would be acquired. With 5 mins being the time for all the three sections baseline, cuff occlusion and recovery, the type of the occlusion done was arterial occlusion. The cuff occlusion was done at 220 mm/Hg for 5 mins which is considered as a complete block of the artery.

4 healthy and youthful subjects who were ready to volunteeringly be a subject were considered for the experiment.

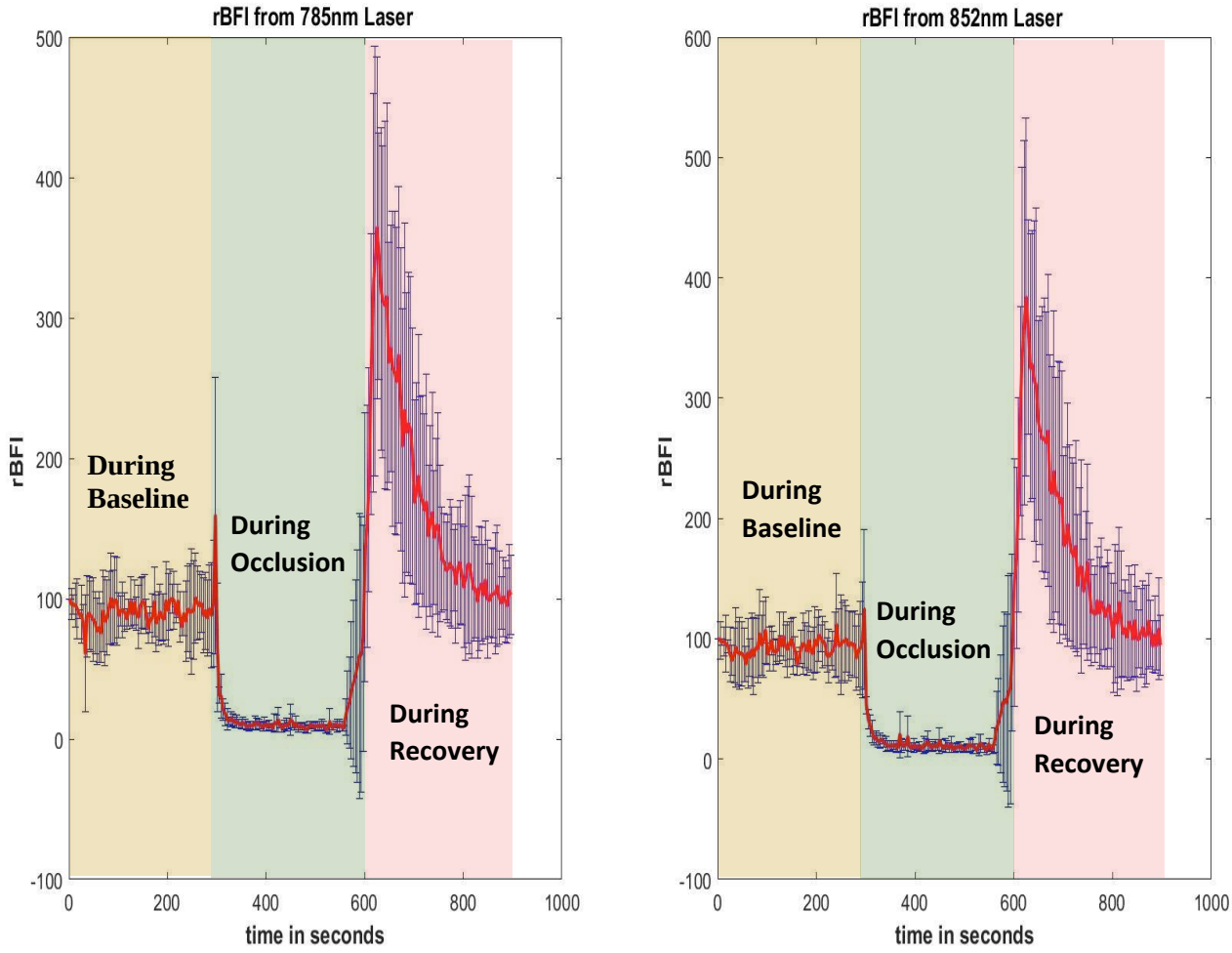

Figure 36(a)

Figure 36(a) represents the plot which depicts the rBFI (Relative Blood Flow Index) during the course of the experiment. From the graph is is evident that the rBFI (Relative Blood Flow Index) from both the lasers during baseline remained stable after which, during cuff occlusion the rBFI (Relative Blood Flow Index) decreased gradually until the cuff was deflated. Once the cuff was deflated, we can see a sudden increase in rBFI (Relative Blood Flow Index) and after a couple of mins they tend to get back to normal.

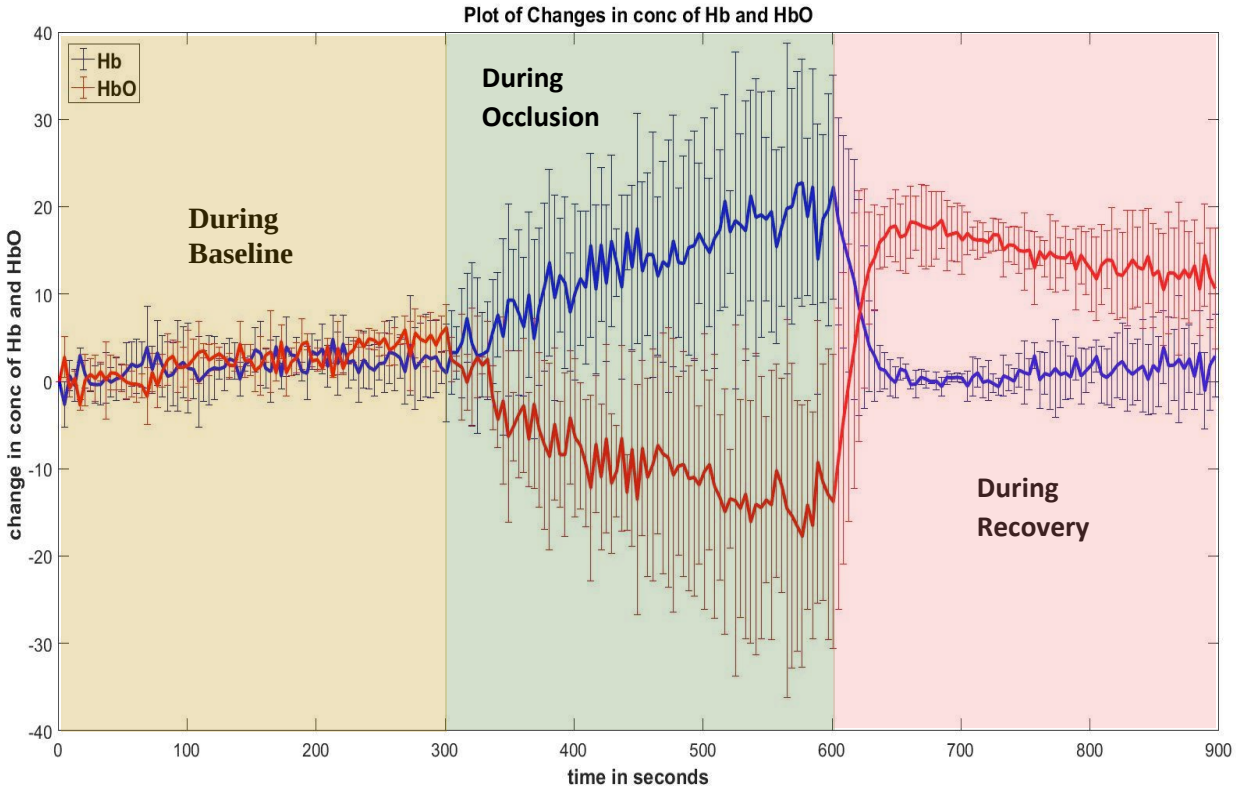

Figure 36(b)

Figure 36(b) represents the plot which depicts the changes in conc. of Hb and HbO during the course of the experiment. From the graph is is evident that the change in conc. of Hb and HbO during baseline remained stable after which, during cuff occlusion the conc of HbO decreased gradually and at the same time conc of Hb increased gradually until the cuff was deflated. Once the cuff was deflated, we can see a sudden increase in conc of HbO and a sudden decrease in the conc of Hb and after a couple of mins they tend to get back to normal.

Based on the conclusions drawn from Figure 36(a) and Figure 36(b) we can conclude by telling that the real-time dual wavelength DCS system was validated for its functioning and performance and is now ready to be used for any experimental purposes.

Chapter 6

Discussion and future work

6.1 Discussions

Microvascular blood perfusion measure using DCS is actually done by keeping a track of the speckle fluctuations of photons caused by the movement of scatterers inside the biological tissue sample. Contemporary researches and studies depict that DCS is feasible technique to surveil microvascular blood perfusion. This emerging technique has a lot of advantages such as non-invasiveness, high temporal resolution, high penetration depth, portability, blood perfusion measurement at microvascular level. DCS Technology has been extensively validated in various tissues through comparisons with laser Doppler flowmetry, power Doppler ultrasound, Xenon-CT, florescent microsphere flow measurement and arterial spin labeled magnetic resonance imaging (ASL-MRI) [16].

In this study, we have demonstrated an implementation of a real-time single wavelength DCS system and a real-time dual wavelength DCS system with a software based autocorrelator, gate signal to control the APD, use of NI USB 6501 to generate logical outputs to control the optical switch, to use MATLAB script inside of LABVIEW, data management and to have a user-friendly interface. Both the systems have been validated and cross validated with an intralipid phantom and a cuff occlusion experiment. The system and the interface was kept user friendly, with an ease to operate, cost effective and portability.

6.2 Limitations

The current DCS system and the technology used will calculate the BFI based on a semi-infinite geometry in which the tissue sample being measured is considered as homogeneous. Hence, the rBFI will be a collective rBFI of skeletal muscle, fat and skin as the light penetrates all these tissues as well [19]. The separation distance between source and the detector cannot be more than 2 cms for the fact that we are using few mode fiber as a detector fiber with which the SNR would decrease. DCS can be subjected to motion artifacts very easily. Hence, following strict protocols by advising the subject to stay calm, relaxed, not to move and fixing the probe firmly without obstructing the blood flow can possibly reduce these artifacts.

REFERENCES

1. David B. (1996). *Diffuse photon probes of structural and dynamical properties of turbid media: theory and applications* (Unpublished doctoral dissertation). University of Pennsylvania, Philadelphia, U.S.A.

2. Jing D., Renzhe B. & Kijoon L. (2015). *Frontiers in Biophotonics for Translational Medicine.*Retrieved from http://books.google.com

3. Dong_J. *et al. Diffuse correlation spectroscopy spectroscopy with fast Fourier transform-based software autocorrelator*. J. Biomed. Opt. **17**,97004 (2012).

4. Wang, L.V. & Wu, H. in *Biomedical optics: principles of imaging* (Wiley-Interscience, Hoboken, N.J, 2007).

5. http://www.vision-systems.com/articles/print/volume-17/issue-10/features/infrared-cameras-enhance-diagnostic-medical-imaging.html

6. Bunce, S. C., Izzetoglu, M., Izzetoglu, K., Onaral, B. & Pourrezaei, K. Functional near-infrared spectroscopy. *Engineering in Medicine and Biology Magazine, IEEE* **25**, 54-62 (2006).

7. Chance, B., Cope, M., Gratton, E., Ramanujam, N. & Tromberg, B. Phase measurement of light absorption and scatter in human tissue. *Rev. Sci. Instrum.* **79**, 3457-3481 (1998).

8. Smith, Andrew M.; Mancini, Michael C.; Nie, Shuming (2009). "Bioimaging: Second window for in vivo imaging". Nature Nanotechnology.

9. Jobsis, F. (1977). *Noninvasive, infrared monitoring of cerebral and myocardial oxygen sufficiency and circulatory parameters*. Science, 198(4323), 1264-1267. doi:10.1126/science.929199

10. Hamblin, M. R. (2008). The role of nitric oxide in low level light therapy. Mechanisms for Low- Light Therapy III. doi:10.1117/12.764918

11. Berne, B. J., & Pecora, R. (1990). Dynamic light scattering: With applications to chemistry, biology, and physics. Malabar, FL: Krieger.

12. Chu, B. (1991). Laser light scattering: Basic principles and practice. New York: Academic Press.

13. Brown, W. (1993). Dynamic Light Scattering: The Method and Some Applications. New York:Clarendon Press.

14. JC, R. & F, G. Low-level light therapy of the eye and brain. *Eye and Brain* **2011**, 49-67 (2011).

15. Boas, D. A., Pitris, C., & Ramanujam, N. (2011). Handbook of Biomedical Optics. Boca Raton: CRC Press.

16. He, L., Lin, Y., Shang, Y., Shelton, B. J., & Yu, G. (2013). Using optical fibers with different modes to improve the signal-to-noise ratio of diffuse correlation spectroscopy

flow-oximeter measurements. J. Biomed. Opt Journal of Biomedical Optics, 18(3), 037001.doi:10.1117/1.jbo.18.3.037001

17. Michael J. Joyner; Darren P. Casey (2015). " Regulation of increased blood flow (Hyperemia) to muscles during exercise: A hierarchy of competing physiological needs. American Physiological Society.

18. Dicon Fiberoptics, INC, MEMS MxN Blocking optical switch operation manual.

19. Yu, K. G. (2013). Diffuse Correlation Spectroscopy (DCS) for Assessment of Tissue Blood Flow in Skeletal Muscle: Recent Progress. Anat Physiol Anatomy & Physiology, 03(02).doi:10.4172/2161-0940.1000128

20. http://archives.sensorsmag.com/articles/0200/63/counter.shtml

Biographical information

Chandan Ganesh Bangalore Yogananda was born in Bangalore, India on 8th January1993. He completed his Bachelors in Medical Electronics from M S Ramaiah Institute of Tecchnology (Autonomous institute, affiliated to Visvesvaraya Technological University), India in June 2015. He worked as a Product design & development Intern at MedNXT organizations Bangalore, India while doing his Bachelors towards development of a low-cost pill dispenser. In Fall 2015, he began his graduate studies at University of Texas at Arlington. To pursue his passion for research he joined Dr. Hanli Liu's Biomedical Optics Lab. His research work during the course involved the Design & development of real-time single and dual wavelength DCS systems to study skeletal muscle blood perfusion and oxygen metabolism. He plans to pursue his interests in medical device research and development by taking up related challenging projects in healthcare and allied fields.